EXPERIMENTAL EVALUATION OF THE LATERAL LOAD BEHAVIOR OF SQUAT STRUCTURAL WALLS

by

Tevfik Terzioğlu

B.Sc., Civil Engineering, Boğaziçi University, 2008

Submitted to the Institute for Graduate Studies in
Science and Engineering in partial fulfillment of
The requirements for the degree of
Master of Science

Graduate Program in Civil Engineering
Boğaziçi University

2011

ACKNOWLEDGEMENTS

I would like to express my gratitude to all the people who in one way or another contributed to the development of this research. I would like to express my sincere appreciation to my thesis advisor Asst. Prof. Kutay Orakçal; thank you for your valuable help in instructing, guiding and supporting me throughout the duration of this research.

Also, I would like to thank the members of my Master's thesis examination committee: Prof. Dr. Uğur Ersoy and Assoc. Prof. Dr. Cem Yalçın for their knowledgeable and in-depth comments and advice.

Special thanks to my friends Dr. Selçuk Altay, Dr. Osman Kaya, Hasan Altun, Furkan Çelenli and Denizhan Uluğtekin for helping me during the experimental procedure and suggestions during the construction and testing of the specimens, and to the technicians, Hasan Şenel, Hamdi Ayar and Ümit Melep for their help in the experimental phase of this research.

This research has been financially supported by University of Chile, Fondecyt Project no.11080010 and Boğaziçi University Research Fund, under project no.09S110. I would like to thank Asst. Prof. Leonardo Massone, from University of Chile, for his guidance throughout the experimental project.

I would like to thank to my true love Fatma Yilmaz for her endless support.

Finally and above all, I am indebted to my family for their self-sacrifice and patience through my education.

ABSTRACT

EXPERIMENTAL EVALUATION OF THE LATERAL LOAD BEHAVIOR OF SQUAT STRUCTURAL WALLS

This experimental study investigates the lateral load and deformation capacity of low-rise (squat) reinforced concrete structural walls designed to resist seismic actions. An experimental program was conducted to assess the lateral strength, degradation of lateral load at large deformations, and hysteretic energy dissipation characteristics of squat structural walls. One important objective was to provide detailed experimental data for development of analytical modeling methodologies, which simulate shear-flexure interaction behavior for low-rise (squat) structural walls.

For this purpose, the experimental program conducted at the Boğaziçi University Structural and Earthquake Engineering Laboratory involved testing of 11 (eleven) squat wall specimens, with different geometries and reinforcement configurations. Eleven large-scale specimens were subjected to cyclic horizontal displacements applied at the top, corresponding to increasing drift levels. Other test parameters included the wall aspect ratio, the amount of vertical and horizontal distributed web reinforcement, the amount of longitudinal boundary reinforcement, and the compressive strength of concrete. The test results were evaluated for characterizing the cracking shear force and drift level, the maximum shear capacity and the corresponding drift level, and the drift level associated with a pre-defined collapse limit state, for each of the specimens tested. Conclusions were drawn regarding the shear capacity, deformation capacity, energy dissipation characteristics, strength deterioration characteristics after capacity is reached, and the influence of vertical distributed reinforcement on the lateral load behavior of walls. Experimentally measured shear capacities and lateral load – top displacement envelope relationships were compared with the existing code provisions on design and assessment of reinforced concrete structural walls.

ÖZET

KISA PERDE DUVARLARIN YATAY YÜK DAVRANIŞLARININ DENEYSEL OLARAK İNCELENMESİ

Bu deneysel çalışma, deprem yüklerine karsı sıklıkla kullanılan kısa betonarme perde duvarların yatay yük ve deformasyon kapasitelerini incelemek amacıyla gerçekleştirilmiştir. Yapılan deneysel çalışmada kısa perde duvarların yatay dayanımları, yüksek deformasyon seviyesindeki yumuşama etkisi ve enerji sönümleme kapasiteleri incelenmiştir. Önemli amaçlardan bir tanesi de kısa perde duvarların kesme ve eğilme sekil değiştirmelerinin birleşik etkisi altında modellemesi ve deneysel kalibrasyonu için detaylı deneysel datayı elde etmektir. Diğer taraftan daha doğru ve tutarlı dizayn kriterleri belirleyebilmek için kısa perde duvarlarla ilgili daha fazla deneysel araştırmaya ihtiyaç olduğu belirtilmiştir.

Bu amaçlarla Boğaziçi Üniversitesi Yapı Laboratuvarında, değişik en-boy oranlarında, farklı donatı oranlarına sahip on bir kısa duvar numunesi test edilmiştir. Bu numunelerin kırılma mekanizmaları, kesme dayanımları ve enerji sönümleme kapasiteleri detaylı olarak incelenmiştir. Numuneler artan deplasman seviyelerinde yatay tersinir yükler altında yüksek deplasman seviyelerine kadar test edilmiştir. Numunelerden iki tanesi değişik eksenel yük seviyelerinde test edilmiştir. Elde edilen deneysel kesme kapasiteleri ve yatay yük – deplasman zarf eğrileri, Amerikan ve Türk şartnamelerinde betonarme kısa perde duvarlar için tanımlanmış dayanım hesaplarıyla ve kısa duvarlar için öne sürülen kesme kuvveti – şekil değiştirme zarf eğrileriyle kıyaslanmıştır.

TABLE OF CONTENTS

LIST OF FIGURES

LIST OF TABLES

LIST OF SYMBOLS

A_{ch}	Cross sectional area of the structural wall that has no openings
A_{cv}	Area of concrete section calculated by web thickness and length of section in the direction of shear force considered
A_{cw}	Cross sectional area of the entire wall section
A_g	Gross concrete area
A_{vf}	Area of reinforcement perpendicular to shear plane
D1	Diagonal 1 for shear measurement
D2	Diagonal2 for shear measurement
F_y	Yield strength of the Wall
f_c`	Concrete compressive strength
f_{ct}	Direct tensile strength of the concrete
F_{cr}	Cracking strength
f_y	Yield stress of web reinforcement
f_{yw}	Yield strength of the transverse reinforcement
h	Wall height
h	Story height for shear measurement
h_w	Total height of the structural wall
K	Stiffness
l_w	Total length of the structural wall
U_f	Flexural displacement at the top of the first story
$U_{s\_original}$	Top lateral shear deformation component using original X configuration
$U_{s\_corrected}$	Corrected top lateral shear deformation component
V_n	Shear strength
V_r	Expected shear strength of the structural wall
α	Relative distance from the top of the first story to the centroid of the curvature distribution
δ	Wall top displacement
Δ_y	Displacement at yield strength

Δ_u	Total displacement
λ	correction factor related to unit weight of the concrete
μ	Displacement ductility
μ	Coefficient of friction
ρ_h	Wall horizontal steel ratio
ρ_n	ratio of distributed shear reinforcement in a plane perpendicular to the direction of the applied shear
ρ_{sh}	Shear reinforcement ratio in the web section
ρ_t	transverse reinforcement ratio
θ	Rotation over story level

1. INTRODUCTION

1.1. Introductory Remarks

Structural walls are widely used to improve the seismic performance of reinforced concrete structural systems. Properly designed and detailed structural walls possess the necessary strength, stiffness, and ductility characteristics to ensure life safety and to minimize damage on a structure subjected to a severe earthquake. In order to demonstrate adequate seismic performance, structural walls should be designed and detailed properly, such that they can undergo inelastic deformation without significant loss of lateral load capacity. An adequate design of a slender reinforced concrete structural wall requires that wall shear failure shall not occur before the wall experiences a ductile flexural response under seismic excitations. However, this may not be achieved when the structural wall is relatively short, and its response is governed by shear deformations. Such walls with aspect (height to width) ratio smaller than 1.5 or 2.0 could be used in the seismic design of low-rise buildings (e.g., parking structures). As well, in buildings with perimeter walls (e.g., hospital buildings in California), the perimeter wall can have large window openings, which results in formation of squat horizontal and vertical wall segments between the openings. Such vertical wall segments are referred to as wall piers, and the horizontal wall segments are referred to as wall spandrels. Figure 1.1 presents a photo that shows wall piers and spandrels within a perimeter wall of a reinforced concrete hospital building. Wall piers and spandrels have generally small aspect ratio, and are subjected to predominant shear actions. The level of existing research, as well as current code provisions and modeling approaches, are not adequate to represent the behavior of such walls. Therefore, estimating the shear capacity, failure mode, ductility, and overall behavior of such squat walls is important, within the context of performance-based seismic design and evaluation.

For seismic-resistant design of structural walls, various performance levels were described, including preservation of functionality, different levels of damage and prevention of loss of life. In conjunction with these damage levels, specific structural properties, including the stiffness, strength, and ductility characteristics, need to be considered. Typical responses of a reinforced concrete structural wall are illustrated in

Figure 1.2. The stiffness of a wall relates the lateral applied load to the resulting lateral displacement. Lateral stiffness (K) is defined as the slope of the idealized linear elastic response, and it is defined as the lateral force at the yield point divided by the lateral displacement at the yield point ($K = F_y/\Delta_y$). For a true (e.g., experimental) load – displacement curve, the lateral stiffness can be defined as the effective secant stiffness at a lateral load corresponding to $0.75F_y$. Ductility of a wall is defined as the ability of the wall component or wall system to sustain large deformations before collapse. Displacement ductility (μ) can be quantified as the ratio of the total imposed displacement to the displacement at yielding, i.e., $\mu = \Delta_u/\Delta_y$.

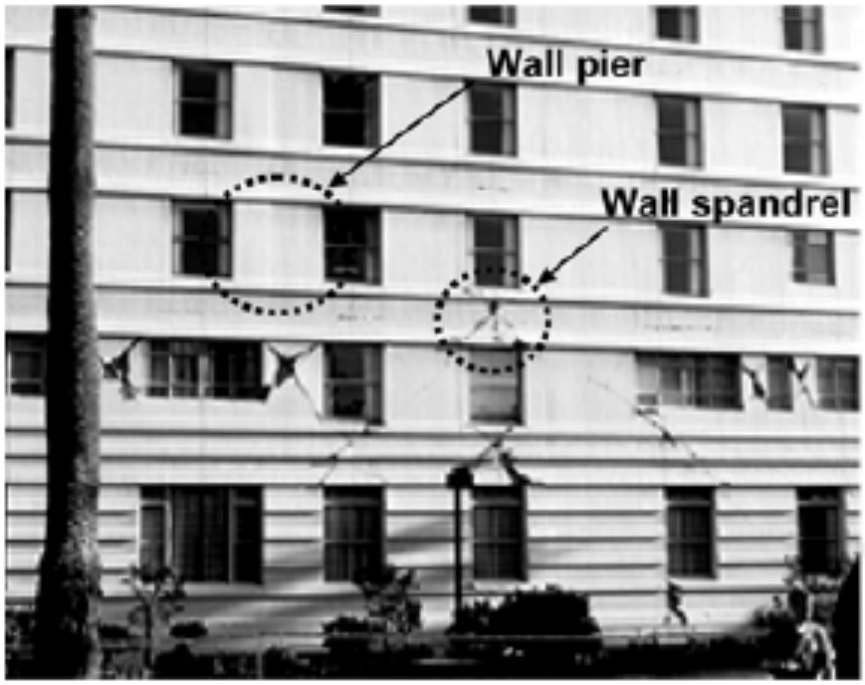

Figure 1.1. Wall Piers and Spandrels in a Perimeter-wall building (Massone, 2006).

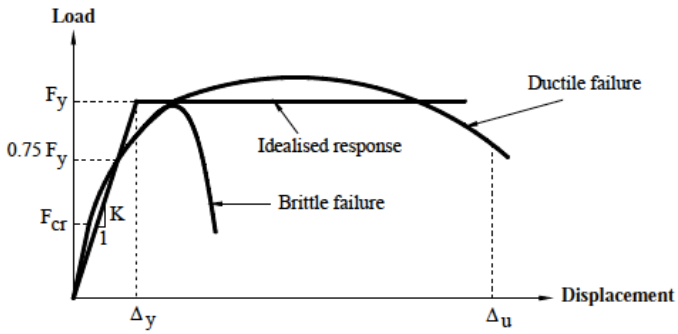

Figure 1.2. Typical Responses of Reinforced Concrete Structural Walls (Paulay and Priestly, 1992).

The desired behavior and failure mode of well-detailed slender structural walls is usually dominated by flexure. However, depending on different conditions including geometrical dimensions, boundary element conditions, the way lateral loads are imposed, and reinforcement detailing, squat structural walls may fail in any of three modes: diagonal tension, diagonal compression or sliding shear (Paulay and Priestley, 1992). Figure 1.3 shows representative figures for the three failure modes observed in squat walls. The diagonal tension failure mode will occur whenever transverse reinforcement is insufficient to carry shear forces or is insufficiently detailed (Figure 1.3a). When adequate the transverse reinforcement is provided but the wall is subjected to a high shear stress, concrete may crush under diagonal compression (Figure 1.3b). This is common for squat walls with boundary elements. Finally, for walls with sufficiently detailed transverse reinforcement but low quantities of longitudinal reinforcement in the web, failure can be due to yielding of longitudinal reinforcement leading to a sliding deformation along the base of the wall (Figure 1.3c). This last failure mode is particularly important for walls subjected to cyclic displacement reversals.

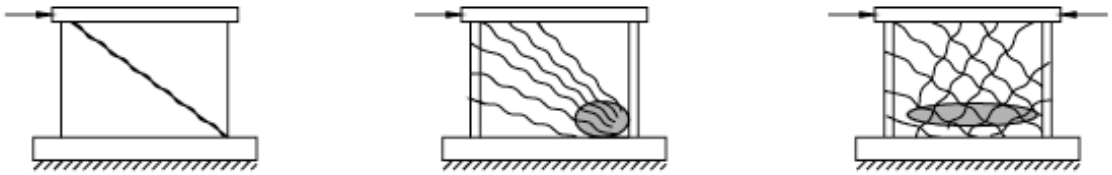

(a) Diagonal Tension (b) Diagonal Compression (c) Sliding shear

Figure 1.3. Failure Modes of Squat Structural Walls (Paulay and Priestly, 1992).

Recent building codes (e.g. ACI 318-08M, 2008, FEMA-356, 2000) place considerable emphasis on understanding the lateral strength, ductility and stiffness of the individual structural members. The guidelines in FEMA-356 (2000) report on seismic evaluation and rehabilitation of existing structures, focuses more on structural walls controlled by flexure (i.e., slender walls). Shear strength provisions provided in FEMA-356 (2000) generally follow ACI 318M-08 requirements, which are developed for the design of new buildings.

In FEMA-356 (2000) particular emphasis is placed on the estimation of the shear strength of squat structural walls, the responses of which are governed by shear. However,

limited information is provided in FEMA-356 on the lateral load versus deformation backbone relationships for shear-controlled walls or wall segments (e.g., wall piers and spandrels), to be used in the seismic evaluation (e.g., pushover analysis) of existing buildings. The FEMA-356 methodology to determine the envelope curve from a cyclic experimental data was shown to potentially result in underestimation of the lateral load versus displacement response characteristics. An alternative procedure was introduced by Massone (2006), which provides better estimation of stiffness and ductility of squat structural walls, as well as better representation of their lateral load – displacement response attributes. Based on the experimental research conducted by Massone (2006), modified backbone curves were provided in the ASCE41/SEI – Suppement1 (2007), which were not verified with further experimental studies.

Overall, performance-based design of new structures, as well as evaluation and rehabilitation of existing structures, relies on assessing the performance of the system for a design level event. One objective of performance-based design or evaluation is to demonstrate that the designed or existing structure could meet the displacement demands generated by the design earthquake, without significant loss in the post yield lateral strength and axial load capacity. Numerous buildings are designed to rely on the performance and ductility structural walls, and many of them incorporate relatively short walls, or wall openings which result in formation of short wall segments (wall piers and spandrels), all of which behave as squat walls under predominant shear effects. Although reliable modeling of such structures requires realistic representation of both the flexural and shear response components of wall elements, current code provisions and rehabilitation guidelines on the strength and ductility of short walls are based on limited research and information.

1.2. Research Significance and Scope

Although extensive research has been conducted on the behavior of slender structural walls, available information on the behavior of squat walls, with aspect ratios smaller than 1.5, is limited. Also, strength calculations given in code provisions and backbone (envelope) curves given in assessment/rehabilitation guidelines may provide unrealistic and over-conservative estimations of squat wall response. As one simplistic

approach, the shear strength defined in ACI 318 – 08M (2008) could be used to model the maximum attainable shear force in a squat wall. Wood (1990) compared the shear strength defined in ACI 318, experimentally against a series of wall tests collected from the literature that presented a shear failure. The work done by Wood (1990) shows that the code equation gives, in general, a slightly conservative estimate of the shear capacity of squat walls, which verifies the equation for shear capacity estimation. On the other hand, there is no direct methodology to estimate the ductility of a squat wall. The general approach is to define the ductility as the capacity of the wall to reach a certain displacement, as it reaches its flexural capacity.

The existing analytical models based on a fiber formulation (e.g. Orakçal, 2004) could provide good estimations of the flexural response of slender walls. However, the nonlinear response of a squat wall cannot accurately estimated by any empirical equation or design parameter. The research conducted by Massone, (2006) showed that the backbone relationships defined in FEMA 356 (2000), incorporate deficiencies related to the initial stiffness and ductility of squat walls, as well as their shear capacity when axial load is applied.

Based on these shortcomings, an experimental program was conducted at the Structural and Earthquake Engineering Laboratory of Bogazici University, to investigate the shear-dominated lateral load behavior of squat structural walls. The objectives of this experimental program include providing detailed information on squat wall behavior and failure modes, in order to develop new analytical modeling approaches, and comparison of the experimental results with code provisions, in order to investigate potential code improvements.

Eleven squat wall specimens, having different aspect ratios and different reinforcement configurations, were constructed. The instrumentation on the wall specimens was designed to characterize the flexural and shear components of the lateral displacement of each wall, and to provide horizontal strain distributions at different levels. Some of the specimens were tested under different axial load levels. The detailed instrumentation and controlled loading allowed segregating the flexural and shear components of the response, as well as investigating the characteristics of the response at

large drift levels. Existing information available in the literature from past experimental studies concentrated on the shear capacity of squat walls; however, since most walls were not tested to large drift levels, information on ductility and strength degradation of walls, required to describe the entire lateral load versus displacement response, was limited.

1.3. Objectives

In summary the objectives of this experimental study are;

i. To investigate the lateral load behavior of squat structural walls, for better understanding and representation of their shear capacity and ductility, as well as different failure modes and residual capacity, for performance-based design and evaluation applications.
ii. To investigate correlations between the global load – displacement response, and the flexural and shear components of the response, since current code provisions and modeling approaches require consideration of the flexural and shear behavior components separately.
iii. To compare the strength and ductility characteristics of the wall specimens tested with existing code provisions and guidelines.
iv. To obtain detailed experimental data to be used in experimental calibration and verification of new analytical modeling approaches.

1.4. Review of Related Research

In this section, previous experimental research on the lateral load behavior of squat structural walls is summarized.

Benjamin and Williams (1957) conducted one of the pioneering experimental researches on squat structural walls. They performed a series of lateral loading tests on low-rise shear walls (aspect ratio of 0.57) subjected to monotonic loading. The test specimens were mainly reinforced concrete frames infilled with monolithic plane or reinforced concrete panels. They proposed an expression to predict the elastic load-displacement curves, and obtained the structural stiffness at various loads. Their purpose

was to identify the lateral load capacity, failure modes and to observe how different variables affect the wall response. The specimens were designed with and without panel reinforcement; the amount of reinforcement at the boundary elements was also changed. Mainly, load–displacement relations for all specimens were provided up to the ultimate lateral load capacity. Most of the early works mainly focused their attention on the stiffness and lateral load capacity, without studying aspects such as strength degradation after the lateral load capacity is achieved.

Another early experimental study on squat walls is the one conducted by Cardenas et al. (1972). In order to develop design information on the behavior and strength characteristics of shear walls for high and low-rise buildings, the PCA Laboratories initiated an experimental investigation. A total of twenty-one specimens were tested. Thirteen specimens dealt primarily with the strength of rectangular shear walls for high and low rise buildings. The last eight dealt with the shear strength of very low rise walls (aspect ratios of 1/2 or less) incorporating cross walls as boundary elements, and subjected to load reversals. Results of these tests were used to formulate the strength section in ACI318-71. As a result, it was emphasized that consideration of energy absorption capacity, reinforcement details and means of avoiding undesirable types of damage are equally important to obtain satisfactory structural performance.

Another experimental study where the specimens were tested under lateral loads up to high drift levels was the one conducted by Barda et al. (1976). The load-displacement response was obtained for large drift levels, and strength degradation characteristic was observed. A series of squat structural wall specimens, which have aspect ratios ranging from 1.0 to 0.25, were tested. Flanges were used in the construction of the specimens, in order to increase the flexural capacity of the specimens for promoting shear failure. The experimental program was designed to observe the effect of boundary longitudinal reinforcement, amount of web vertical and horizontal reinforcement, and aspect ratio on the response of short walls. No axial load was applied on the walls. Besides the behavior of squat walls, repair and strengthening techniques on walls was also investigated in this test program.

The findings of this study indicated that severe load reversals reduced the shear capacity by around 10%. Vertical reinforcement was more effective than the horizontal reinforcement in resisting shear, and vertical reinforcement was also effective in producing a distributed crack pattern. Boundary elements enhanced the post–ultimate load carrying characteristics. Load carrying capacity beyond ultimate load depended mainly on the ability of the boundary elements to act as a frame. For the specimens with aspect ratios of 1/2 and less, the horizontal reinforcement did not increase the shear strength, whereas horizontal reinforcement was effective for producing a distributed cracking pattern. And simple repair techniques were found to provide improved strength and improved energy dissipation capacity. The behavior of short-flanged walls was found to be more complex. Even a small amount of vertical reinforcement in wide flanges could provide a flexural capacity that is associated with excessive shear load on the web. The effectiveness of vertical web reinforcement was also confirmed for such walls.

Several tests results from Japanese researchers were reported by Hirosawa (1975). The collection of test results included different specimens having a large range of aspect ratios, horizontal and vertical web reinforcement ratios, boundary reinforcement amounts and axial load levels. Material properties, loading conditions, and lateral load–displacement curves were provided for each test. Most of the reported tests were carried out only until the lateral load capacity was achieved, not providing information on ductility characteristics.

Maier and Thurlimann (1985) studied the behavior of barbell-shaped and rectangular walls subjected to monotonic and cyclic loading. The specimens were tested as cantilevers, with uniformly distributed vertical reinforcement and horizontal reinforcement ratios of 0% and 1.1%. Particularly for two specimens, constant axial load monotonically increasing lateral loads were applied. These two specimens were identical, except one had no horizontal web reinforcement. It was observed that the horizontal reinforcement had only minor influence on the lateral load capacity. However, the failure mode changed and the ultimate drift decreased for the specimen with no horizontal web reinforcement. Diagonal tension failure was observed for that specimen, whereas diagonal compression failure was observed for the specimen with horizontal web reinforcement. The test program included specimens with and without boundary elements, cyclic and monotonic loading, and high

and low levels of axial load. The specimens were heavily instrumented, which allowed determination of axial, horizontal and vertical strain distributions.

Paulay et al. (1982) also studied the behavior of squat structural walls, with an extensive experimental program. They tried to identify the failure modes of the squat walls, depending on the parameters such as type of cross-section, reinforcement ratio, properties of reinforcing steel, compressive strength of concrete and boundary conditions. Paulay et al. have reported failure modes for squat structural shear walls that are likely to fail in shear. Accordingly, diagonal tension failure was found to occur when a diagonal crack forms from corner to corner, due to insufficient horizontal web reinforcement. If the wall has high flexural capacity and adequate horizontal reinforcement, it might fail under diagonal compression. The concrete crushes in the compression zone near to the base of the wall. For cyclic loading, two sets of diagonal crack appear and concrete crushing can extend over the entire length of the wall due to degradation that is provoked by the load reversals. Another failure mode was found to be sliding shear. If the flexural capacity of the wall is not adequate, a continuous horizontal crack develops along the base of the wall. Since the efficiency of the aggregate interlocking decreases as the number of cycles increases, the crack slip becomes significant, and the wall lateral displacement includes considerable amount of sliding deformation. This phenomenon was found to result in pinching of hysteretic loops, which reduces the hysteretic energy dissipation capacity of the wall.

Another experimental research program was conducted by Hidalgo et al. (2002). The behavior of reinforced concrete structural walls experiencing shear mode of failure was investigated. Twenty-six reinforced concrete walls having aspect ratios between 0.35 and 1.0 were constructed. Other test parameters included the amount of vertical and horizontal reinforcement and compressive strength of concrete. The specimens were tested under cyclic lateral loading, under double curvature, with zero rotation conditions at both ends. Test results characterized the shear strength, stiffness, and failure modes for each specimen. Energy dissipation and displacement capacities were also studied. However, the tests were carried out only until the lateral load drops to 75% of the ultimate lateral load capacity, which means the behavior mostly up to the lateral load capacity was investigated. Conclusions were drawn concerning the deformation capacity, the energy absorption, the

dissipation characteristics and strength degradation characteristics after maximum lateral load. The influence of vertical distributed reinforcement on the behavior of walls was also investigated.

It is widely recognized that the horizontal web reinforcement is essential for the shear strength of a wall, and also for maintaining the strength after diagonal cracks in the concrete have developed. Horizontal web reinforcement improves redistribution of stresses after formation of cracks, and adds post-cracking inelastic behavior to the response. These phenomena were supported by this experimental study of Hidalgo et al (2002). On the other hand, the results obtained indicated that the amount of vertical web reinforcement has little or no influence on the lateral load capacity of the walls that fails under shear failure mode. It was also suggested that the test setup has a significant influence on the effect of vertically reinforcement on wall response.

In terms of the influence of vertical web reinforcement on the response, test results by Hidalgo et al. (2002) did not agree with previous experimental observations for squat walls, such as those obtained by Barda et al. (1976), who highlighted the importance of the vertical reinforcement on wall shear capacity. The results also did not agree with ACI 318 provisions, which suggest using a vertical web reinforcement ratio at least equal to the horizontal web reinforcement ratio. Hidalgo et al. (2002) suggested that the importance of vertical web reinforcement did arise during these tests, due to the type of boundary conditions applied on the wall specimens. The specimens were enforced zero rotation conditions at the top and bottom, with double curvature bending moment distribution, as illustrated in Figure 1.4. When cantilever-loading conditions are used during testing, the top of the specimen is free to rotate, and vertical web reinforcement may contribute to the lateral load capacity. On the other hand, wall specimens tested in a double curvature loading condition experience largest rotations in the sections close to wall mid-height, however, cracking and inelastic behavior in these regions are less pronounced, compared to the top and bottom sections of the specimen.

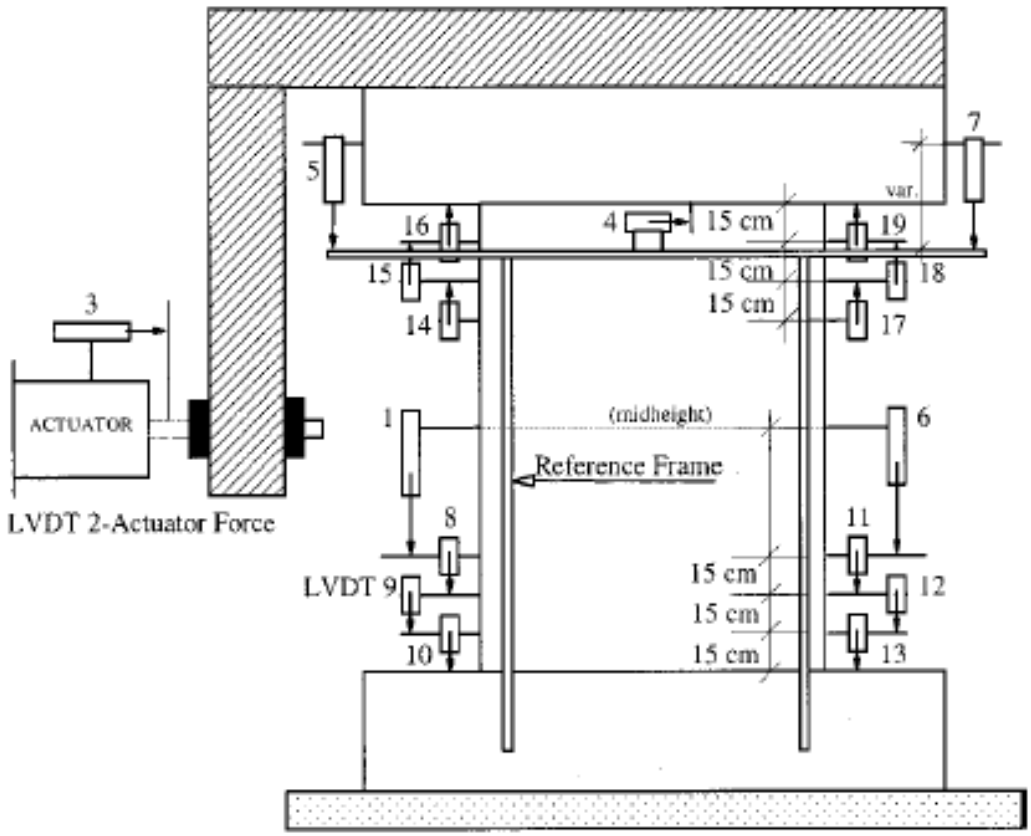

Figure 1.4. Double Curvature Loading setup.

According to the test results by Hidalgo et al. (2002), although the cracking pattern for all specimens was not significantly different, the horizontal web reinforcement provided a more ductile wall behavior. Deformation capacities of the specimens were reduced, as the wall aspect ratio decreases. The energy dissipation capacity of the walls appeared to be independent of the aspect ratio and of the variation in both horizontal and vertical web reinforcement amounts. Strength deterioration characteristics became more severe with the decreasing aspect ratios and decreasing horizontal and vertical web reinforcement ratios.

Another experimental program on the behavior of squat structural walls was conducted by Massone (2006) at the University of California at Los Angeles. The test program consisted of testing six wall piers and eight wall spandrels specimens. Relatively low shear span to depth ratios (corresponding to one half of the aspect ratio) were achieved by fixing the base of the walls and restraining rotations at the top of the walls and applying the lateral load at specimen mid-height, producing a double curvature loading condition.

Specimens having shear-span-to-depth ratios of 0.44 and 0.5, horizontal reinforcement ratio of 0.28%, vertical reinforcement ratios between 0.23% and 0.43% and different boundary reinforcements were tested. The experimental program was conducted on selected lightly reinforced wall pier and spandrel configurations to investigate various response attributes including shear strength, stiffness, and deformation capacity, as well as the effect of outdated construction practices on the shear strength and lateral load behavior of wall segments in existing buildings.

For all of the specimens, lateral load failure (degradation of lateral load capacity) was associated with crushing of concrete close to the center of the wall (where the constraining effect of the top and bottom pedestals are minimized), followed by spalling of diamond-shaped wedges of concrete on both sides. The specimens were tested for high drift levels to obtain the residual capacity.

Orakçal et al. (2009) investigated the lateral load capacities of these lightly reinforced wall piers and spandrels that fail in shear or shear sliding. Test results were compared with the shear strength equations provided in ACI 318 and FEMA-356. Also shear friction capacities of the specimens were calculated according to ACI 318 equations. Shear friction capacity was found to be important for one of the specimens, which failed due to sliding at the bottom portion because of the weakened plane joint provided at that section. Use of FEMA356 nominal shear strength calculations showed good agreement with test results. The results also indicated that the FEMA-356 nominal shear strength calculation may provide a more reasonable lower bound estimate of the shear strength of wall segments with boundary reinforcement ratios larger than 3% (assuming there are no boundary columns, that is, the wall cross section is rectangular). For rectangular walls with boundary reinforcement ratios smaller than 3%, the FEMA nominal shear strength calculation was found to provide a slightly unconservative estimate of wall shear strength.

Massone, (2006) investigated lateral load versus deformation response characteristics (for example, stiffness, deformation capacity, strength degradation, and axial load collapse) of shear-controlled wall piers and spandrels based on the same experimental database. FEMA 356 methodology to determine the envelope curve from a cyclic experimental data was shown to potentially result in large underestimations of shear

forces. An alternative procedure was suggested for determination of the experimental envelope curve, which overcomes such inconsistencies. As well, modifications to the FEMA356 backbone curves were suggested, in order to better represent the overall shear-controlled load-deformation responses of squat walls.

2. EXPERIMENTAL PROGRAM

This chapter presents the details of the specimen construction procedure, as well as the test setup and instrumentation used in the experimental program. Basic technical information on hydraulic loading system and the sensors is also provided.

2.1. Description of Wall Specimens

In this section, the design, specifications, and detailing of the wall specimens tested in in this experimental study are described. Three sets of specimens, with a total of eleven squat wall specimens were tested at the Bogazici University Structural Engineering Laboratory.

The first set of specimens included three squat walls with aspect ratios of 0.5. Squat walls have aspect ratios of 1.5 or smaller, according to the definition in FEMA356. The second set consists of four structural walls, one having 0.33 aspect ratio, one having 1.0 aspect ratio and two having 0.5 aspect ratio. The third set includes one 1.0 aspect ratio specimen and three 0.5 aspect ratio specimens. Two of the specimens were tested under different level constant axial loads. Specimens are differentiated by reinforcement ratio, aspect ratio, the amount of boundary reinforcement, steel properties and the compressive strength of concrete. No axial load was applied during first two set of tests. Two specimens from third set were tested under axial load. The naming of the specimens is done according to their aspect ratio, reinforcement ratio and the testing sequence. A representative naming scheme is shown in the Figure 2.1.

The specimens of identical type are the ones having the same aspect ratio, same horizontal and vertical web reinforcement ratios and same boundary reinforcement ratio. If any of these three properties change, the type of the specimen changes. Same type specimens are classified with specimen numbers (e.g. S1, S2 …) and testing sequence (e.g. 1, 2 …).

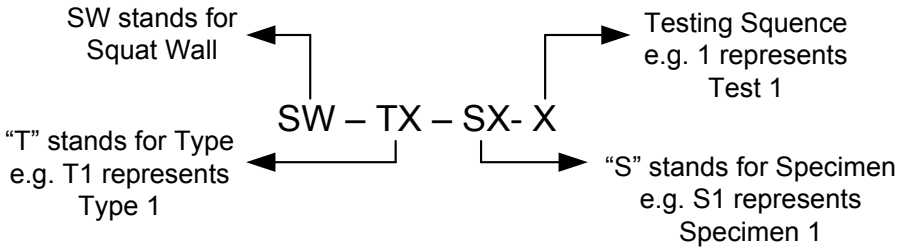

Figure 2.1. Naming of Specimens.

Specimen designs and reinforcement ratios are provided in Table 2.1. The specimen SW-T2-S1-1 and the specimen SW-T2-S2-3 differ only in terms of their horizontal reinforcement anchorage conditions. Specimen SW-T2-S1-1 has U-cap hooks at the ends of the horizontal reinforcement bars, for anchorage. On the other hand specimen SW-T2-S2-3, as well as all other specimens, has 180^{o} hooks on the horizontal bars. Figure 2.2 shows the details of the hooks used. Another variation exists in the Type1 specimens. The longitudinal boundary reinforcement of specimen Type1-S2 was confined with ties, whereas no confinement was provided for specimen Type1-S1, in order to observe the difference between these two specimens in terms of strength and ductility.

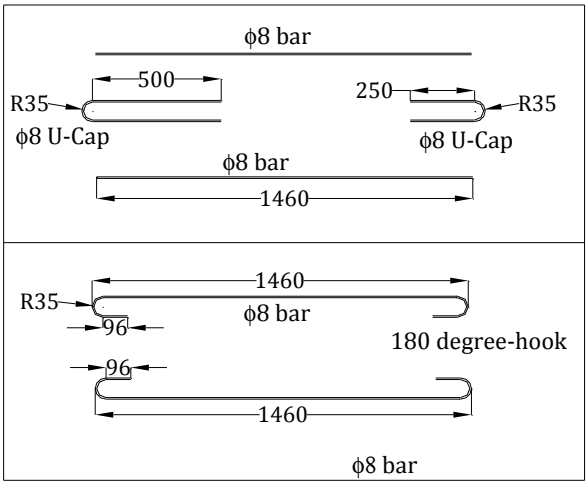

Figure 2.2. Hook Types.

The steel reinforcement ratios were calculated as the total steel area divided by the tributary area of concrete. For the boundary reinforcement, the tributary area is defined as the thickness of the wall multiplied by the length between boundary reinforcing bars, added to two clear cover lengths (one on each side). For the specimens, clear cover was 40 mm and the distance between boundary bars along the length was 50 mm. Therefore the

boundary tributary area width corresponded to 130 mm. For vertical web reinforcement, the tributary area corresponded to the cross-sectional area minus two boundary tributary areas. For horizontal web reinforcement, the tributary area corresponded to the vertical cross-sectional area of the wall specimen.

Table 2.1. Specimen properties.

Specimen	l_w cm	h_w cm	h /l cm	Horizontal		Vertical		Boundary	
				Reinf. Bars	ρ_t (%)	Reinf. Bars	ρ_l (%)	Bars	ρ_b (%)
SW-T2-S1-1	150	75	0.50	ϕ8@125 mm	0.68	ϕ8@125 mm	0.68	4ϕ16	5.15
SW-T2-S2-3	150	75	0.50	ϕ8@125 mm	0.68	ϕ8@125 mm	0.68	4ϕ16	5.15
SW-T2-S3-4	150	75	0.50	ϕ8@125 mm	0.68	ϕ8@125 mm	0.68	4ϕ16	5.15
SW-T3-S1-5	150	75	0.50	ϕ8@125 mm	0.68	ϕ8@125 mm	0.68	2ϕ8	0.65
SW-T4-S1-6	150	50	0.33	ϕ8@125 mm	0.68	ϕ8@125 mm	0.68	4ϕ14	3.95
SW-T5-S1-7	150	150	1.00	ϕ8@125 mm	0.68	ϕ8@250 mm	0.34	4ϕ22	9.75
SW-T6-S1-8	150	150	1.00	ϕ8@125 mm	0.68	ϕ8@250 mm	0.68	4ϕ22	9.75
SW-T1-S2-9	150	75	0.50	ϕ8@250 mm	0.34	ϕ8@250 mm	0.34	4ϕ16	5.15
SW-T1-N5-S1-10	150	75	0.50	ϕ8@250 mm	0.34	ϕ8@250 mm	0.34	4ϕ16	5.15
SW-T1-N10-S1-11	150	75	0.50	ϕ8@250 mm	0.34	ϕ8@250 mm	0.34	4ϕ16	5.15
SW-T1-S1-2	150	75	0.50	ϕ8@250 mm	0.34	ϕ8@250 mm	0.34	4ϕ16	5.15

Notes: h /l: thickness of the wall, l_w: length of the wall, h_w: height of the wall, ρ_t: transverse reinforcement ratio, ρ_l: longitudinal reinforcement ratio, ρ_b: boundary reinforcement ratio, thickness of the wall is 12 cm for all specimens.

During the first set of tests, there were some concerns about the placement of the concrete during casting of specimen SW-T2-S2-3. Therefore, an identical specimen was constructed during the second set of tests. The identical specimen is named as SW-T2-S3-4, which corresponds to Test Sequence No. 4.

2.1.1. General Description of 0.5 Aspect Ratio Specimens

In the tests, there were a total of five 0.5 aspect ratio wall specimens. These specimens have length of 1500 mm, height of 750 mm and thickness of 120 mm. They differ by their web reinforcement ratio or boundary reinforcement amount. Four of the 0.5 aspect ratio specimens has transverse (horizontal) and vertical (longitudinal) web reinforcement ratios of $\rho_t = \rho_l = 0.34\%$. These four specimens were identical in terms of their horizontal and vertical reinforcement ratios, and their aspect ratios. However, two of these Type-1 specimens were tested under different axial load levels. These two specimens named as SW-T1-N5-S1-10 and SW-T1-N10-S1-11. The abbreviations N5 and N10 represent the axial load level applied. Type1-N5 means the axial load applied at a level of $5\%f'_cA_g$ (5% of wall axial load capacity) and Type1-N10 means that the axial load was applied at a level of $10\%f'_cA_g$. The specimens with axial loads were tested as 10 and 11^{th} specimens, as the last two tests. Another Type-1 specimen was Type1-S2, which had confined boundaries at the ends. This specimen was constructed in order to see the effect of confined boundaries on the behavior. Figure 2.3 shows the geometry and reinforcement details of specimen types T1-S1, and Figure 2.4 shows the geometry and reinforcement details specimen type T1-S2.

The vertical and horizontal web reinforcement was distributed in two curtains. Equally distributed vertical reinforcement was ϕ8-reinforcing steel bars and placed uniformly along the wall section. Since there is enough space for embedment length in top and bottom pedestals, vertical reinforcing steels have not been hooked. For all specimens the distance between two curtains of vertical reinforcement was 62 mm. The horizontal reinforcement was distributed uniformly along the height of the wall with equal spacing.

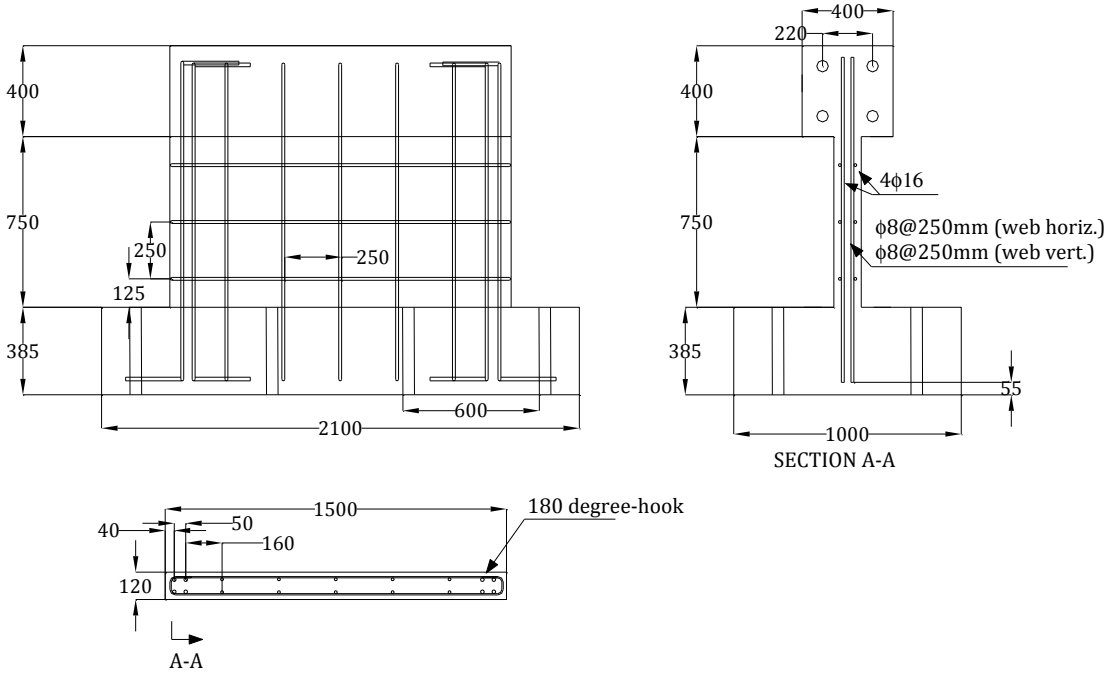

Figure 2.3. Geometry and Wall Reinforcement of Specimen T1–S1.

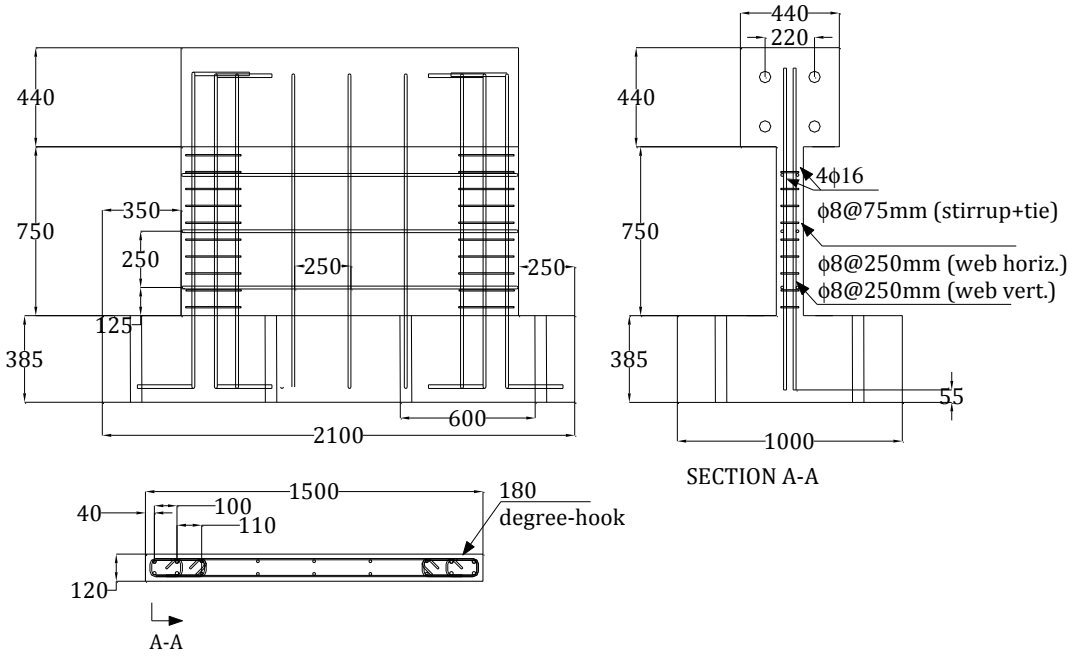

Figure 2.4. Geometry and wall reinforcement of specimen T1–S2.

Since there is not enough space at the edges of the wall, the horizontal reinforcing bars were anchored with 180^{o} hooks at the ends. Only for the T2-S1 specimen, horizontal reinforcing bars were terminated at the edges and U-caps were used instead of hooks. The

inner distance between two rows of horizontal bars was 70 mm. Figure 2.5 shows the geometry and reinforcement details of specimen type T2-S1, which have horizontal (transverse) and vertical longitudinal web reinforcement ratios of $\rho_t = \rho_l = 0.68$ and U-caps at the end of the horizontal reinforcing bars. The parameters used for the construction of the third Type 2 specimen (T2-S3) were the same as the T2-S2 specimens. All the parameters were kept identical; however, due to time of testing after concrete is placed, concrete compressive strength comes out to be a different parameter for the T2-S3 specimen. Figure 2.6 shows the reinforcement details and the geometry of T2-S2 specimens. All the geometric properties and the reinforcement details of specimen T2-S3 was the same as the two T2-S2 specimens.

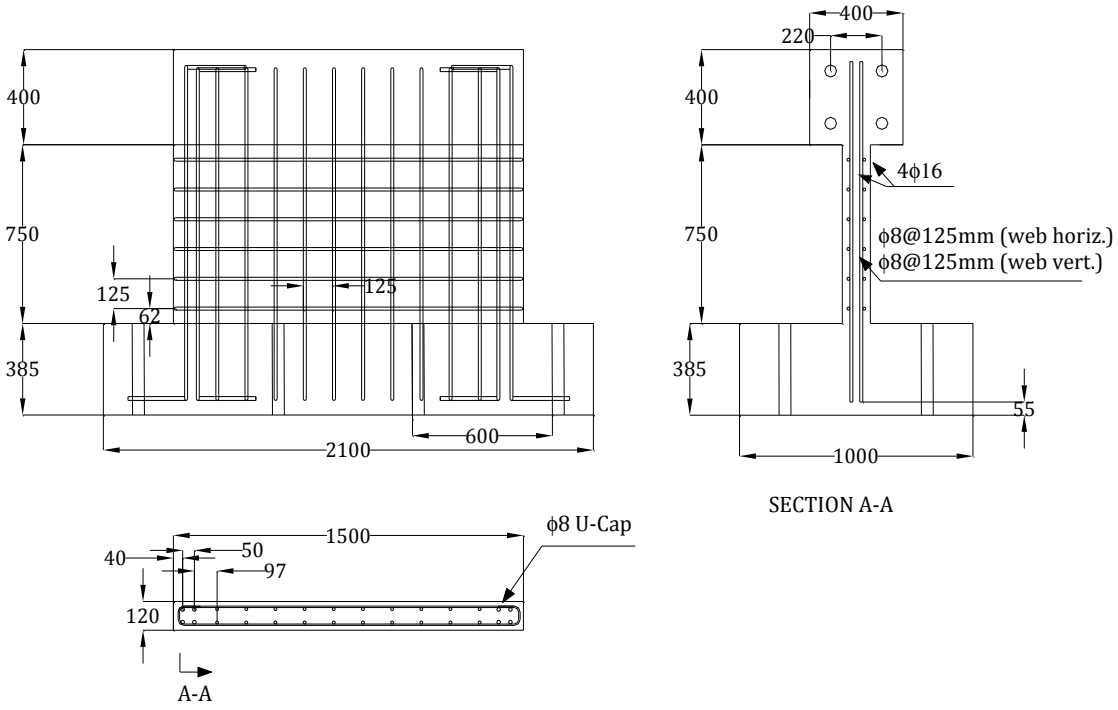

Figure 2.5. Geometry and wall reinforcement of specimen T2-S1.

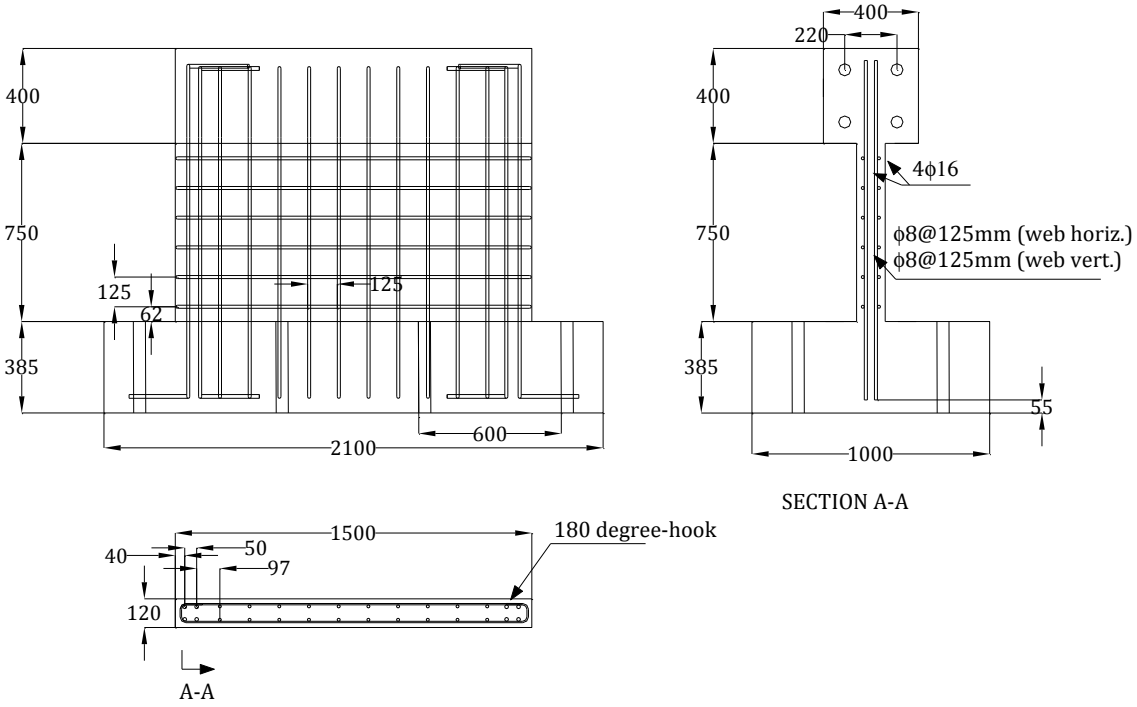

Figure 2.6. Geometry and wall reinforcement of specimen T2-S2.

The longitudinal boundary bars were placed at both edges of the wall. They were placed inside the hooks of horizontal bars. However, the boundary regions were not confined with ties, except for specimen T1-S2. Two different types of boundary reinforcement were used for the 0.5 aspect ratio structural walls. Seven of the structural walls had 4ϕ16-reinforcing bars at their boundaries. T3-S1, which has similar web reinforcement with Type2 structural walls, has 2ϕ8 boundary reinforcement at both edges. Figure 2.7 shows the reinforcement details and geometric dimensions of specimen type T3-S1. The differentiating parameter for this specimen is the amount of boundary reinforcement. The flexural yielding of the boundary reinforcement was targeted in the design of this specimen.

2.1.2. General Description of 0.33 Aspect Ratio Specimen

The specimen having a 0.33 aspect ratio was 1500 mm long, 500 mm tall and 120 mm thick. It had web reinforcement ratios of $\rho_t = \rho_l = 0.68\%$. Figure 2.8 shows the geometry and reinforcement details of specimen T4-S1.

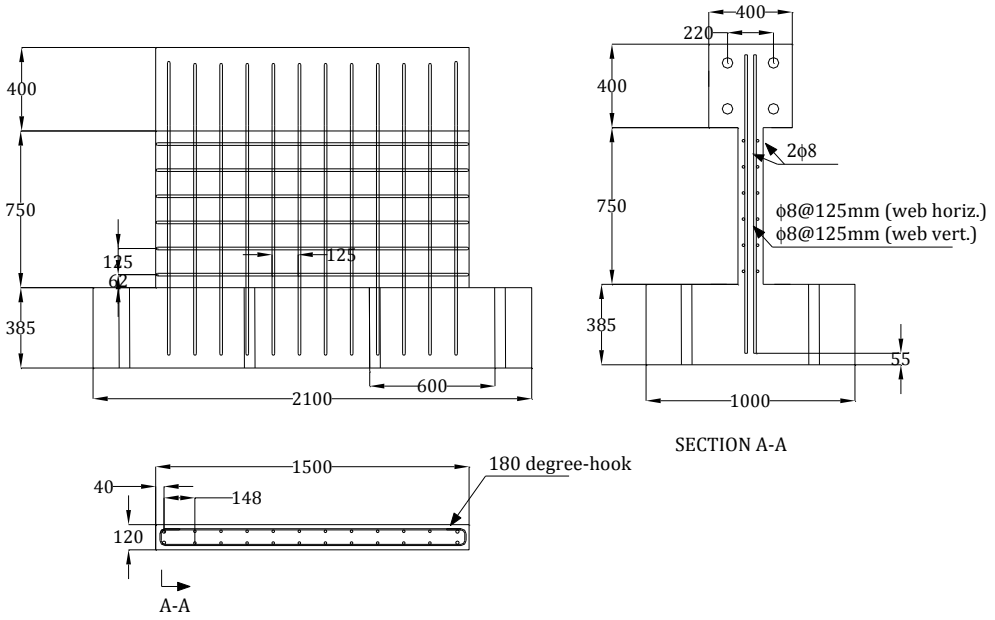

Figure 2.7. Geometry and reinforcement of specimen type T3-S1.

The longitudinal boundary bars were placed at both edges of the wall. They were placed inside the hooks of the horizontal web bars. The boundary regions were not confined with ties. For this specimen, 4-ϕ14 boundary bars were provided at both ends of the wall. The amounts of boundary bars provided targeted simultaneous reaching of flexural and shear capacities of the wall.

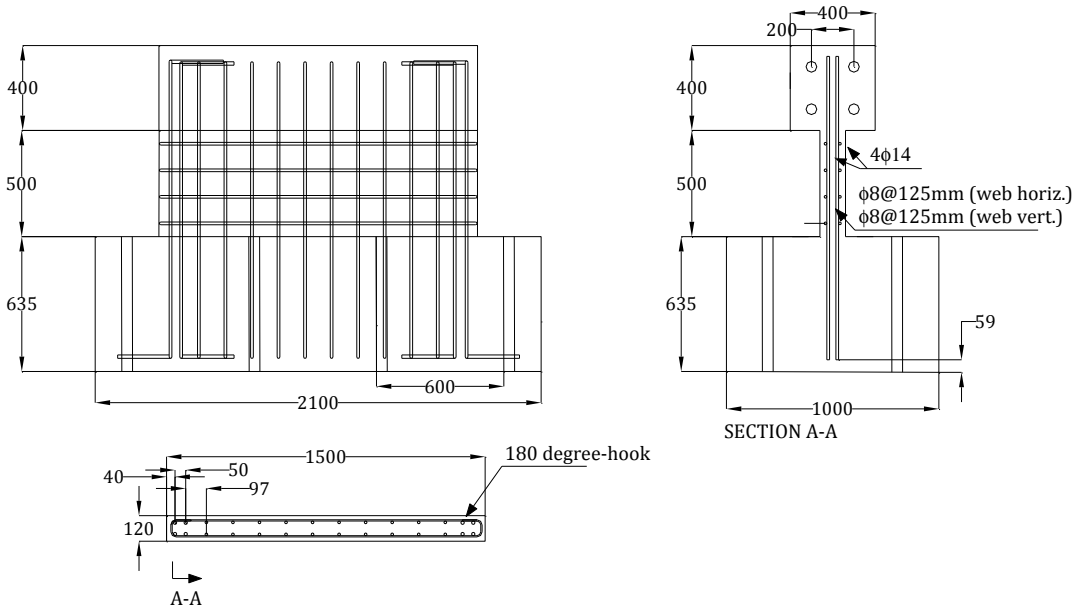

Figure 2.8. Geometry and wall reinforcement of specimen T4-S11.

2.1.3. General description of 1.0 Aspect Ratio Specimens

Two structural walls having 1.0 aspect ratio were constructed. The Type5 and Type6 specimens were designed with identical horizontal web reinforcement amounts. Both of the walls had 0.68% horizontal reinforcement ratios, whereas the Type5 specimen had 0.34% vertical web reinforcement ratio, and the Type6 specimen has 0.68% vertical web reinforcement ratio. Figure 2.9 shows the geometry and reinforcement details of specimen T5-S1.

The height of the wall specimens was 1500 mm, the length was 1500 mm, and the thickness was 120 mm. For specimen T5-S1, ϕ8 vertical bars were placed with 250 mm spacing, and for specimen T6-S1, they were placed with 125 mm spacing. The vertical bars did not incorporate hooks at the ends, since there was enough embedment space in the top and bottom pedestals for the bars to develop. ϕ8 horizontal web bars were distributed along the height, with 125 mm spacing and terminated at the edges of the wall with 180^o hooks.

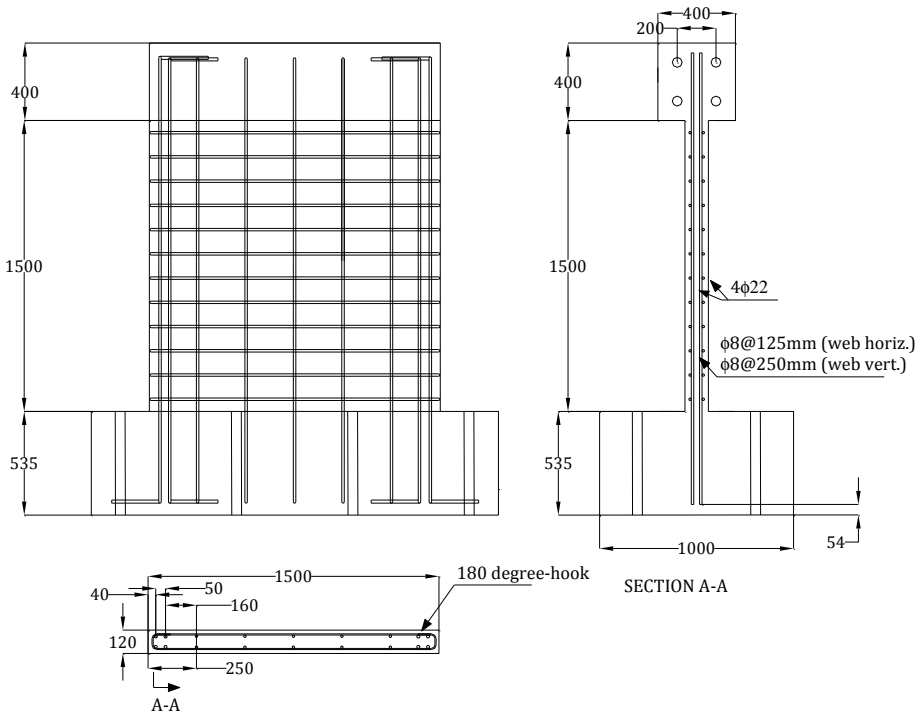

Figure 2.9. Geometry and wall reinforcement of specimen T5-S1.

The boundary reinforcement was placed inside the horizontal bars at both edges. Boundary regions were not confined with ties. 4ϕ22 bars were used at both edges as

boundary reinforcement. The boundary bars were anchored with 90^{o} hooks inside the top and bottom pedestals.

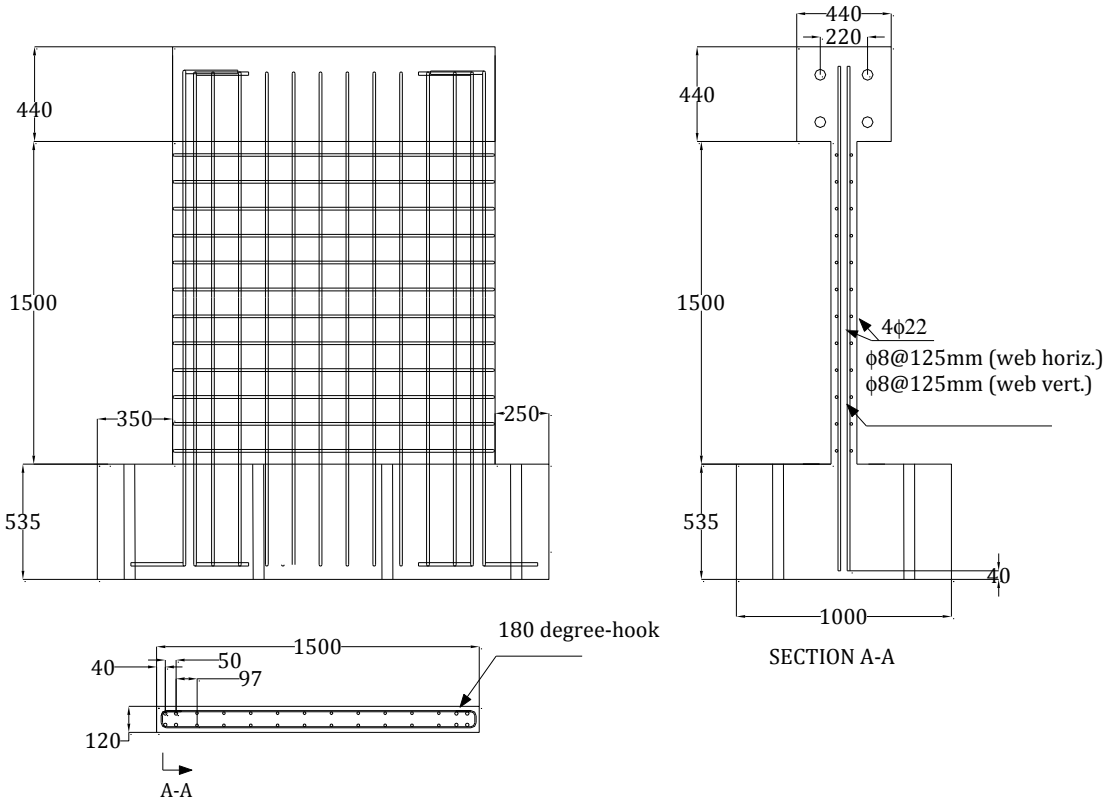

Figure 2.10. Geometry and wall reinforcement of specimen T6-S1.

2.1.4. General Description of Pedestals

The specimens were connected to the strong floor by means of bottom pedestal. The top pedestal (load transfer beam) was connected to the horizontal actuator. The two pedestals were designed such that they can withstand shear forces and bending moments generated by the applied lateral load. The bottom pedestal had dimensions of 1.0 m width and 2.1 m length. The dimensions of the bottom pedestal were also designed to create enough frictional area so that the specimen does not slide under high lateral loads. The bottom pedestal incorporates eight 50 mm diameter holes, four on both sides of the wall, for connecting the specimens to the strong floor.

The top beam had 400 x 400 mm cross sectional dimensions and 1500 mm length. There were four 50 mm plastic (PVC) tubes passing through the length of the beam. Those

pipes were placed for the connection of the beam to the actuator. Figure 2.11 shows the dimensions and reinforcement details of top beam and bottom pedestal. The third set of specimens constructed had 440 x 440 mm beam cross-section, for easier placement of the 50 mm diameter plastic (PVC) tubes inside the beam stirrups.

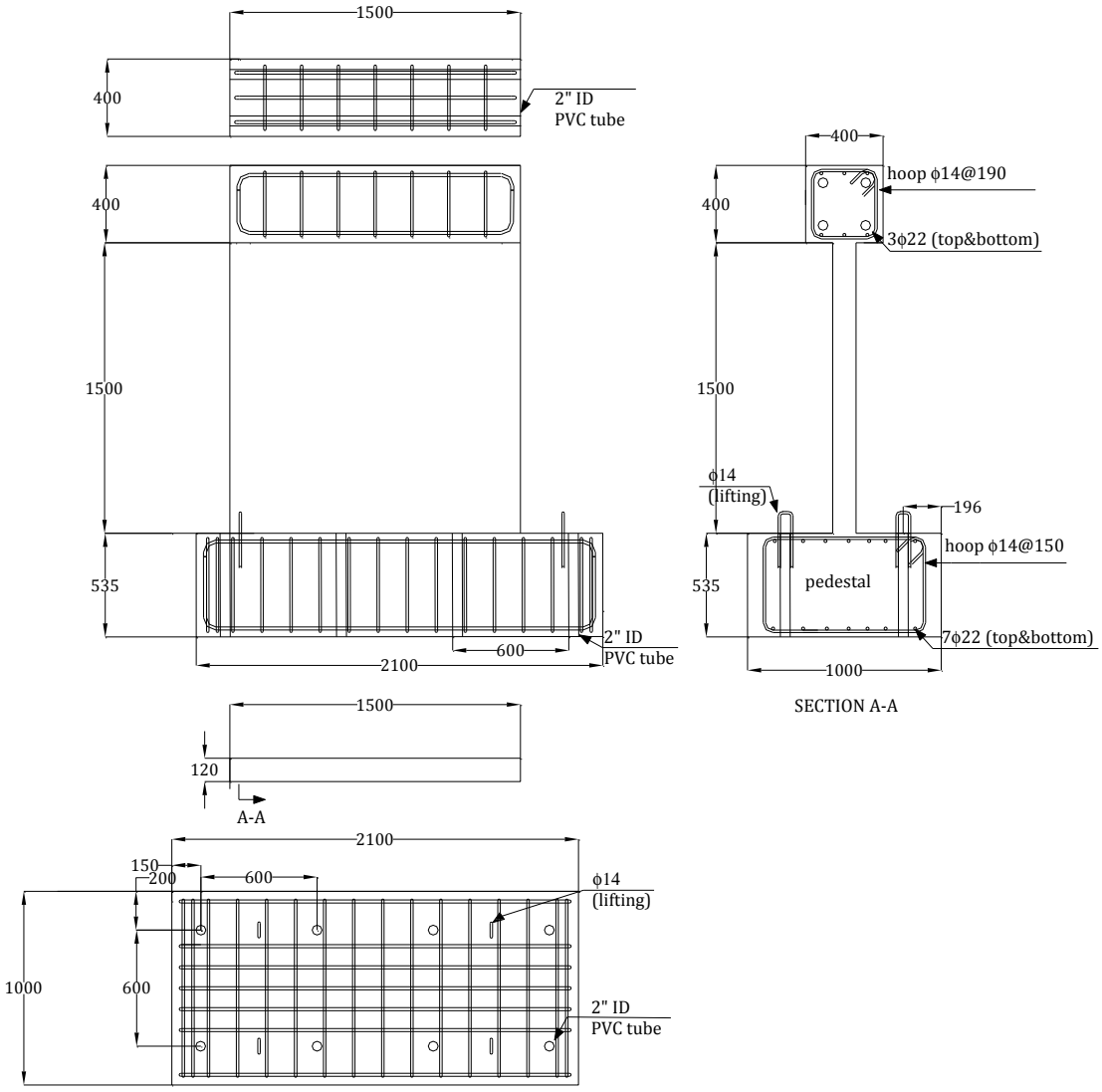

Figure 2.11. Beam and Pedestal Reinforcement.

2.2. Material Properties

The material properties were chosen to represent general construction conditions in Turkey. The concrete was chosen to have 25 MPa compressive strength and the reinforcing bars were chosen to have 420 MPa yield stress. The materials were ordered with such

grades, but they were tested in the laboratory to determine their actual mechanical properties. The measured mechanical properties of the materials used are described in this section.

2.2.1. Reinforcing Steel

Tensile coupon samples having 600 mm length were tested for each diameter reinforcing steel bar. Throughout the experiments, two different reinforcing steel suppliers provided the steel. For the first set of specimens, there were two different diameter types, ϕ8 and ϕ16. The tension test results for the first set of specimens are provided in Figure 2.14.

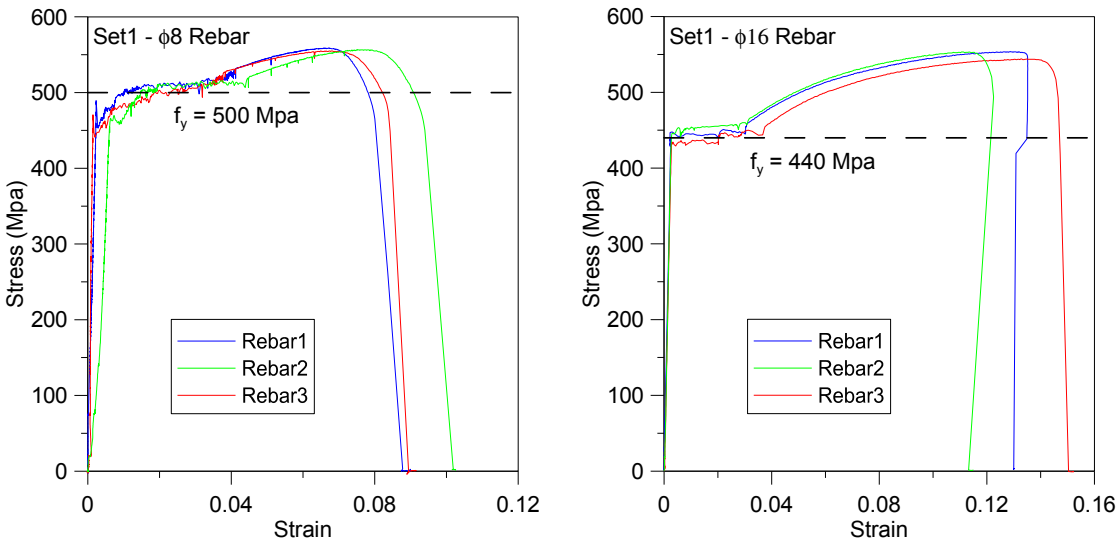

Figure 2.12. Steel Stress-Strain Curves, specimen set 1.

Reinforcing steel bars were provided by the same supplier for the second and third set of specimens. ϕ14 reinforcing bars were used only for the boundary elements of 0.33 aspect ratio specimen and ϕ22 reinforcing bars were used for the boundary bars of the 1.0 aspect ratio specimens. The tensile stress- strain properties of the bars used for the second and third sets are provided in Figure 2.13 and Figure 2.14.

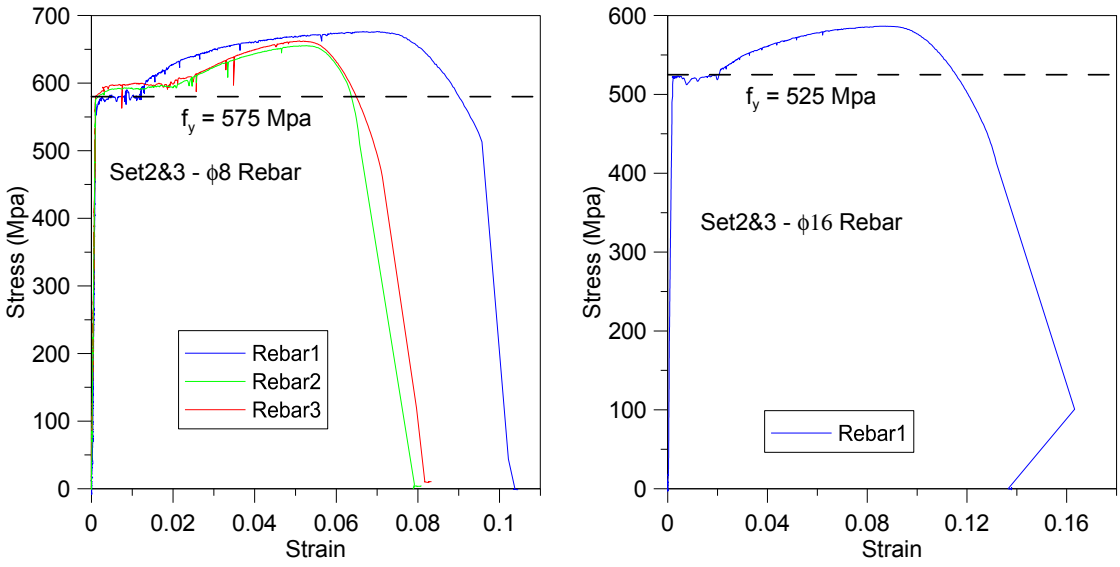

Figure 2.13. Steel Stress-Strain Curves, specimen sets 2 and 3.

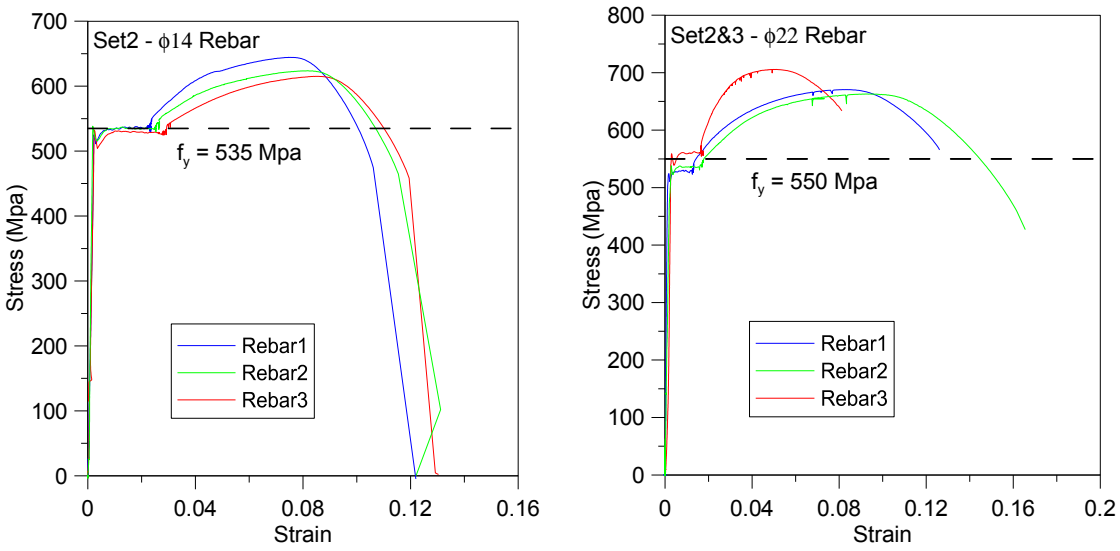

Figure 2.14. Steel Stress-Strain Curves, specimen sets 2 and 3.

2.2.2. Concrete

The target concrete compressive strength was 25 MPa for all specimens. The provided concrete had different test-date cylinder compressive strengths, ranging between 20 MPa – 35 MPa, also depending on the date of testing. The specimens were heavily reinforced; therefore, the concrete was ordered to have a maximum aggregate size 1 cm. For improved workability, plasticizers were added to the concrete mix. The slump for all three castings (for the three sets of specimens) ranged between 17 cm and 20 cm. For each

wall specimen, 3 standard (150 x 300 mm) cylinders were tested at the test date. Table 2.2 presents the average cylinder concrete compressive strength for all the tested specimens.

Table 2.2. Concrete Compressive Strengths.

Specimen	f_c' (MPa)
SW-T2-S1-1	19.3
SW-T2-S2-3	25.8
SW-T2-S3-4	29
SW-T3-S1-5	32.1
SW-T4-S1-6	34.8
SW-T5-S1-7	35
SW-T6-S1-8	22.6
SW-T1-S2-9	24
SW-T1-N5-S1-10	26.3
SW-T1-N10-S1-11	27
SW-T1-S1-2	23.7

2.3. Specimen Construction

Three sets of specimens were constructed for in this experimental program. The first set consists of three specimens having 0.5 aspect ratio, constructed in June 2009. The first sets of specimens are specimens T1-S1and T2-S1 and T2-S2. The second set contains four specimens constructed in June 2010. The second group consists of T2-S3, T3-S1, T4-S1, and T5-S1. One of the specimens, T2-S3, in the second set, was identical to one of the specimens in the first set. The third set was constructed in May 2011. Four specimens were constructed, three of which are identical to Type1 specimen and tested under axial load. One of the specimens in the third set had 1.0 aspect ratio and 0.68% vertical reinforcement ratio being different than Type5 specimen.

The first group of specimens were constructed in a construction site in the city of Gebze and shipped to the laboratory. Casting was conducted while the specimens standing up with their bottom pedestals being on the floor. During the construction of first two sets, concrete was casted at one stage, to avoid cold joints between the bottom pedestal and the wall. The casting of the concrete for the third set was performed in two stages. First the bottom pedestal concrete was casted followed by casting of the wall and the top pedestal. This was done due to the experienced construction and concrete placement difficulties experienced during first two sets.

The reinforceng bars were ordered as bent bars. As the first step of construction the bars of beam and pedestal were tied. At the same time construction of the formwork of the pedestals was started. For the holes on the pedestal, 50 mm diameter plywood pieces were nailed to the pedestal floor with 600 mm spacing. And 50 mm pipes were placed over these pieces. Figure 2.15 shows a representative photo of pedestal formwork and reinforcement.

Figure 2.15. Pedestal Formwork and Reinforcement.

The formwork of the wall section was prepared at the same time with the steel cage assembly of the pedestals. One face of the wall section plywood placed on top of the pedestal box in order to create a reference plane for the wall section reinforcement assembly. Beam steel cages were assembled after finishing the wall reinforcement. Four PVC pipes having 1500 mm length were placed inside the beam cage. These holes were required to connect the top pedestal to the actuator. Figure 2.16 and Figure 2.17 show representative photos of wall and beam reinforcement.

Figure 2.16. Wall and Beam Reinforcement.

Figure 2.17. Formwork and reinforcement of Beam.

Installation of strain gauges was performed at the same time with the construction of beam reinforcement. The selected bars were prepared for the strain gauge installation. First the surface of the bars were smoothened by grinding machine, then the surfaces were cleaned with alcohol and then the strain gauges were glued on the bars. 10 mm length uniaxial strain gauges were used for measuring steel strains. After finishing this operation the wiring of the strain gauges were done with 2 m cables. Following the wiring procedure, protective coating was applied to the strain gauges to prevent any kind of deformation

during the casting of concrete. Every cable named with the corresponding strain gauge. The strain gauge cables were guided out from the formwork through the drilled holes on the formwork. The cables of the strain gauges were put into plastic bag to protect them from rain and concrete pouring. In Figure 2.18, representative strain gauge application is shown. A detailed explanation about the placement of strain gauges will be provided in the instrumentation section.

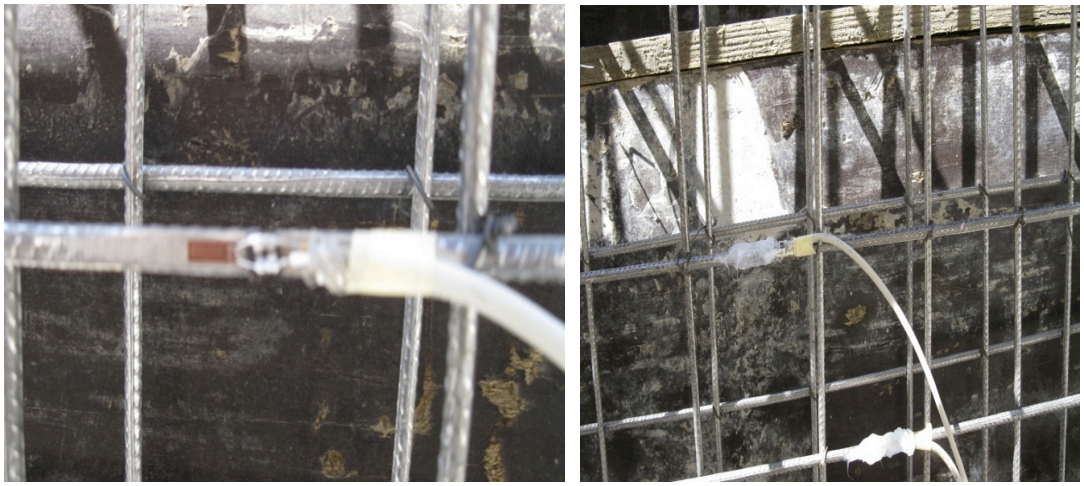

Figure 2.18. Strain Gauge Installation.

After finishing the strain gauge installation, the other face of the formwork was nailed and the formworks were finished. At the end top face of the beam, the formwork was left open. For the casting of pedestal concrete a small portion of the pedestal box was left open. For the installation of displacement sensors, 6 mm-threaded rods were placed on the specimens. In order to avoid any harm to the specimens and avoid extra workmanship, these rods were placed before the casting of the concrete. 6 mm holes were drilled through predefined locations and M6 threaded rods installed through these holes. These rods were tightened by nuts in order to provide some shoring. Shoring or supporting the long spans of the formwork was required to prevent opening or bulging of the formwork. Shoring was provided by means of 10 x 10 cm wood studs connected by steel threaded rods. Figure 2.19 shows the completed formwork and the shoring of the wall sections. The pedestal and beam were also provided some kind of reinforcement. 5 x 10 cm wood studs were nailed on top of the specimens connecting them together. Diagonal studs supported the pedestals.

The casting of the concrete took place in September 2009 for the first set specimens. Before starting the casting of the concrete, a slump test was conducted and plasticizer was added to the concrete mix for workability. The final slump of the concrete was 20 mm, before casting. During casting, concrete was placed using a pump and vibrators. Concrete was also cast into 150 x 300 mm cylinders to test the compressive strength of the concrete. Figure 2.20 shows the cylinders and freshly cast concrete in the wall formwork.

Figure 2.19. Shoring of the Formwork.

After the casting of the concrete, top faces of the pedestals and beams were left open. However, proper curing was applied during the first week. Those open surfaces were covered with wet clothing, at all times. After 10 days, the forms were removed, and the specimens were transported to the laboratory.

Figure 2.20. Freshly-cast concrete and cylinder specimens.

Second and third set of specimens was constructed just outside the laboratory. The same construction procedure was applied, as in the first set of specimens. In second set, four specimens were constructed. Figure 2.21 shows the construction of the second set of specimens.

Figure 2.21. Construction of the second set of specimens.

In May 2011, the third set of specimens were constructed. This time the casting of the concrete was achieved in two stages. First the bottom pedestal formwork was constructed and the concrete was cast in the bottom pedestals only, for better placement of concrete. Figure 2.22 shows the pedestal formwork and reinforcement of the wall section.

In this set, there were two specimens, which were tested under different level axial load levels. For applying axial load it was decided to use a set up that includes axial load cables connected to the bottom pedestal of the specimens. For this purpose, 16 mm threaded rods were placed inside the bottom pedestal formwork before the casting of the concrete. In order to connect a hinge to the bottom pedestal, four threaded rods provided at both sides. Figure 2.23 provides a representative picture showing the shape and placement of the threaded rods, which will be connected, with a hinge, to the axial load cables during testing.

Figure 2.22. Bottom Pedestal Formwork and Wall Reinforcement.

Figure 2.23. Pedestal Threaded Rods for the Axial Load Assembly.

2.4. Test Setup

Before placing the specimens in the testing area around 2-cm thick plaster was applied on the strong floor, and the specimens were placed on top of the plaster. This was done since the surface of the strong floor and the bottom of the pedestal was not perfectly smooth. By applying the plaster, possible cracking of the pedestal during attachment of the specimen to the strong floor was avoided and sliding of the pedestal during testing was prevented. The specimens were tested in the upright position. A representative sketch of the test setup is illustrated in Figure 2.24.

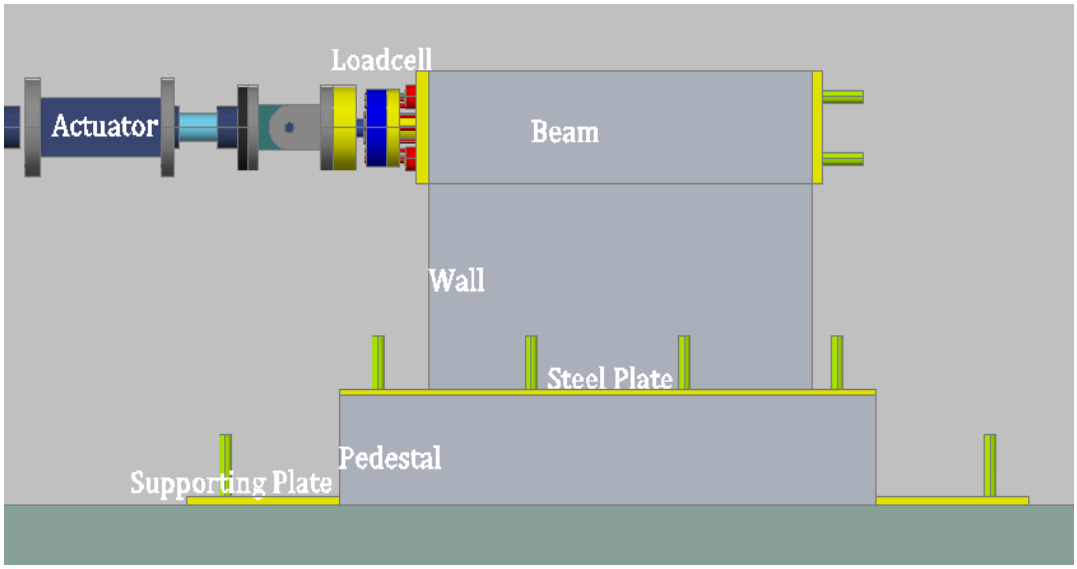

Figure 2.24. Test setup

Anchor bars (threaded rods) were passed through the holes on the pedestal. Prior to tightening of the anchor bars, steel plates were placed on top of the pedestal, in order to distribute the compressive load coming from the nuts used to tighten the anchor bars. Since the plaster was not hardened in the first day the anchors were tightened in the following day of the placement of the specimen on the strong floor. The anchor bars were 45 mm high strength threaded rods. The yield capacities of the threaded rods were chosen such that they would not yield under the tensile force that occurs due to the bending moment as a result of 1000 kN of lateral loading. A more detailed 3-dimensional scheme of the test setup is illustrated in Figure 2.25. Figure 2.26 presents a photo of test setup.

In order to apply enough torque to tighten the nuts on the anchor rods, a wrench was used, with a 3 m lever arm. In the first test, post-tensioning forces of 300kN were applied on the anchor rods, prior to tightening of the nuts. Afterwards, the nuts were tightened further with the wrench. In later tests, it was decided to use only the wrench for tightening, without applying post-tensioning on the rods.

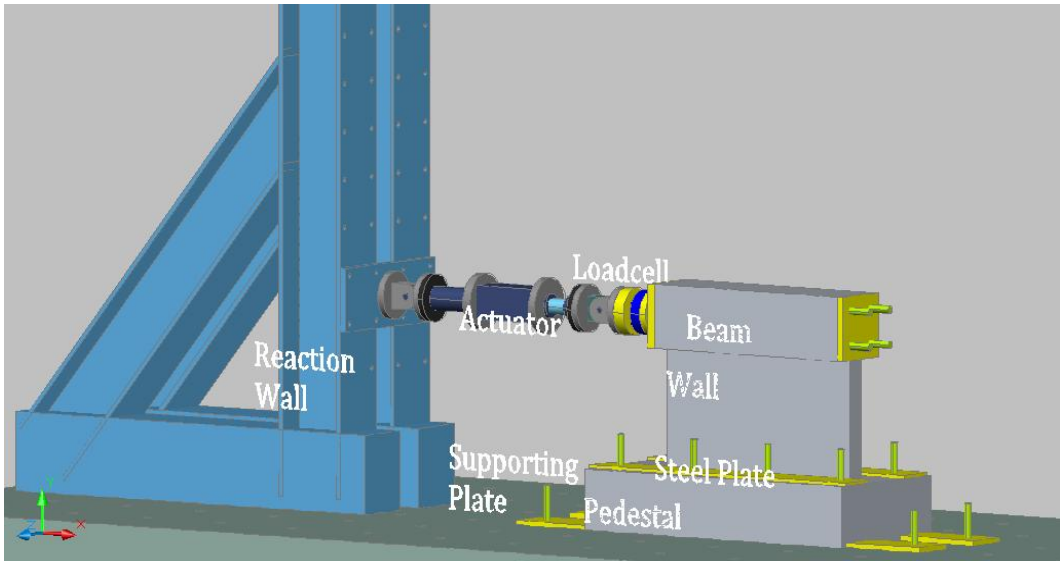

Figure 2.25. 3D Scheme of Test Setup.

As a precaution against pedestal sliding, four 30 mm thick supporting plates were placed at both ends of the pedestal (Figure 2.25). Noticeable pedestal sliding was not observed during any of the tests.

Lateral loading was applied with an actuator having a capacity of 1000 kN. One end of the actuator was fixed to a steel reaction wall. The reaction frame was connected to the strong floor by twelve 60 mm diameter high-strength threaded rods. Before placing the reaction frame in place, 2 cm thick grout was poured on the strong floor for leveling, as well as to avoid sliding. Each threaded rod of the reaction frame was post-tensioned with 300 kN of tensile force, and the bolts were tightened before the post-tensioning loads were removed. During the first test, the displacement of the reaction frame relative to the ground was monitored. Although 900 tons of lateral load was applied, no sliding of reaction wall was measured.

Figure 2.26. Test Setup Photo.

There were two specimens tested under at 5%$A_g f_c$` and 10%$A_g f_c$` axial load levels. The axial load was applied using four pre-stressed steel cables each having 250 kN axial tension capacities. The cables were connected to the bottom pedestals of the specimens with special steel hinges, and to transverse steel beams at the other ends. The axial load was applied through a hydraulic cylinder placed between the steel beams and the top pedestal (load transfer beam) of each specimen. Figure 2.27 shows a photo of the axial load setup.

Figure 2.27. Axial Load Test Setup

During the tests, a high level of lateral load was expected. At such levels of lateral load, it is likely to have out of plane movements of the specimen due to asymmetry in specimen geometry or accidental eccentricity effects. To prevent such out-of-plane movement, or possible lateral-torsional buckling, four triangular-shaped steel out-of plane frames (two at each side of the specimen) were used to support the specimens in the transverse direction. These frames supported the top pedestals (load transfer beams) in the out-of-plane direction, but did not restrain in-plane motion. In order to minimize their resistance to applied lateral loads; greased steel plates were placed on the surface of the top beam, and the out-of-plane frames were in contact with these plates through roller (socket and ball) supports. Figure 2.28 presents details of the out-of-plane support frames.

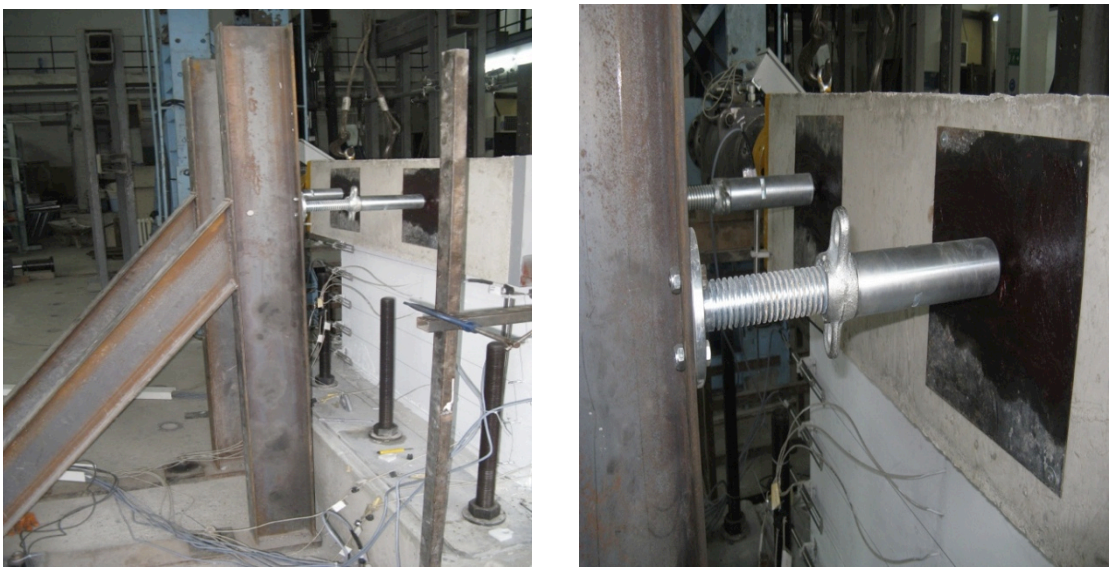

Figure 2.28. Out of Plane Frames.

2.5. Test Equipment

The testing equipment included hydraulic control units, control software, data acquisition system, LVDT's (Linear Variable Differential Transducers) and strain gauges. In this section, a property of the testing equipment is briefly described.

2.5.1. Hydraulic Control System and Actuator

The lateral load was applied with an actuator having a capacity of 1000 kN. The hydraulic oil needed to create the required pressure is stored in two oil tanks. A hydraulic circuit controls the pressure and drainage oil. The hydraulic oil is pumped to the actuator by means of two electric motors, and two dynamic (differential-displacement) pumps. An electronic panel controls the hydraulic system. Figure 2.29 shows the components of the hydraulic system.

A CAS 100-TF tension-compression load cell measured the applied lateral load. Before the tests, the actuator did not incorporate a servo-control valve and a load cell. The load cell was calibrated externally and mounted to the actuator using of steel connection plates.

Figure 2.29. Hydraulic System.

In order to be able to control the actuator accurately, a servo-valve was installed on the actuator. The servo-valve was connected to a control box, which was controlled by TESTLAB software. The actuator had an externally mounted displacement transducer. This transducer enabled controlling the actuator under displacement control. However, during the tests, two externally connected LVDT's, measuring the top displacement of the specimens, for displacement controlled loading. The actuator had 300 mm stroke capacity, 150 mm in tension and 150 mm in compression. Figure 2.30 shows the components of the actuator.

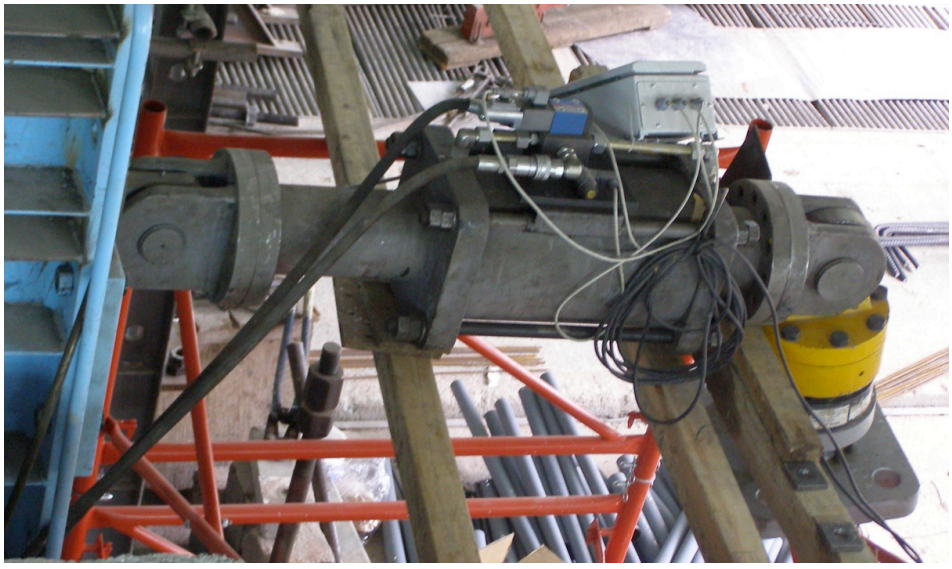

Figure 2.30. Horizontal Actuator.

2.5.2. Instrumentation

For measuring average concrete strains and steel strains on the specimens, strain gauges and DC-LVDTs (DC excited Linear Variable Differential Transducers), also known as DCDTs were used. The applied lateral load was measured from the load cell mounted on the actuator.

Strain gauges were installed on the reinforcing bars of the wall section at different locations. The strain gauge data was collected for general comparisons and to monitor if there is yielding in a specific reinforcing bar. Thirteen strain gauges were installed on each specimen. Three strain gauges were placed on the exterior boundary-reinforcing bar on both sides, and four strain gauges were distributed along the wall-pedestal interface. Three other strain gauges were attached to the horizontal (transverse) reinforcing bars, distributed along the wall height.

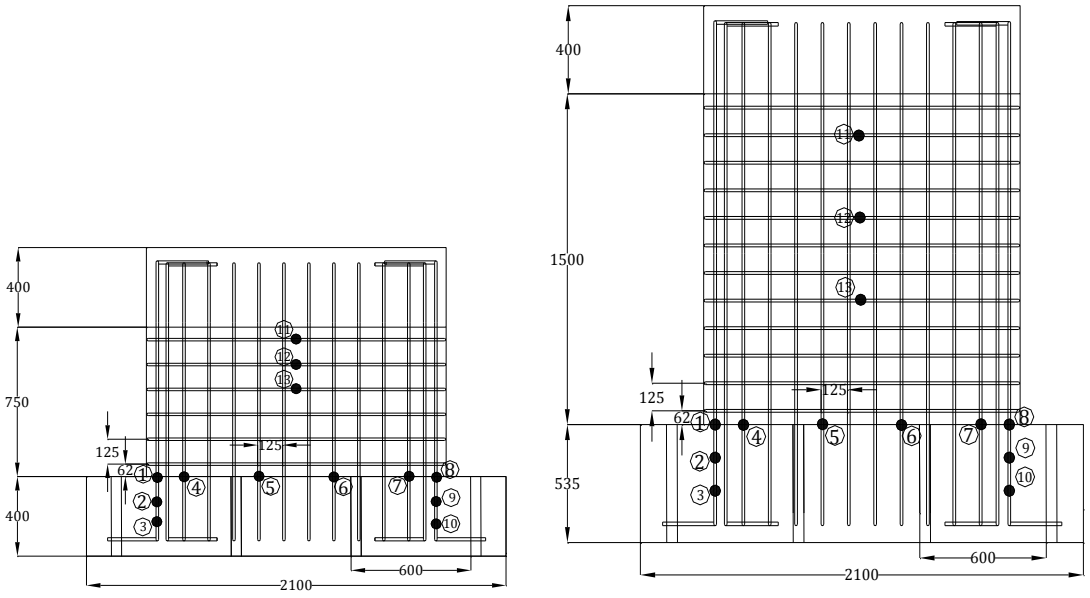

Figure 2.31. Strain Gauge Positions.

The three strain gauges on the horizontal web bars allowed monitoring of horizontal steel strain distributions. The other six placed along the bottom wall-pedestal interface on the vertical reinforcing bars, where the maximum moment occurs, allowed observing whether the vertical reinforcement (both boundary and web) yields under flexural deformation. Additional strain gauges were installed on the boundary reinforcement,

within the pedestal, to observe strain distributions along the pedestal height, in order to observe strain penetration effects on the boundary reinforcement.

External instrumentation of the specimens was performed using LVDTs. There were three main configurations that were used for all of the specimens. Different configurations other than these three were also used during the tests. The first configuration is for measuring the shear deformation of the specimens. Two spring-mounted and wire-mounted LVDTs are placed diagonally on the wall. And another two LVDTs are placed diagonally from bottom pedestal to top pedestal (beam). These are placed in order to be able to monitor the shear deformation until the end of the experiment, because the shear LVDTs on the wall were removed after crushing of the concrete, typically at the base and corners of the wall specimen. The second group of LVDTs is used for measuring flexural deformations of the specimens. Again, two spring-loaded and wire-mounted LVDTs were mounted on the wall sections, and another two were placed from pedestal to pedestal. The third group is for measuring the horizontal strain distributions along the wall height. 5 LVDTs were placed horizontally along the wall height for walls having 0.5 and 0.33 aspect ratios, and 9 LVDTs were placed along the wall height for structural walls having 1.0 aspect ratio. Figures 2.32 and 2.33 represent the LVDT locations on the specimens. The LVDTs had stroke capacities of +/-25 mm, +/-50 mm, and +/-75 mm, and were placed at different locations depending on the expected level of deformations.

The top displacement of the specimens was measured relative to the bottom pedestal. Two +/-75 mm LVDTs were used, and the average of the two measurements was recorded. These displacement sensors were mounted on a steel reference frame, which was connected to the bottom pedestal of the specimens. Therefore, in case of an accidental sliding of the pedestal, the sensors would still measure the correct relative displacement of the wall, with respect to the bottom pedestal. Figure 2.34 shows the reference frame used to support the top displacement sensors.

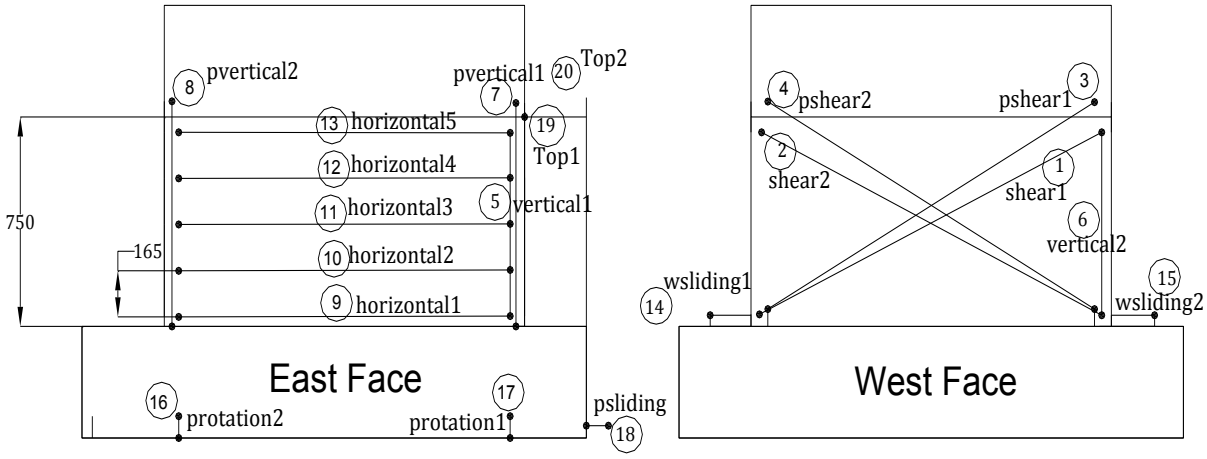

Figure 2.32. LVDT locations – 0.5 aspect ratio Walls.

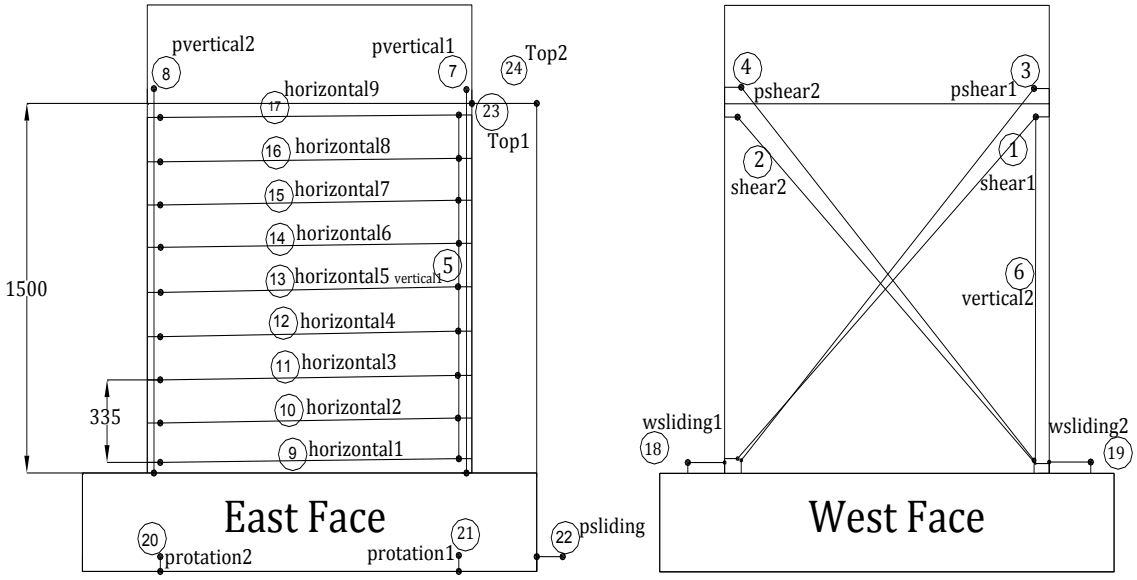

Figure 2.33. LVDT Locations – 1.0 Aspect ratio Walls.

The sensor configurations used are adequate to collect data representing shear, flexural and base sliding deformation contributions to the top displacement. The vertical sensors at the wall sides (e.g. sensors 7 and 8, and 5 and 6 in Figure 2.32) were used to determine average curvature values.

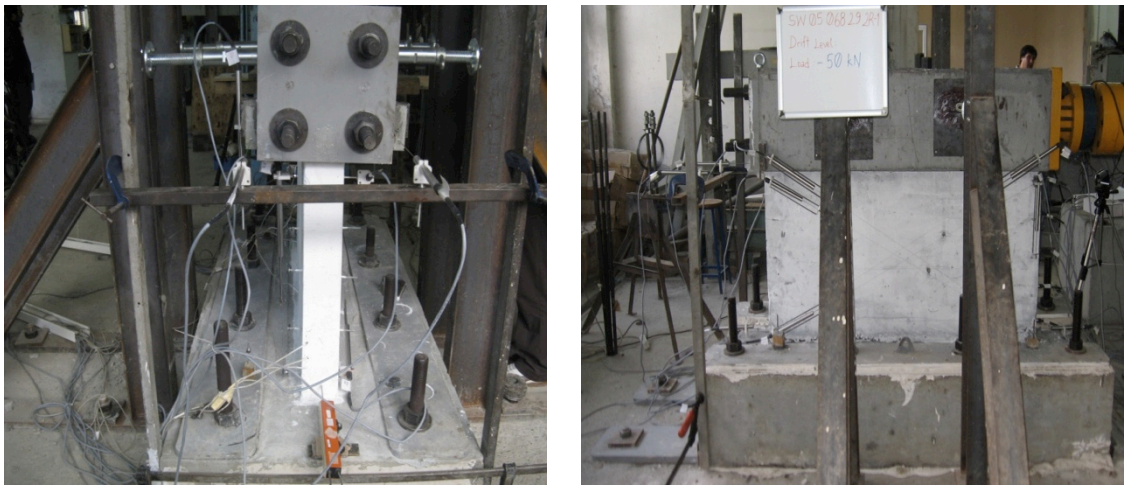

Figure 2.34. Top Displacement Sensors and Reference Frame.

These values were used to estimate flexural component of the top deformation. Figure 2.35 shows the vertical sensor configurations both on the wall and from top beam to bottom pedestal. The horizontal sensors at the wall base (e.g. sensors 14 and 15 in Figure 2.32) were used to determine average sliding deformation at the wall-pedestal interface. Shear deformations were determined from the data collected with pairs of diagonal sensors in 'X' configuration (e.g. sensors 1 and 2, and 3 and 4 in Figure 2.32).

Figure 2.35. Vertical and Horizontal LVDTs.

2.5.3. LVDT Details and Installation

The displacement sensors used for external instrumentation were DC-excited Linear Variable Differential Transducers. These transducers simply convert the linear movement of an object (transducer core) into an electrical signal. They incorporate the sensitivity to measure movements as small as millionths of a millimeter and to collect data up to 300 Hz.

Figure 2.36 shows the components of a typical LVDT used in the tests. The transformer's internal structure consists of a primary winding centered between a pair of identically wound secondary windings, symmetrically spaced about the primary. The coils are wound on a one-piece hollow form of thermally stable glass reinforced polymer, encapsulated against moisture, wrapped in a high permeability magnetic shield, and then secured in cylindrical stainless steel housing. This coil assembly is usually the stationary element of the position sensor.

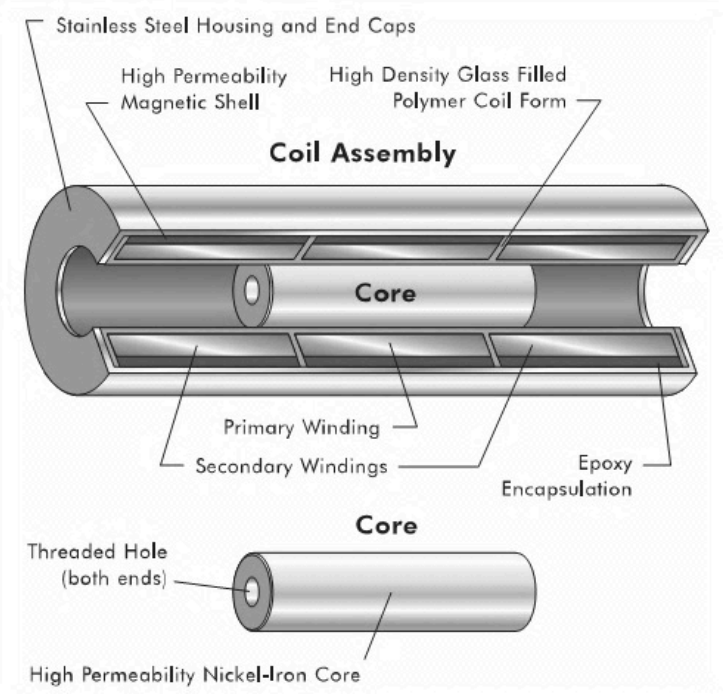

Figure 2.36. Components of an LVDT.

The moving element of an LVDT is a separate tubular armature of magnetically permeable material called the core, which is free to move axially within the coil's hollow bore, and mechanically coupled to the object whose position is being measured. This bore

is typically large enough to provide substantial radial clearance between the core and bore, with no physical contact between it and the coil. In operation, the LVDT's primary winding is energized by alternating current of appropriate amplitude and frequency, known as the primary excitation. The LVDT's electrical output signal is the differential AC voltage between the two secondary windings, which varies with the axial position of the core within the LVDT coil. Usually this AC output voltage is converted by suitable electronic circuitry to high level DC voltage or current that is more convenient to use.

Since the cores are short they need to be extended. 2 mm diameter extension rods were prepared using 304-stainless steel. One end of the extension rods threaded using 1-72 NF thread size in order to fit the inner rods of the core. After assembling of the extension rods, all the sensors were calibrated.

Since the sensors are simply composed of hollow cylinder and a core they need mounting devices for specific applications. For the tests, two different mounting configurations were used. And all the sensors were attached by the mounting devices and connected to 6 mm diameter threaded bars embedded in the specimens. The main component of the mounting device is a hard plastic clips made of kestamid. It has 6 mm inner threads at the bottom and two 5 mm holes at the corners for the spring connection. Figure 2.37 shows a detailed picture of this mounting assembly.

The white clips hold the LVDT securely and are connected to the 6 mm diameter threaded rods embedded in the wall specimens before casting of concrete. The tension springs on the sides of the LVDT, are connected to the clips, creating a spring-loaded assembly. The other ends of the springs were attached to a thin steel plate, which is connected to the end of the extension rod. This mounting assembly used for long distance deformation measurements. A 0.5 mm diameter steel wire is tied to the end of the extension rod and the other end of the wire is tied to another threaded rod embedded in the wall, resulting in a wire-connected spring-loaded assembly.

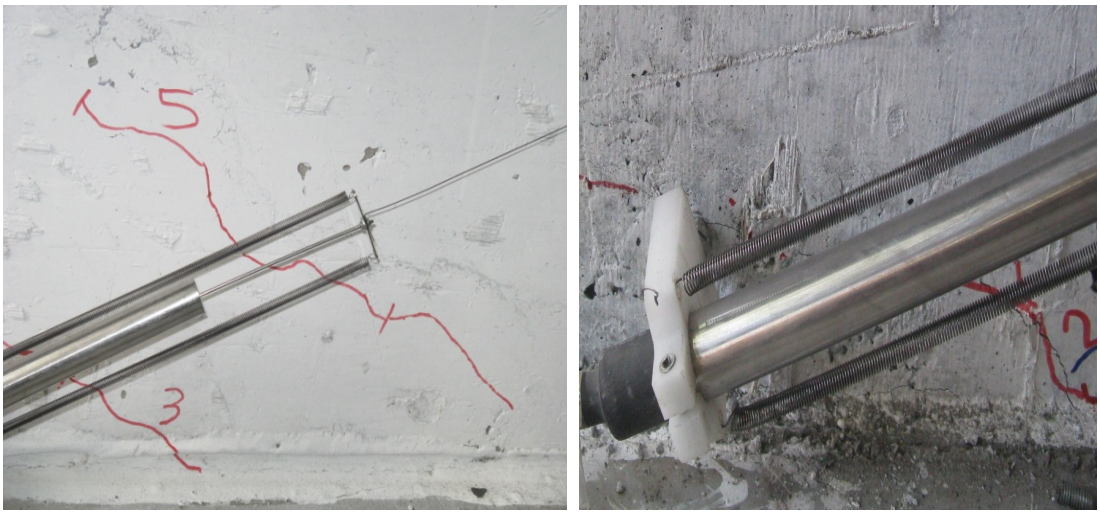

Figure 2.37. LVDT Spring-Loading and Mounting Assembly.

3. EXPERIMENTAL OBSERVATIONS AND BEHAVIOR

In this chapter, experimental observations on the wall specimens are evaluated and characterized. All of the specimens tested are investigated in terms of experimentally observed damage and behavior. Experimental observations are discussed for each specimen type.

The experimental procedure was discussed in the previous chapter. Reversed cyclic lateral loading is applied at the height of each specimen, resulting in single curvature loading condition. Three full cycles were applied at each drift level. First two or three drift (or lateral load) levels might differ from specimen to specimen. After these initial small displacement drift levels, all of the specimens were subjected to drift levels of 0.05%, 0.1%, 0.15%, 0.2%, 0.3%, 0.4%, 0.6%, 0.8%, 1.0%, 1.2%, 1.4%, 1.6%, 1.8%, 2.0%, 2.4%, 3.2%. Depending on the residual lateral load capacity, one or two more drift levels were imposed on some of the specimens.

All of the wall specimens were heavily instrumented in order to be able to collect as much data as possible, to characterize the behavior and the deformation components. LVDTs were used in specific configurations, which allow decomposing of the shear and flexural components of wall lateral displacement at the top. In order to determine the shear component of the top lateral displacement, two diagonal displacement sensors were placed in the X configuration described previously. For the first two tests, the diagonal sensors were placed on the wall sections only. For other specimens additional diagonal sensors were used connected at the top pedestal (beam) at one end, and the bottom pedestal at the other. This configuration allowed measurement of shears deformations at larger drift levels (even when the wall section is significantly damaged), and also accounting for sliding shear deformation at the wall-pedestal interface, in the shear deformation measurement.

3.1. Behavior of Type1 – Specimen1 (SW-T1-S1-2)

Type-1 specimens had 0.34% vertical and horizontal web reinforcement ratios. Specimen-1 is subjected to zero axial load. It had 4-ϕ16 boundary bars at each boundaries.

This specimen was the second specimen tested in the experimental program. The specimen was tested under reversed cyclic loading at increasing drift levels. Initial (small displacement) drift levels were applied as load-controlled cycles, due to the high lateral stiffness of the specimen. Two load-controlled drifts were applied at 50 kN and 100 kN load levels, each with three loading cycles. No visible damage occurred during the load controlled cycles. After the initial load controlled cycles, displacement controlled loading was applied at eighteen different drift levels. These drift levels are: 0.05%, 0.1%, 0.15%, 0.2%, 0.3%, 0.4%, 0.6%, 0.8%, 1.0%, 1.2%, 1.4%, 1.6%, 1.8%, 2.0%, 2.4%, 3.2%, 4.8%, 7.2%.

The first visible diagonal crack formed during the first cycle to 0.05% drift level in the positive direction. Cracking produced an instantaneous degradation in the lateral load. However, the degradation was not permanent, and the lateral load increased in the following drift levels. The load level was around 35% of the lateral load capacity, when the first diagonal tension crack formed.

After the formation of the first major diagonal crack, smaller diagonal cracks formed at the bottom corner in the negative loading direction. The first major diagonal tension crack from corner to corner in the negative direction, formed during the first cycle of the 0.1% drift level. Figure 3.1 shows the orientation of first diagonal tension cracks in positive and negative directions.

The major diagonal cracks could be easily heard, as they formed. The diagonal cracks in push and pull directions were almost perpendicular to each other. After the formation of the first diagonal cracks, the stiffness of the wall degraded.

Figure 3.1. Initial Diagonal Cracks (T1-S1).

At 0.2% drift level, the second major diagonal tension crack formed during loading in the positive direction, with sudden load degradation and jump in the lateral displacement. This time, stiffness degradation was more pronounced than the first crack. The load level was around 56% of the lateral load capacity. In the negative direction, a new major diagonal crack did not form; instead, the first crack extended and widened. After the formation of the second major crack, the stiffness degradation was gradual up to the maximum lateral load level. There was no sudden occurrence of any load degradation, up to the lateral load capacity.

For the successive drift levels, new diagonal cracks were observed, the previous cracks extended (elongated), and crack widths increased. New cracks generally formed in zones with no cracks. At 0.8% drift level, crushing of the concrete started at the bottom corners. The largest crack width went up to 1.5 mm. At 1% drift level, the maximum lateral load capacity of 635 kN was reached. When the lateral load capacity was reached, none of the transverse (horizontal) reinforcing bars had yielded. On the other hand, longitudinal boundary reinforcement had yielded at the 1.0% drift level, when the capacity was reached. Figure 3.2 shows the cracking pattern of the specimen at the lateral load capacity.

Figure 3.2. Cracking Pattern at Ultimate Load (T1-S1).

At the 1.2% drift level, strength degradation started and concrete started to crush at the center section of the wall. After the ultimate load level, crushing and spalling of the concrete concentrated at the center. This specimen had 0.34% vertical and horizontal reinforcement ratio, which is greater than the minimum reinforcement ratio (0.25%) in most design codes. This specimen failed under diagonal tension. The main cracks followed the direction of the principle compressive stresses. Figure 3.3 shows photos for medium and high damage levels of this specimen. The main diagonal cracks opened and closed at every cycle, and eventually the crushing of concrete propagated along the diagonal tension and compression struts, indicating a general diagonal tension type of squat wall failure, as described by Paulay and Priestley (1992).

Figure 3.3. Medium and High Damage Levels (T1-S1).

3.2. Behavior of Type2 – Specimen1 (SW-T2-S1-1)

Type2 specimens had 0.68% vertical and horizontal web reinforcement ratios. Type2 specimens had 4-ϕ16 longitudinal reinforcement at each boundary, which was the same as Type1 specimens. Three specimens were tested as Type2 specimens. During the first set of tests, two Type2 specimens were tested. Specimen1 had U-caps at the end of straight horizontal reinforcing bars, to provide anchorage. On the other hand, Specimen2 had 180-degree hooks at the ends of the horizontal reinforcing bars. This anchorage difference did not significantly influence the observed behavior. Both anchorage conditions performed adequately in preventing slipping of the horizontal web bars.

Specimen1 was tested under reversed cyclic loading at different drift levels. The first three drift levels were applied as load-controlled drifts at 50 kN, 100 kN and 150 kN lateral load levels. After these three load-controlled drift levels, displacement-controlled loading at eleven drift levels were applied. The applied drift levels were 0.1%, 0.15%, 0.2%, 0.3%, 0.4%, 0.6%, 0.8%, 1.2%, 1.6%, 2.0%, and 2.4%. It was realized that 0.4% increase after 0.8% drift level may be excessive, since the ultimate lateral load capacity was reached at approximately 1% drift level. Also, during the strength degradation drifts, 0.4% increase was found to be excessive. For the other specimens, the drift level was increased by 0.2% increments, after the 0.4% drift level.

First small cracks formed at the first positive and negative cycles of 150 kN load level at the bottom corners. These were not major diagonal cracks; they resembled small hairline cracks. The first main diagonal cracks formed at the 0.1% drift level at both positive and negative loading directions. Sudden strength degradation and a sudden jump in the lateral displacement were observed together with the formation of the main diagonal cracks.. The strength degradation was not permanent; in the following cycles the lateral load level continued to increase. Figure 3.4 the diagonal tension cracks, which have occurred due to loading in positive and negative directions.

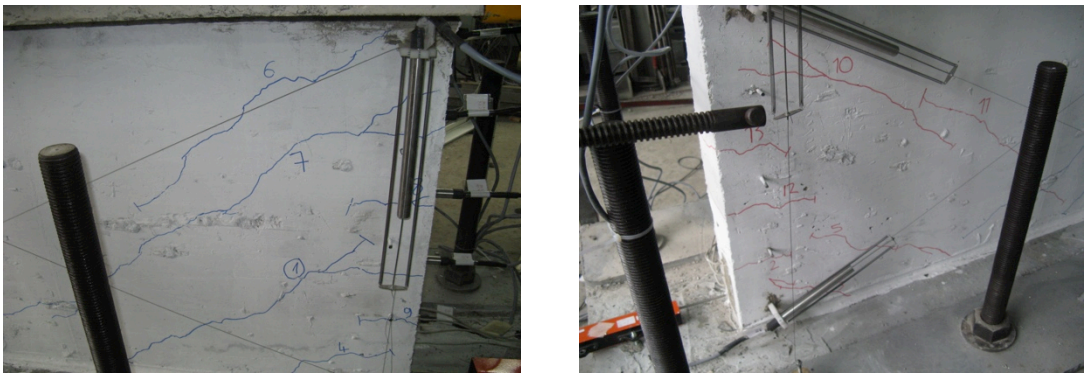

Figure 3.4. Initial Diagonal Cracks (T2-S2).

These cracks occurred at around 32% of lateral load capacity. After the formation of these cracks, the stiffness of the wall degraded.

At 0.15% drift level, the cracks that formed during the previous cycles extended (elongated) and widened. Also a new main diagonal crack formed, causing a sudden strength degradation and displacement jump. At 0.2% drift level, at around 52% of the lateral load capacity, one more diagonal tension crack formed, making a loud noise. After the formation of the diagonal tension cracks at 0.2% drift level under loading in both positive and negative directions, the lateral stiffness remained almost constant up to lateral load capacity of the specimen.

At the higher drift levels the crack formation concentrated on the previously uncracked regions. As well, the existing cracks continued to open and close at each cycle, and the main cracks extended from bottom pedestal to top pedestal. Some of the cracks initiated formation of small hairline cracks within the top pedestal. The lateral load capacity was reached at the 1.2% drift level, at around 800 kN load level. At this drift level, concrete started to crush at the bottom corners of the specimen. Figure 3.5 shows the diagonal tension cracks at the ultimate lateral load level. It was seen that at the ultimate load level, the main diagonal tension cracks close to the center of the specimen did not crush. On the other hand the small diagonal tension cracks at the corners started to widen and crushing of the concrete was observed first at these cracks.

Figure 3.5. Cracking Pattern at Ultimate Load (T2-S1).

As Park and Paulay (1975) first discussed it, it is almost impossible to have diagonal tension failure mode, when the wall has a high ratio of transverse (horizontal) reinforcement. In this case, Type2 specimens have 0.68% transverse reinforcement ratio, which is twice that of Type1 specimens. For Type2 specimens, although the diagonal tension cracks formed, they did not substantially widen, and the failure mode resembled a diagonal compression failure, under combined shear and flexure effects, since the large amount of transverse reinforcement prevented the widening of the main diagonal cracks and crushing along diagonal compression struts between the cracks..

Crushing was first observed at the bottom corners of the wall, where the first inclined cracks were formed. After the crushing of the corner regions, the effective shear area that resists shear sliding was reduced. The crushing of the concrete then propagated inwards, along the wall-pedestal interface. Eventually, the entire base of the wall crushed, and the crushing extended upwards towards the center of the wall. Figure 3.6 shows the medium and high damage levels observed on the wall specimen.

3.3. Behavior of Type2 – Specimen2 (SW-T2-S2-3)

Type2 – Specimen2 has same reinforcement characteristics with Type2 – Specimen1. The only difference is the anchorage conditions of transverse reinforcement.

Figure 3.6. Medium and High Damage Levels (T2-S1).

Type2 - Specimen2 was tested as the third specimen after the testing of Type1 – Specimen1. Based on the results of the first test, it was expected that the first diagonal cracks may form at the 150 kN load level. When the main diagonal tension crack forms, the lateral load level can decrease suddenly, which may cause stabilization problems in the hydraulic loading system. Therefore, the 3rd drift level was changed to a displacement controlled drift level, similarly to the second test (Type1 – Specimen1). The first two drift levels were applied at 50 kN and 100 kN load levels. In following, 0.05%, 0.1%, 0.15%, 0.2%, 0.3%, 0.4%, 0.6%, 0.8%, 1.0%, 1.2%, 1.4%, 1.6%, 1.8%, 2.0%, 2.4%, 4.8%, 7.2% drift levels were applied under displacement control. Three cycles were applied at each drift level. The 3.2% drift level was not applied for this specimen, since the lateral load capacity had already dropped to a residual strength level at 2.4% drift.

The first diagonal tension cracks, due to loading in both positive and negative directions, formed close to the bottom corners at 0.05% drift level, at a load level of 20% of the lateral load capacity. Although they have caused instantaneous strength degradation, it was not significant. Figure 3.7 shows the diagonal cracks formed during the initial drift levels. At 0.05% drift, cracks 1 and 2 formed during loading in the positive (push) direction and crack 3 formed during loading in the negative (pull) direction.

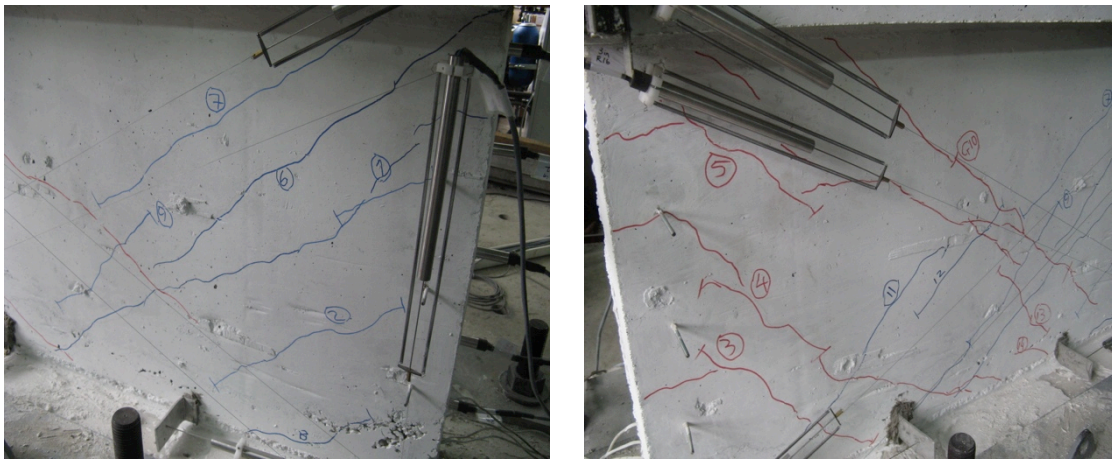

Figure 3.7. Initial Diagonal Cracks (T2-S2).

At each drift level up to 0.2%, new diagonal cracks formed, each getting closer to the center (mid-length) of the wall. At the first cycle of each drift, newly formed cracks caused instantaneous strength degradation and a sudden lateral displacement increase. At 0.1% drift, the main diagonal cracks, cracks 5 and 7 formed in due to loading in the negative and positive directions, successively. These crack caused degradation of lateral stiffness. At 0.15% drift, new cracks developed at the center of the wall, and the existing cracks extended and widened. At 0.2% drift level, cracks 5 and 7 extended to the bottom corners, almost perpendicular to each other. These cracks progressed as the main diagonal cracks, from corner to corner of the wall. At the first cycle of the 0.2% drift level, the main diagonal cracks joined to the other cracks extending to the bottom corners.

The stiffness degradation started with formation of the first diagonal crack at the 0.05% drift level, and gradually continued up to 0.2% drift. After 0.2% drift, until the lateral load capacity was reached, the stiffness almost remained constant. At the 0.2% drift level, at the instant the diagonal tension crack formed, the lateral load level was around 50% of the lateral load capacity.

During following drift levels, new cracks formed close to the bottom of the wall, and the existing cracks extended. The diagonal tension cracks formed a rectangular mesh pattern. Figure 3.8 shows the crack pattern at the ultimate load level. Concrete started to crush at 1% drift level at the bottom of the wall. The overall behavior and diagonal-compression failure mode was the same as that of Specimen T2-S1.

After the ultimate load capacity, the strength of the specimen degraded gradually. At 1.8% drift level, a residual strength of around 12% of ultimate lateral load capacity remained. The lateral load did not degrade beyond this point. At higher drift levels, the crushing of the concrete propagated through the center, but remained in the lower half of the wall height. This type of behavior proved that when the transverse reinforcement ratio is high, it is unlikely to have crushing along diagonal struts. The failure mode of this specimen was also diagonal compression failure, under combined shear and flexure effects. After the crushing of the corners, crushing propagated towards the wall center at the base, and the wall underwent sliding along the crushed base. Figure 3.9 shows observed medium and high damage levels for Type2 – Specimen2.

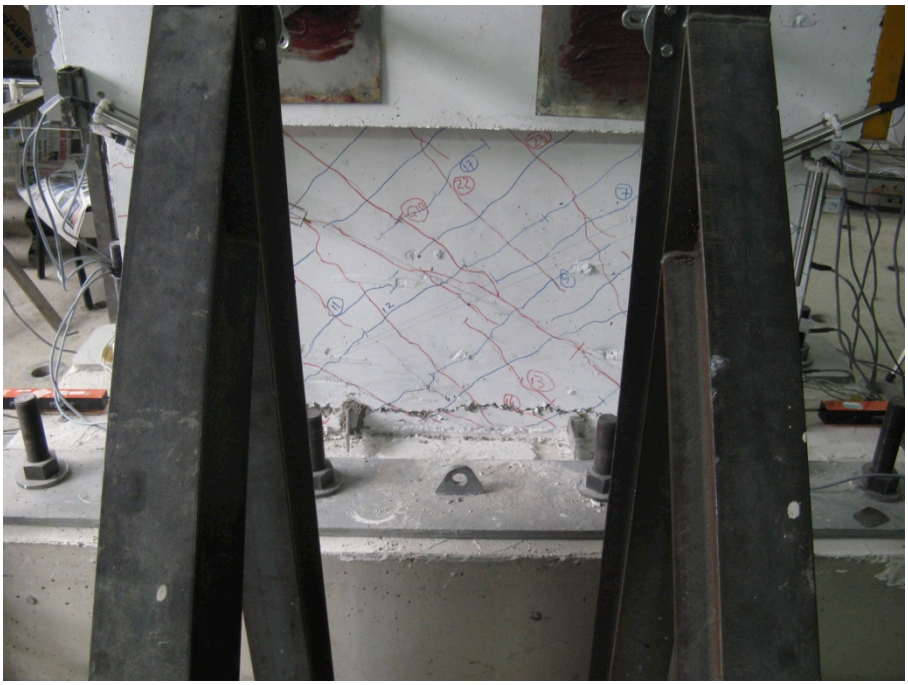

Figure 3.8. Cracking Pattern at Ultimate Load (T2-S2).

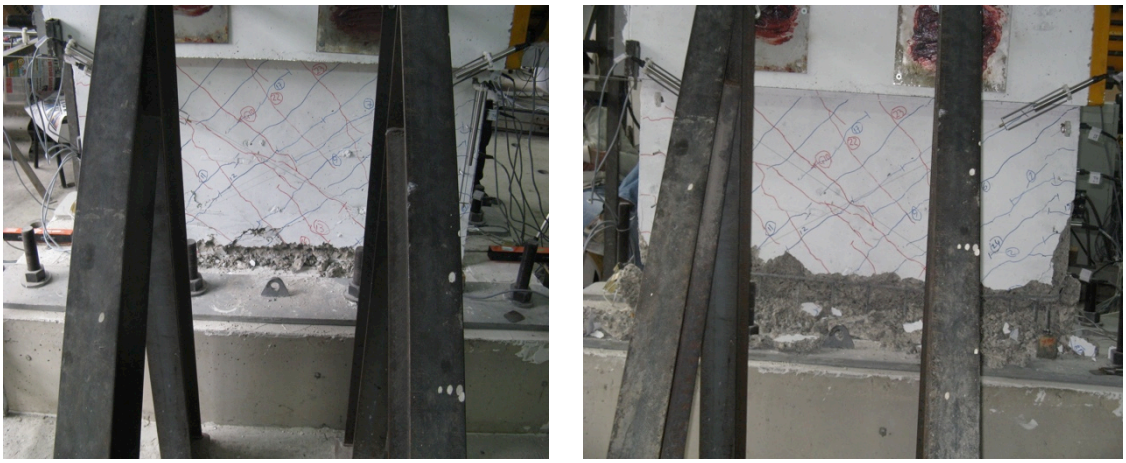

Figure 3.9. Medium and High Damage Levels (T2-S2).

3.4. Behavior of Type2 – Specimen3 (SW-T2-S3-4)

During the first set of tests, Type2 specimens showed different load – displacement response characteristics. Therefore, one more specimen with the same configuration was constructed together with the second set specimens. The second set specimens composed of one of Type2, Type3, Type4, and Type5 specimens. Type2-Specimen3 was tested under seventeen drift levels. This time, only the first drift level was load-controlled at 50 kN load level. In following, 0.025%, 0.05%, 0.1%, 0.15%, 0.2%, 0.3%, 0.4%, 0.6%, 0.8%, 1.0%, 1.2%, 1.4%, 1.6%, 1.8%, 2.0%, 2.4% displacement-controlled drift levels were applied.

The cracking pattern and the drift levels when the diagonal cracks formed was the same as other Type2 specimens. Initial diagonal tension cracks formed during 0.05% drift level. These cracks were close to the bottom corners. At the following drift levels up to 0.3% drift, two main diagonal cracks formed under positive and negative loading directions at each drift level. Figure 3.10 shows the first diagonal tension cracks formed under positive and negative loading directions. Cracks 5 and 7 formed during loading to 0.1% drift level. Then at 0.15% drift, two major cracks developed from pedestal to pedestal in each direction. These cracks formed at a lateral load level of 57% of the capacity. As it can be seen from the crack propagation, the first cracks formed at the corners and at each drift level after the first crack, a new and longer diagonal crack formed closer to the wall center.

For this specimen, other major diagonal tension cracks formed at 0.2% and 0.3 % drift levels, both causing instantaneous strength degradation. Figure 3.11 shows the crack pattern at 0.3% drift. Cracks 9 and 10 formed during the 0.2% drift level and cracks 11 and 12 formed during 0.3% drift. The diagonal tension cracks occurred at 0.15%, 0.2%, and 0.3% drift levels caused stiffness degradation of the specimen. Beyond that point, the stiffness almost remained linear, until reaching the lateral load capacity.

Figure 3.10. Initial Diagonal Cracks (T2-S3).

Figure 3.11. Cracking Pattern at Ultimate Load Level (T2-S3).

Strain gauge data shows that transverse reinforcement at the center of the wall yielded at 0.4% drift level. Boundary reinforcement also yielded at the same drift level.

The specimen has reached its lateral load capacity at 0.6% drift, at a load level of around 810 kN. When the lateral load capacity was reached, the vertical web reinforcement close to the wall ends also yielded. At 0.8% drift level, the lateral load level remained almost same as the capacity. Strength degradation started at 1% drift level. Crushing of the concrete started at the bottom corner at the negative loading cycle to 1% drift, and crushing propagated along the width of the wall at the bottom during larger drift levels. Also at 1% drift, relatively minor concrete crushing was observed along one of the diagonal cracks. However, crushing at the bottom was much more pronounced and progressive.

Figure 3.12. Medium and High Damage Levels (T2-S3).

The failure mode of this specimen was also diagonal compression failure, under combined shear and flexure effects, as in the previous Type2 specimens. However, higher lateral load capacity was observed for this specimen, due to higher material strengths. The materials used for construction of the second set of specimens, was different. The concrete compressive strength was around 30 MPa for this set of specimens, whereas it was around 25 MPa for the first set. The yield strength of web reinforcement was around 575 MPa for this set, whereas it was around 480 MPa for the first set.

3.5. Behavior of Type3 – Specimen1 (SW-T3-S1-5)

This specimen was designed such that it has same web reinforcement amount with Type2 specimens, but it has only two – ϕ8 boundary reinforcement at each boundary, which was intentionally kept low in order to observe either flexural yielding or a sliding

shear failure mode at the base of the wall. After a 50 kN load-controlled initial drift level, 0.0125%, 0.025%, 0.05%, 0.1%, 0.15%, 0.2%, 0.3%, 0.4%, 0.6%, 0.8%, 1.0%, 1.2%, 1.4%, 1.6%, 1.8%, 2.0%, 2.4%, 3.2% drift levels were applied under displacement control. At the 0.0125%, 0.025%, and 0.05% drift levels, there was no visible damage on the specimen. At 0.1% drift a few initial inclined cracks formed, as shown in Figure 3.13.

Figure 3.13. Initial Diagonal Cracks (T3-S1).

As seen from Figure 3.13, the first crack is parallel to the bottom wall-pedestal interface and the other cracks make small angles with the horizontal. The stiffness of the wall decreased after the formation of these initial cracks. At the following drift levels the stiffness remained almost constant up to lateral load capacity. The lateral load capacity was reached at the 0.6% drift level, at around 380 kN lateral load. Figure 3.14 shows the cracking pattern at the ultimate lateral load capacity. At this point, the horizontal crack at the wall pedestal interface had extended along the entire width of the wall, the crack had widened, and the wall started experiencing sliding shear failure along the interface crack. The concrete along the interface crack started to crush at this drift level.

The strain gauge data showed that none of the horizontal web reinforcement bars yielded during the test, whereas all boundary reinforcement yielded at 0.4% drift level, and all vertical reinforcement bars yielded at 0.6% drift level. This data also shows that the sliding shear failure mode was triggered by flexural cracking and initiation of flexural yielding at the wall-pedestal interface.

Figure 3.14. Cracking Pattern at Ultimate Load Level (T3-S1).

At 1% drift the interface crushed along the entire wall width, and the interface crack widened significantly at each loading cycle. After 1.2% drift, the vertical reinforcing bars fractured one by one, at each successive drift level. At the end of the test, all of the vertical reinforcing bars were fractured at the interface. Figure 3.15 shows the medium and high damage levels for the specimen. Interestingly, after the ultimate lateral load level capacity was reached, strength degradation was gradual, possibly due to kinking of the vertical bars during sliding of the specimen.

Figure 3.15. Medium and High Damage Level (T3-S1).

3.6. Behavior of Type4 – Specimen1 (SW-T4-S1-6)

The only Type4 specimen had four – ϕ14 boundary reinforcement at each boundary, and 0.68% horizontal and vertical reinforcement ratios. This specimen had 1/3 aspect ratio, which differentiated it from the Type2 specimens. Again the transverse reinforcement ratio was relatively large compared with the Type1 specimens. The specimen was tested under reversed cyclic loading at 0.00625%, 0.0125%, 0.025%, 0.05%, 0.1%, 0.15%, 0.2%, 0.3%, 0.4%, 0.6%, 0.8%, 1.0%, 1.2%, 1.4%, 1.6%, 1.8%, 2.0%, 2.4%, 3.2%, 4.0% displacement controlled drift levels.

At the initial three drift levels, no damage was observed. First diagonal tension cracks formed at 0.05% drift level at the bottom corners. Figure 3.16 shows the positions of initial diagonal cracks. Under larger drifts, new diagonal cracks formed closer to the wall center at each successive drift level. The crack formation and alignment were similar to Type1 and Type2 specimens. Diagonal cracks formed at 0.1% and 0.2% drift levels caused instantaneous strength and stiffness degradation. Up to 0.6% drift, new cracks formed, while existing cracks extended and widened.

Figure 3.16. Initial Diagonal Cracks (T4-S1).

At 0.6% drift, the wall reached its lateral load capacity of 875 kN Maximum crack width measured was around 1.5 mm. At 0.8% drift, concrete started to crush over the lower

half of the wall height, close to the center. Figure 3.17 shows the diagonal cracking pattern at the ultimate load capacity.

Figure 3.17. Diagonal Cracking Pattern at Ultimate Load Level (T4-S1).

Strain gauge data showed that the horizontal reinforcement yielded at 0.6% drift level. At the 0.8% drift level, boundary reinforcement also yielded. Starting from 1% drift, concrete crushed at the bottom portion of the wall, at the corners and at the center. The crushing propagated along the wall width, again indicating a diagonal compression failure similar to the Type2 specimens. Figure 3.18 shows the crushing of the concrete for medium and high damage levels.

Figure 3.18. Medium and High Damage Levels (T4-S1).

3.7. Behavior of Type5 – Specimen1 (SW-T5-S1-7)

The first Type5 specimen had four ϕ22 reinforcing bars at each boundary, 0.34% vertical and 0.68% horizontal web reinforcement ratios, and an aspect ratio of 1.0. This specimen was one of the two most slender specimens tested in scope of the experimental program. The specimen was tested under reversed cyclic loading at 0.00625%, 0.0125%, 0.025%, 0.05%, 0.1%, 0.15%, 0.2%, 0.3%, 0.4%, 0.6%, 0.8%, 1.0%, 1.2%, 1.4%, 1.6%, 1.8%, 2.0%, 2.4%, 3.2% and 3.6% displacement controlled drift levels.

No damage was observed on the specimen during the first three drift levels. At 0.05% drift, the first diagonal tension cracks were formed at the bottom corners. Figure 3.19 shows the location and orientation of these cracks. The cracks were oriented at about 45 degrees with the horizontal. The stiffness of the wall decreased by the formation of initial diagonal cracks. At the instant these cracks occurred, the lateral load level was about 28% of the lateral load capacity.

At 0.1% and 0.15% drift levels, larger diagonal cracks formed. The cracks also caused stiffness degradation. At the instant the diagonal crack formed at 0.15% drift level, instantaneous strength degradation observed and the lateral load level was around 45% of the lateral load capacity. After that drift level the stiffness remained almost constant up to the lateral load capacity.

Figure 3.19. Initial Diagonal Cracks (T5-S1).

At each successive drift level, new cracks formed progressively closer to the wall center, and the existing cracks were extended. At 0.4% drift, diagonal cracks at the corners extended towards the center and became horizontal, such that they continued as flexural joint cracks at the wall-pedestal interface. During the following drift levels, these cracks opened and closed at each cycle.

At 0.6% drift, the lateral load capacity was reached at a load level of around 710 kN. Concrete crushing started at the corners. Figure 3.20 shows the cracking pattern at the ultimate load level. The strain gauge data showed that the transverse reinforcement yielded at the ultimate load level. As well, the boundary reinforcement yielded at 0.8% drift.

The horizontal web reinforcement ratio of the specimen was 0.68%. The diagonal tension cracks were prevented from widening, by the significant amount of horizontal web reinforcement. Although at the ultimate load level, crushing of concrete had initiated at the wall center due to diagonal compression, the bottom corners of the specimen also crushed under flexural compressive stresses. The specimen is believed to fail under a combined shear and flexure failure mode.

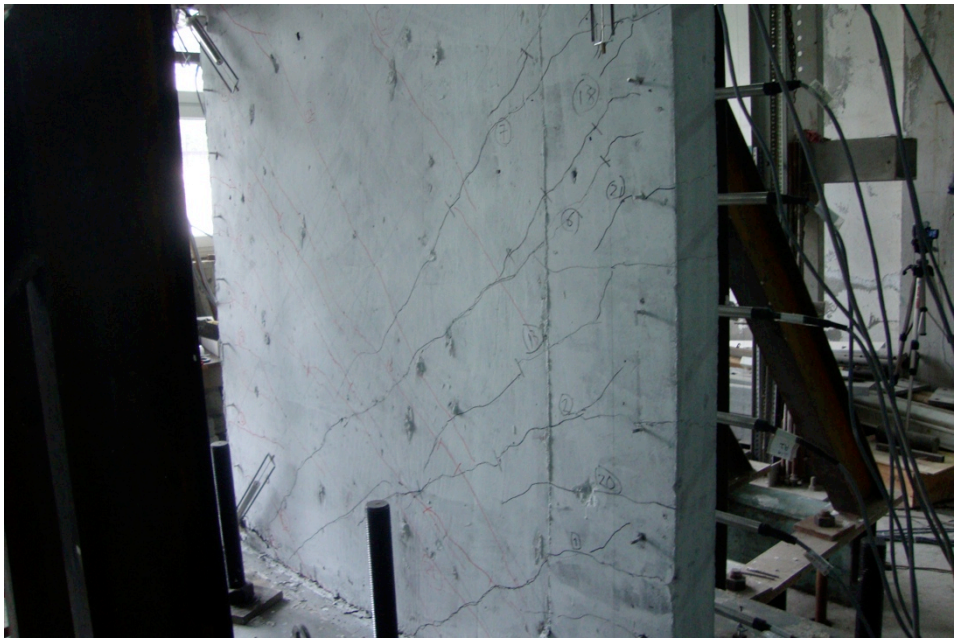

Figure 3.20. Diagonal Cracking Pattern at Ultimate Load Level (T5-S1).

At 1% drift, the bottom corners of the wall started crushing. At 1.2% drift, crushing was also observed along the main diagonal crack, and the largest crack width became 1.2 mm. At 1.4% drift, both corners of the wall crushed completely and the crushing along the diagonal strut became severe, especially close to the bottom. Figure 3.21 shows the crushing of concrete at two different damage levels.

Figure 3.21. Medium and High Damage Levels (T5-S1).

3.8. Behavior of Type6 Specimen1 (SW-T6-S1-8)

This specimen had 0.68% vertical reinforcement ratio, which differentiated it from the Type5 specimen. All other geometric properties and the reinforcement characteristics were the same as the Type5 specimen. In terms of material strength; both specimens incorporated close steel yield strength and concrete compressive strength values. However, since the Type6 specimen had been cast as part of the third set, of specimens, the concrete compressive strength was 23 MPa. On the other hand, the Type5 specimen had a concrete compressive strength of 35 MPa. The specimen was tested under reversed cyclic loading at 0.00625%, 0.0125%, 0.04%, 0.05%, 0.1%, 0.15%, 0.2%, 0.3%, 0.4%, 0.6%, 0.8%, 1.0%, 1.2%, 1.4%, 1.6%, 1.8%, 2.0%, 2.4%, 3.2% and 3.6% displacement controlled drift levels. No axial load was applied during testing of the specimen.

No damage was observed on the specimen during the first three drift levels. The first diagonal tension crack formed at 0.04% drift. At this drift level, the load was around 20% of the lateral load capacity.

Figure 3.22 shows the initial diagonal tension cracks formed on the specimen. After the formation of these cracks, the stiffness of the wall degraded. During the following three drift levels (0.05%, 0.1%, and 0.15%) new diagonal cracks formed, and caused relatively small stiffness degradation compared to the initial crack. It can be said that after the initial crack formed, the stiffness of the wall remained almost unchanged up to the lateral load capacity.

Figure 3.22. Initial Diagonal Cracks (T6-S1).

During successive drift levels, new diagonal cracks formed and the existing cracks widened. The largest crack width reached 1.6 mm, and the specimen reached is lateral load capacity at 1.0% drift level, at a load level of 735 kN. Figure 3.23 shows the distribution of the diagonal cracks at the capacity. It can be seen that the diagonal cracks were uniformly distributed all around the specimen. Compared to the Type5 specimen, the cracking pattern is better distributed, which may be attributed to the larger vertical web reinforcement ratio used in this specimen. It can be deduced that the additional vertical reinforcement improved the distribution of the cracks.

Although the concrete compressive strength of the Type6 specimen is lower, the lateral load capacity of this specimen was marginally higher than the Type5 specimen. This

suggests that the larger vertical reinforcement ratio has increased the shear strength of the wall, which is consistent with the work by Barda et al. (1976), which suggests that the vertical web reinforcement ratio significantly improve the lateral load capacity of squat walls.

Figure 3.23. Diagonal Cracking Pattern at Ultimate Load (T6-S1).

The strain gauge data showed that the horizontal web reinforcement did not yield during the test. On the other hand, the boundary reinforcement and the vertical web reinforcement yielded, only after the specimen reaches its lateral load capacity. This supports that the specimen has experienced shear failure. If the specimen is classified according to its failure type, it can be said that it failed under diagonal compression. The horizontal web reinforcement ratio was high, and the specimen also had high flexural capacity. After the formation of diagonal cracks, the cracks did not significantly widen, and the concrete first crushed at the bottom corners of the specimen, and the crushing propagated along the base of the wall, towards the center. The crushing initiated at 1.2% drift level, when the strength degradation had started. During successive drift levels, no additional cracks formed. However, crushing was also observed along the diagonal cracks close to the bottom. Nevertheless, first crushing was due to diagonal compression effects and initiated at the bottom corners. Figure 3.24 shows the medium and high damage levels for this specimen.

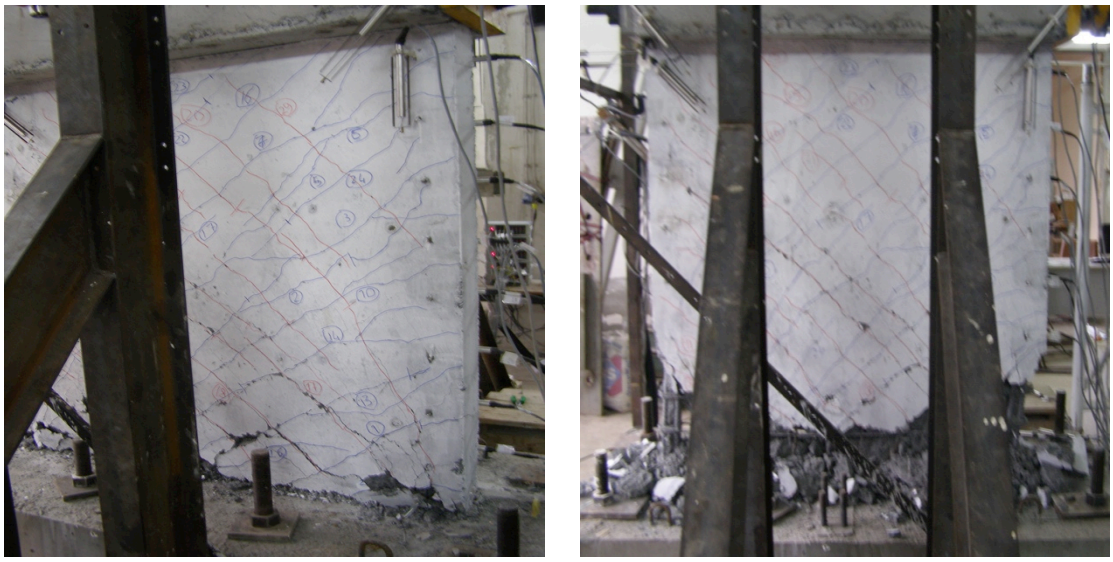

Figure 3.24. Medium and High Damage Levels (T6-S1).

3.9. Behavior of Type1 Specimen2 (SW-T1-S2-9)

This specimen had 0.34% horizontal and vertical web reinforcement ratios and 0.5 aspect ratio, similarly to Specimen T1-S1. However confinement was provided in the boundary regions, with ties at 75 mm spacing along the height of the wall. The type naming remained unchanged since the naming of the specimen is defined according to the web reinforcement ratios and aspect ratio of each specimen. The specimen was tested under reversed cyclic loading at 0.00625%, 0.0125%, 0.04%, 0.05%, 0.1%, 0.15%, 0.2%, 0.3%, 0.4%, 0.6%, 0.8%, 1.0%, 1.2%, 1.4%, 1.6%, 1.8%, 2.0%, 2.4%, 3.2% and 3.6% displacement controlled drift levels. No axial load was applied. The compressive strength of concrete was 24 MPa, similarly to Type1 – Specimen1.

The first diagonal cracks on the specimen formed during the first cycle to 0.05% drift level, in both loading directions. These cracks were located close to the bottom corners. By the formation of the initial crack the stiffness of the wall degraded. During the following three drift levels, new diagonal cracks formed, one of which was from corner to corner of the wall. The main diagonal crack angle orientation was around 45 degrees, and the cracks were approximately perpendicular to each other.

During following drift levels, new cracks formed and the main diagonal cracks crossing each other at the center, widened. Maximum crack width became 1.6 mm at the end of the 0.6% drift level, and the specimen reached its lateral load capacity at 0.8% drift. Figure 3.25 shows the orientation of the main diagonal crack formed due to loading in the positive direction.

Figure 3.25. Main Diagonal Crack at Ultimate Load (T1-S2).

The crushing of the concrete initiated at 0.8% drift, at the center of the specimen along the diagonal strut. It was expected that the orthogonal diagonal crack (strut) would also experience crushing. However, during following cycles, the bottom part of the specimen crushed under diagonal compression, and this prevented crushing along the negative diagonal strut.

Strain gauge data showed that the horizontal web reinforcement did not yield. On the other hand, the boundary and vertical reinforcement yielded before the ultimate load capacity. The specimen reached capacity and failed under diagonal tension, but at larger drifts, crushing occurred at the bottom corner and the crushing propagated along the wall base, as is the case for diagonal compression failure.

Figure 3.26. High Damage Level (T1-S2).

3.10. Behavior of Type1-N5-Specimen1 (SW-T1-N5-S1-10)

This specimen had the same geometric and reinforcement properties as the other Type1 specimens. The only difference was the axial load applied on the specimen, corresponding to a level of 5% of its axial load capacity. The concrete compressive strength was also similar to other Type1 specimens. Therefore, it allowed characterizing the axial load effect on the lateral load capacity. The specimen was tested under reversed cyclic loading at 0.025%, 0.05%, 0.14%, 0.16%, 0.2%, 0.3%, 0.4%, 0.6%, 0.8%, 1.0%, 1.2%, 1.4%, 1.6%, 1.8%, 2.0%, 2.4% and 3.2% displacement controlled drift levels. At the test day the concrete compressive strength was 26 MPa; therefore, an axial load of 240kN was applied on the specimen, and held constant during testing, using a hydraulic hand-pump.

Formation of diagonal cracks and the failure mode of this specimen was very similar to Type1 – Specimen1 (with zero axial load). The main diagonal cracks were formed in both positive and negative directions at 0.3% drift levels. These cracks were extended from bottom corner to top corner crossing at around 90 degrees to each other. At 0.6% drift,

maximum crack width became 1.4 mm, and at 0.8% drift level, the specimen reached its lateral load capacity at a load level of 780 kN. This load level is about 23% higher than the one that was tested under zero axial load. Figure 3.27 shows the medium and high damage levels for this specimen. It can be seen that crushing of the concrete has initiated at the center of the specimen, indicating that the mode of failure was diagonal tension. At later drift levels, the bottom corners of the specimen crushed due to the compressive stresses on the diagonal struts.

Figure 3.27. Medium and High Damage Levels (T1-N5-S1).

3.11. Behavior of Type1-N10-Specimen1 (SW-T1-N10-S1-11)

This specimen was the last specimen tested within the scope of this experimental program. It had identical geometry and reinforcement details as the previous Type-1 specimen tested under 5% axial load level. The axial load level applied to this specimen was increased to 10% of its axial load capacity, which corresponds to an axial load of 480 kN. Drift levels of 0.0125%, 0.025%, 0.05%, 0.1%, 0.15%, 0.2%, 0.3%, 0.4%, 0.6%, 0.8%, 1.0%, 1.2%, and 1.4% were applied under displacement control. For this specimen, higher drift levels could not be applied, due to sudden degradation of the lateral load, just after the ultimate lateral load capacity was reached.

The initial diagonal cracks were formed at 0.05% drift, similarly to other specimens of same type. At following drift levels, the propagation and distribution of the cracks were similar to other Type1 specimens, excluding the one that formed at 0.8% drift level. At that drift level, a horizontal crack formed along at the center of the wall. This crack connected

two diagonal cracks; one coming from the bottom corner and the other from the opposite top corner. The diagonal cracks were formed previously under loading in the positive direction. Figure 3.28 shows the orientation and alignment of the two main diagonal cracks, connected by the horizontal crack segment in between. Then crushing of concrete developed around these diagonal and horizontal cracks. Apparently, the large level of axial load changed the orientation of the main diagonal crack, making it horizontal close to the wall center. The reason for the horizontal crack to develop may be that the axial load forces the specimen to slide along the main diagonal tension cracks.

Figure 3.28. Main Crack (T1-N10-S1).

The specim-en reached its lateral load capacity at 0.8% drift level. At the first cycle of the following (1%) drift level, the specimen experienced very sudden degradation in lateral load capacity, together with crushing along then main tri-linear crack. The lateral load dropped drastically to 40% of the lateral load capacity. Strain gauge data showed that the horizontal web reinforcement did yield during the test.

After the sudden strength degradation, crushing and sliding continued along the tri-linear crack, with no crushing occurring elsewhere. Figure 3.29 shows the high damage level for this specimen, illustrating that the damage on the specimen is concentrated along

the tri-linear diagonal crack. The lateral load reached to a value close to the specimen that was tested under 5% axial load level; therefore, the increase in the axial load level did not result in any serious increase in lateral load capacity of the specimen, compared with the specimen subjected to 5% axial load level.

Figure 3.29. High Damage Level (T1-N10-S1).

4. EXPERIMENTAL RESULTS

4.1. Shear and Flexural Deformation Components

Recent research has shown that lateral load versus displacement response of slender walls can be captured reasonably by simple analytical models (e.g., Thomsen and Wallace, 2004). Such models usually consider uncoupled shear and flexural responses. These models give inconsistent results for relatively short and squat walls. In order to capture the behavior of squat walls and walls with shear mode of failure, shear flexure interaction should be modeled. For all these modeling purposes the shear and flexural components of top lateral displacement is needed. Therefore a widely used method, for measuring shear and flexural components, was used during the experiments.

4.1.1. Shear and flexural deformation components (on wall)

Based on a common approach, for measuring the shear and flexural components of top lateral displacement, two sensors were placed vertically at the wall boundaries and two sensors were placed diagonally from corner to corner. These sensors were attached at 50 mm inside the wall ends and pedestal interfaces. Figure 4.1 presents the positions and configurations of diagonal X configuration sensors and the vertical sensors used. Axial displacements were measured using the two vertically placed displacement sensors at the boundaries. These measurements were used to calculate wall rotations by dividing the relative axial displacements by the distance between two vertically placed sensors.

To determine the flexural contribution to the top lateral displacement, the location of the centroid of the curvature distribution (center of rotation) must be defined. The flexural displacement at the top of the wall, for a given curvature distribution can be calculated as:

$$U_f = \alpha . \theta . h \qquad (4.1)$$

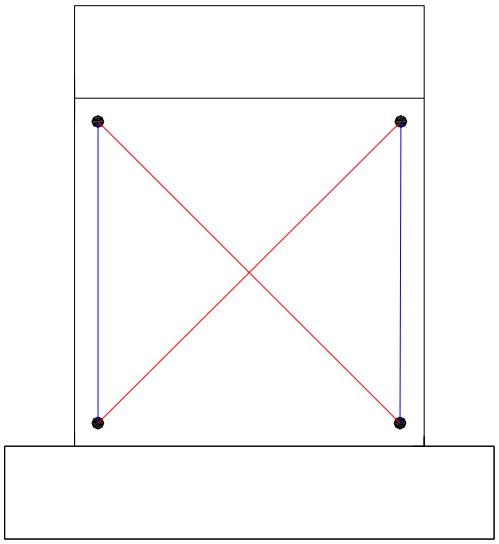

Figure 4.1. Vertical and Diagonal Displacement Sensors on Wall.

Where α is the distance of the center of rotation from the top of the wall, θ is rotation over story level and h is the wall height. In this experimental program, all the structural walls were loaded under single curvature and the curvature distribution of all the wall specimens are triangular, assuming linear elastic flexural behavior, corresponding to a value of $\alpha = 0.67$.

Shear deformation of the wall specimens were determined using the diagonally placed sensors as shown in the Figure 4.1. If the center of rotation does not coincide with the geometric center of the wall height, the measurement from the diagonal sensors are influenced by the flexural deformations and need to be corrected (shown by Massone and Wallace, 2004). The uncorrected shear component of the top lateral displacement can be calculated as:

$$U_{s\_original} = \delta = \frac{\sqrt{D1^2 - h^2} - \sqrt{D2^2 - h^2}}{2} \qquad (4.2)$$

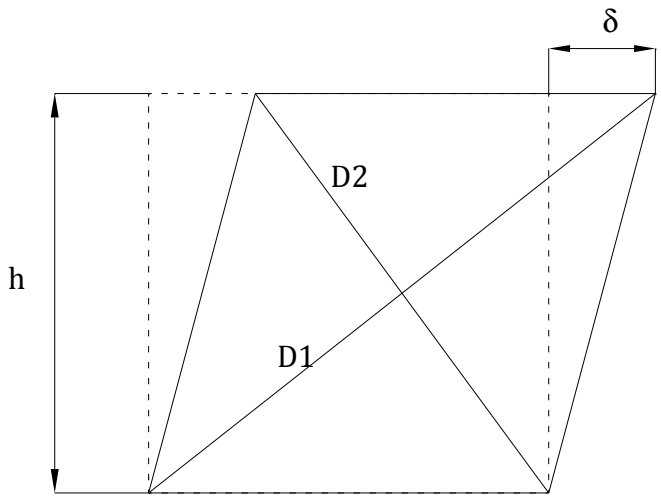

Figure 4.2. Uncorrected Shear Deformation.

As suggested by Massone and Wallace (2004), the uncorrected shear deformation measured using X configuration diagonal potentiometers and the wall flexural deformation can be used together in order to determine the average corrected shear deformation as:

$$U_{s\_corrected} = U_{s\_original} + \left(\frac{1}{2} - \alpha\right).\theta.h \qquad (4.3)$$

For shear deformation, using the $U_{s\_original}$ value obtained using only the diagonal sensors provides a biased estimation of the wall shear deformation, due to negligence of the contribution of flexural deformation on the measurements.

In this approach, using on-wall diagonal and vertical sensors (sensors connected to the wall section) has a few drawbacks. First of all, it is impossible to place the potentiometers and reference points exactly at the ends or corners of the wall section. The threaded rods used to attach the on-wall displacement sensors are around 5 cm inside, from wall corners. Therefore, this configuration cannot measure the interface (e.g., sliding shear) deformation at the top and bottom pedestal interfaces, which may be of considerable amount. In case of flexural deformation measurements, this approach neglects the flexural deformation that occurs at the interfaces between the wall and the pedestals. As well, since the concrete starts to crush and spall at the bottom corners, the rods starts to dislocate around the ultimate load levels, and it is impossible to obtain accurate measurements at higher drift levels.

4.1.2. Shear and flexural deformation components (pedestal-to-pedestal)

Wall top displacement was measured from a rigid reference frame connected to the bottom pedestal. Since the bottom pedestal was used as reference for external lateral displacement measurements, it was not necessary to make any corrections on wall displacement measurements to account for pedestal sliding and rotation (uplift). Figure 4.3 shows a representative figure of lateral top displacement LVDTs, pedestal-to-pedestal vertical LVDTs, and pedestal-to-pedestal diagonal (X configuration) LVDTs. Although the lateral top displacement measurements were independent of pedestal sliding and uplift, displacement sensors were still attached to the pedestal to detect possible sliding and rotation.

The two vertical potentiometers were placed at the wall boundaries for measuring the relative vertical displacements from pedestal to pedestal. Since the top and bottom pedestals can be assumed as rigid, the vertical displacement of the wall top end is equal to the measured displacement from the pedestal sensors, which were located at around 5 cm above the bottom of the top pedestal.

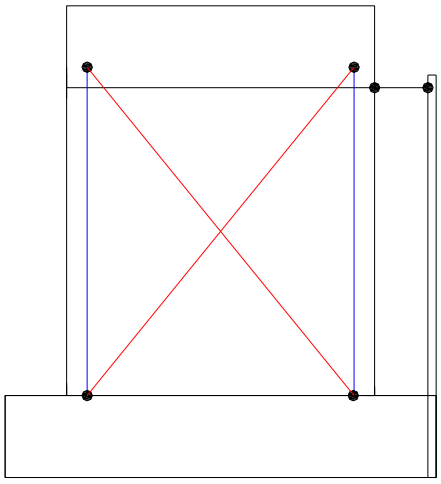

Figure 4.3. Top displacement, Vertical and Diagonal LVDTs (pedestal to pedestal).

The shear component of the top lateral displacement can be calculated with the same procedure as the previous shear deformation formula. However, in this case, the calculated shear deformation also contains the sliding shear deformation at the wall-pedestal interfaces, and . the uncorrected shear deformation takes the form:

$$U_{s\_original} = \delta + s = \frac{\sqrt{D1^2 - h^2} - \sqrt{D2^2 - h^2}}{2} \quad (4.4)$$

Where, s is the sliding deformation relative to the bottom pedestal. The diagonal X configuration sensors and vertical sensor configurations are shown in Figure 4.4.

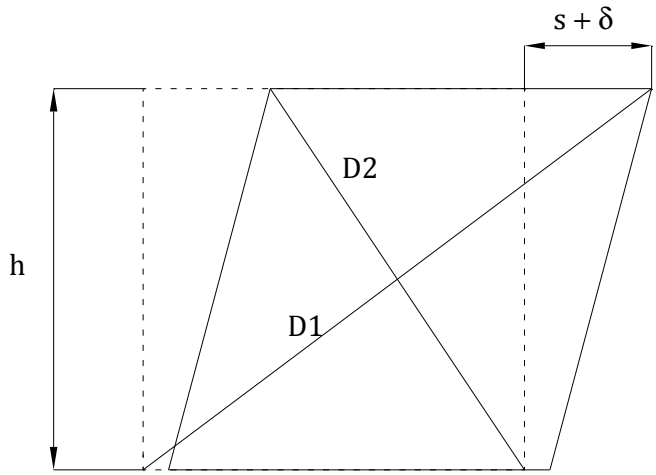

Figure 4.4. Uncorrected Shear Deformation Calculation Pedestal-to-Pedestal.

4.2. Lateral Load versus Top Displacement Relations

As discussed in the previous chapter three main failure modes were observed for the specimens, including diagonal tension, diagonal compression and shear sliding. In this section, the lateral load – top displacement behavior of four representative specimens will be presented and discussed. Results for all other specimens are presented in the Appendix. The lateral load on the specimens was applied by a 1000 kN capacity horizontal actuator. The top displacement of the specimens was measured by two LVDTs having +/-75 mm stroke. They were placed at the top level of the wall section at both faces. The top displacement recorded as the average of these two sensors, was used for displacement-controlled loading. The top displacement sensors were mounted on a steel reference frame, supported by the bottom pedestal. Therefore top displacement sensors measured the lateral top displacement of the wall, relative to the bottom pedestal.

Figure 4.5 presents the lateral load – top displacement response for the Type1 Specimen1, which has experienced a diagonal tension type of failure mode. The concrete

crushed along the main diagonal cracks and the crushing concentrated at the center of the specimen. The lateral load was degraded as the lateral load capacity was reached, which is indicative of sudden failure due to crushing of concrete. After reaching the lateral load capacity, the hysteresis loops showed high pinching. At the high drift levels, the specimen showed a residual capacity of 15% of the lateral load capacity, which is very low and can be neglected.

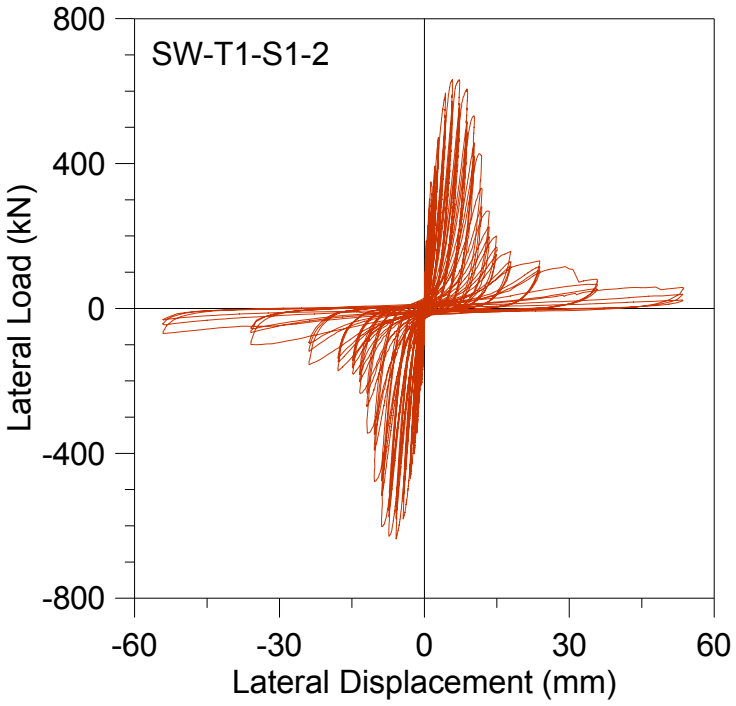

Figure 4.5. Load – Top Displacement, Specimen T1-S1.

As discussed previously, the initial stiffness reduced after the formation of the first main diagonal crack. The first crack causes an instantaneous load reduction. This load reduction is recovered at the following drift levels. However the stiffness degrades permanently. The stiffness degradation occurs generally at 0.05% drift level when the first diagonal crack occurs. And this degradation followed by small stiffness degradations at the following drift levels up to 0.2% drift level. After that the stiffness remains unchanged up to lateral load capacity. Generally the load level is between 20 -30 % of the ultimate load capacity when the first crack occurs. And the lateral load level was around 45 – 55 % of the lateral load capacity when the stiffness degradation stops at 0.2% drift level.

Another Type1 specimen was tested as the last specimen, under an axial load level of 10% of its axial load capacity. The specimen had shown very sudden lateral load degradation after capacity was reached. The lateral load capacity of this specimen was higher by 25%, compared to an identical specimen where no axial load was applied.. Figure 4.6 shows the original load – displacement plot for that specimen. The actual load – displacement curve includes a 5 mm jump in lateral displacement, at the instant of the sudden load degradation. Figure 4.7 shows a modified load – displacement relation for the specimen, for better representation of the response. As seen from the plots, the specimen experienced a very sudden load decrease at approximately 1% drift level. It loses almost all of its the lateral load capacity after the subsequent two drift levels.

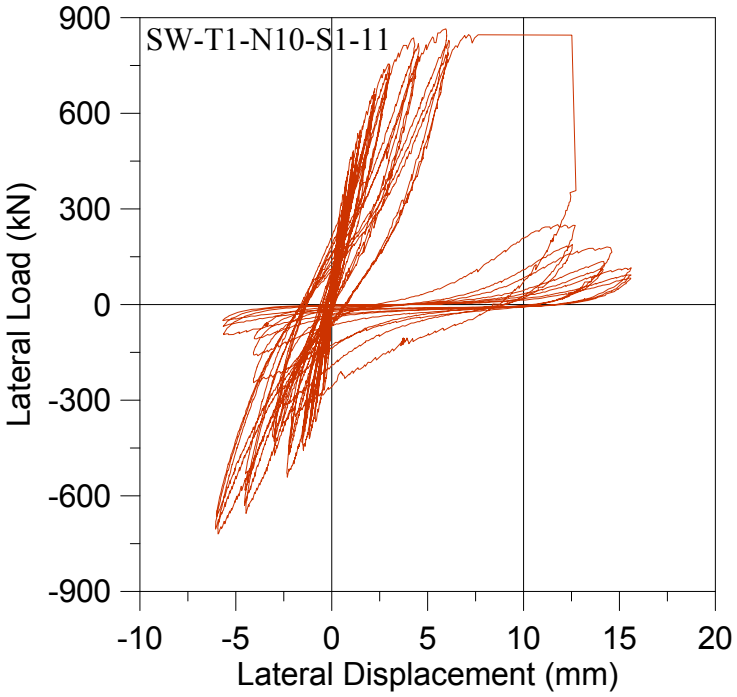

Figure 4.6. Load – Top Displacement , Specimen T1-N10-S1 (original).

Type 2 specimens presented a different failure mode. All Type2 specimens were tested under zero axial load, and had higher vertical and horizontal web reinforcement (0.68%) ratios, compared to Type1 specimens (0.34%). Figure 4.8 shows the load – displacement response obtained of Type2 – Specimen2. Type 2 specimens as well as Types 4, 5 and 6, experienced diagonal compression failure. These specimens have large amount of horizontal web reinforcement, which prevents diagonal tension cracks to widen.

Therefore, the concrete crushes under diagonal compression starting at the bottom corners and propagating along the base of the wall.

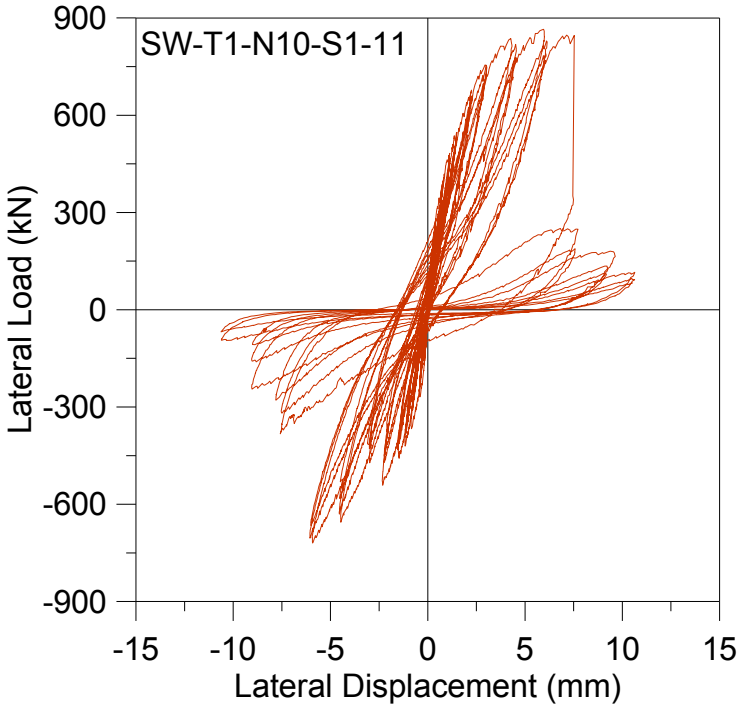

Figure 4.7. Load – Top Displacement, Specimen T1-N10-S1.

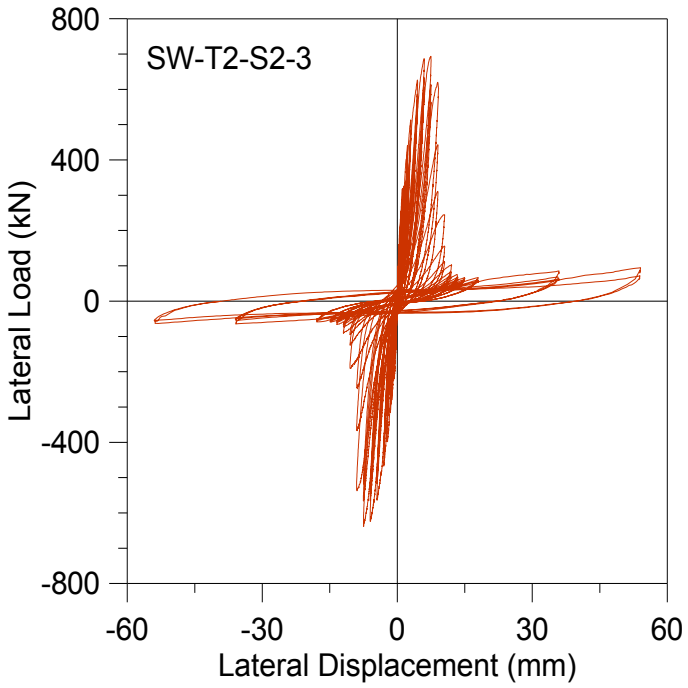

Figure 4.8. Load – Top Displacement, Specimen T2-S2.

As it can be seen from the load – displacement response, the lateral load degraded rapidly after the capacity was reached. The residual strength was again, about 10% of the lateral load capacity.

Another type of failure was observed for the Type3 specimen, which was the only specimen tested with very low amount of boundary reinforcement. The observed failure mode showed that in the case of inadequate boundary reinforcement (low-flexural capacity), the specimen fails under sliding shear mode triggered by flexural cracking. The failure was initiated with formation of flexural cracking on the wall-pedestal interface. This flexural crack propagated along the entire width of the wall at the base, and triggered a premature sliding shear failure.

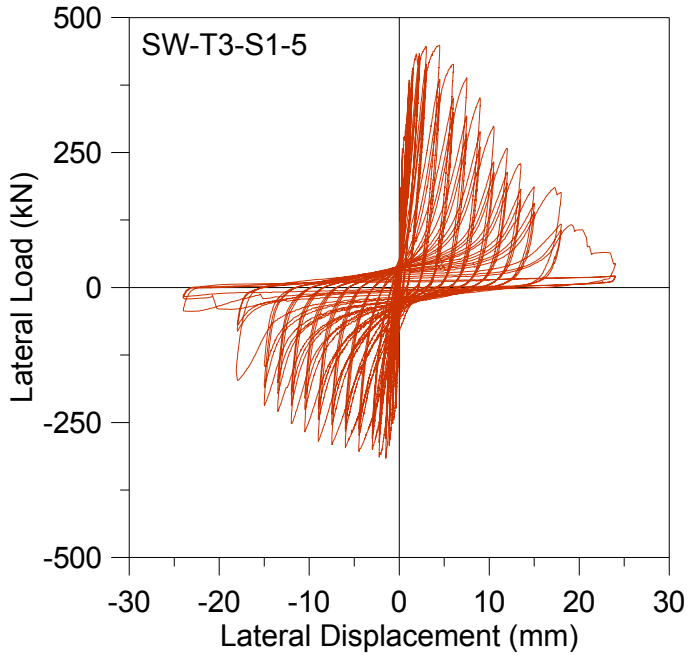

Figure 4.9. Load – Top Displacement, Specimen T3-S1.

Figure 4.9 shows the load – displacement relations for a Type3 specimen. The lateral load capacity is significantly lower than specimens of other type. The maximum lateral load attained was around 380 kN. The specimen has also shown a somewhat unsymmetrical response in the positive and negative loading directions. The maximum load in the positive direction was 440 kN whereas in the negative direction it was 320 kN.

The load degradation after reaching the capacity was gradual, contrary to the sudden degradation observed in Type1 and Type2 specimens.

4.3. Shear, Flexural and Sliding Lateral Deformation Components

As mentioned previously, the wall specimens were instrumented such that decomposition of shear, flexural, and sliding components of the top lateral displacement was possible. This was achieved via attachment of vertical displacement sensors at the wall ends and X – configuration sensors from corner to corner of the walls. Both flexural and shear sensors were placed on the wall sections close to the edges, as well as from bottom pedestal to top pedestal (beam). When the data was processed, it was observed that the flexural deformation (rotation) readings from the on-wall sensors exhibited inconsistencies, due to dislocation of the threaded rods, to which the sensors were attached to, with progressive cracking and damage. Therefore the sensors attached on the top and bottom pedestals were used for identifying the flexural component of the top displacement. For the shear deformation measurements, the on-wall X-configuration (diagonal) sensors provided systematic and reasonable data, up to some point during testing. Therefore, for shear component, both the on-wall and pedestal-to-pedestal shear deformation measurements were provided. All of the deformation data provided was plotted until the displacement sensor readings were not distorted due to local damage and crushing. In this section, representative plots for selected spacimens are presented. Additional deformation plot for all specimens are provided in Appendix A.

4.3.1. Lateral Deformation Components of Specimen T1-S1

For the first two specimens tested, Type1-Specimen1, Type2-Specimen1, only on-wall readings were available for flexural and shear deformation components, since pedestal-to-pedestal sensors were not installed on these specimens. Therefore, the top displacement components shown here are obtained from on-wall sensor measurements.

Figure 4.10 compares the lateral load vs. the top lateral displacement values measured from external sensors (measuring the top lateral displacement of the specimen),

with the lateral load vs. total of the deformation components measured using the shear, flexure and sliding sensors.

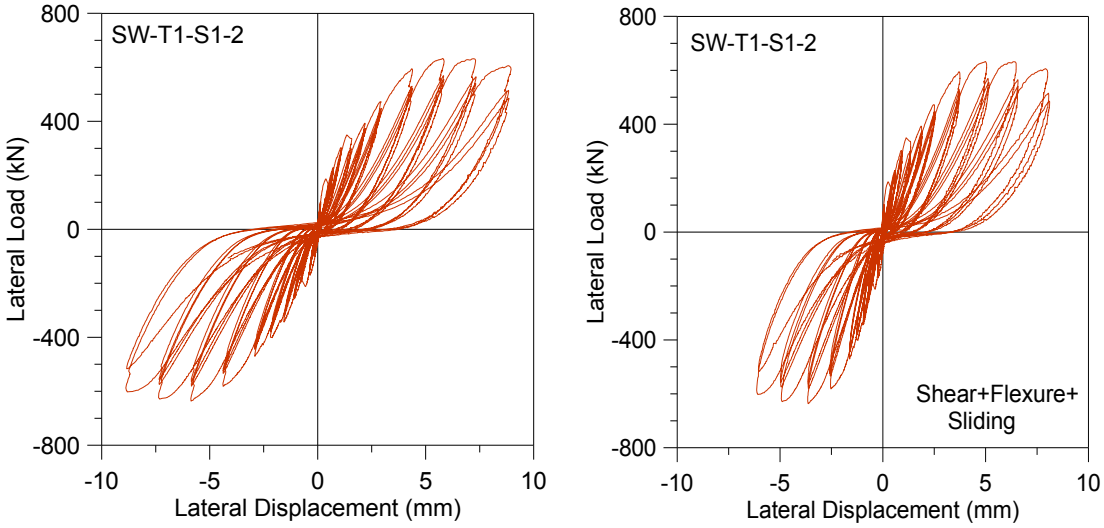

Figure 4.10. Lateral Load vs. Displacement Response from External and Local Sensors, T1-S1.

The total of the shear, flexure, and sliding deformations appears to be lower than the lateral displacement measured at the top. This is possibly due to the deformations developing at the interfaces between the wall section and the top and bottom pedestals, since the on-wall shear and flexural sensors were placed at approximately 50 mm distance from the top and bottom wall-pedestal interfaces.

The average percentage (average of positive and negative loading directions) of shear, flexural and sliding deformation contributions to the top lateral displacement of Specimen T1-S1 are provided in Figure 4.11. The results show that the flexural deformation contribution to the top displacement decreases with the increasing drift levels, whereas the shear deformation contribution increases. When the lateral load capacity is reached, flexural deformation contribution is only around 20% of the top displacement. However, at the end the data, the total of the deformation component measurements can only predict approximately 80% of the total lateral displacement, as the deformation measurements get less accurate with increasing damage on the specimen.

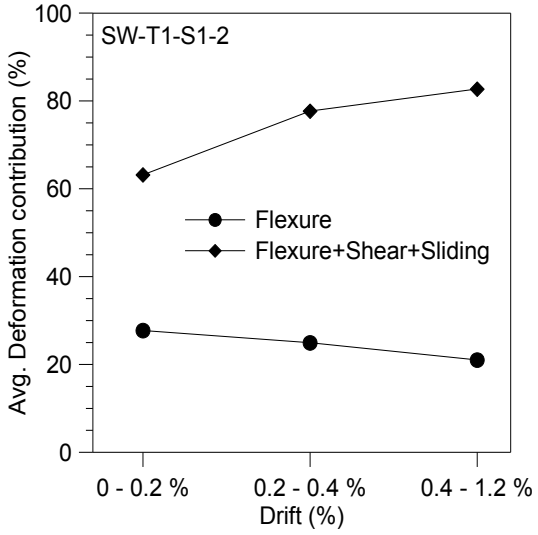

Figure 4.11. Average Deformation Contributions, Specimen T1-S1.

Figure 4.12 compares the flexural and shear deformation components of the top lateral displacement. Most of the lateral deformations were due to shear deformations. The flexural deformation component of the response remains practically linear elastic. As well, the shape of the hysteresis loops and the pinching properties of the shear deformation component of the response resemble the overall lateral load – displacement response, indicating that the behavior of the wall is dominated by shear deformation.

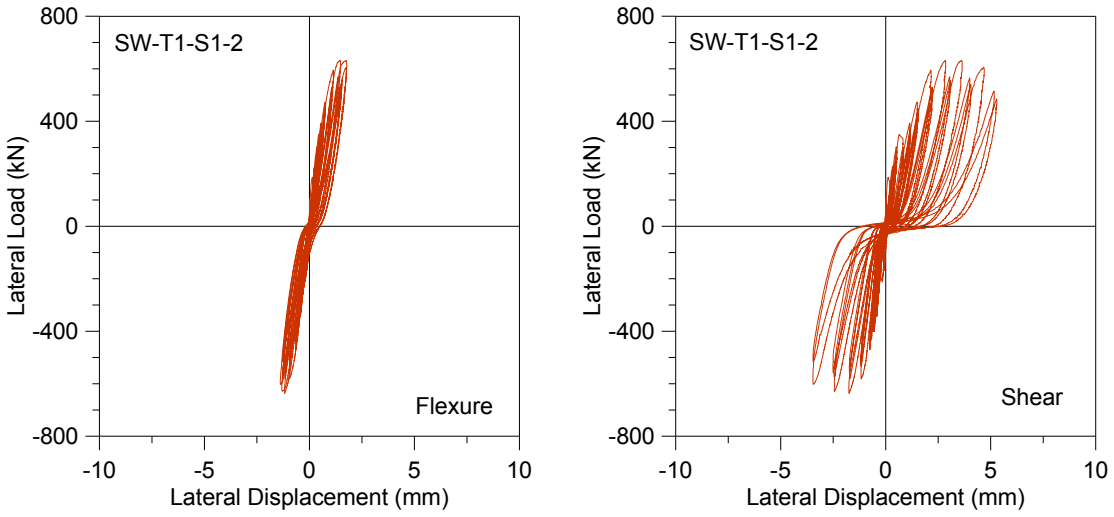

Figure 4.12. Flexural and Shear Deformation Components, Specimen T1-S1.

Figure 4.13 provides the lateral load – sliding deformation measurements for Type1-Specimen1. Magnitude of the sliding deformation is close to the flexural deformation

component, at approximately 2 mm in both positive and negative loading directions, until the data point for which reliable deformation data was obtained.

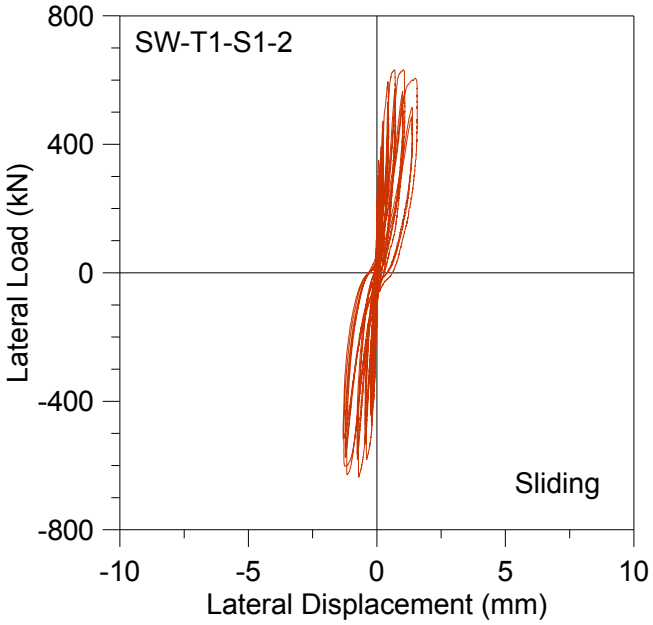

Figure 4.13. Sliding Deformation Component, Specimen T1-S1.

4.3.2. Lateral Deformation Components of Specimen T2-S2

The instrumentation of Specimen T2-S2 was similar, except pedestal-to-pedestal flexural and shear deformation sensors were installed on this specimen (as well as all of the specimens tested subsequently). These applications allowed more reliable measurements of flexural and shear deformation components of the response, as the pedestals did not suffer damage during the tests. Figure 4.14 compares the measured lateral load vs. top displacement response until first strength degradation drift level, to the lateral load vs. the total of shear and flexural deformation components, until same data point. The total deformation does not include sliding deformation component, since the shear deformation measured from pedestal to pedestal includes sliding deformations.

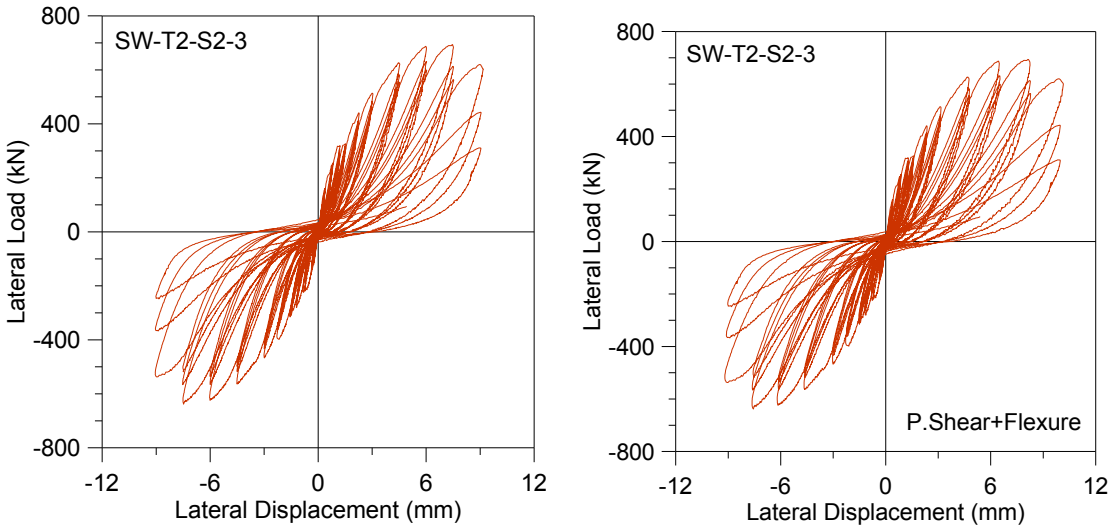

Figure 4.14. Lateral Load vs. Displacement Response from External and Local Sensors, T2-S2.

The average percentage of shear, flexural and sliding deformation contributions to the top lateral displacement of Specimen T2-S2 are provided in Figure 4.15. The results indicate that the measurements obtained from the pedestal-to-pedestal sensors represent the shear and flexural deformation contributions more accurately than the on-wall sensors, as the sum of the pedestal-to-pedestal deformation contributions add up to approximately 100% of the measured lateral displacement of the wall. At high drift levels, flexural deformation contribution decreases below 20% of wall lateral displacement.

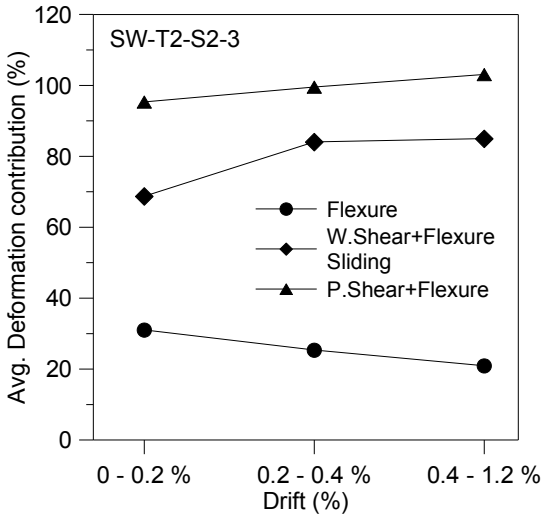

Figure 4.15. Average Deformation Contributions, Specimen T2-S2.

Figure 4.16 shows the flexural and shear deformation components of the lateral load vs. displacement response, separately. The shear deformation component of the response is non-linear, and resembles the shape of the lateral load vs. top displacement response obtained using the sensors mounted on the external reference frame. Therefore, the pinching observed in the overall lateral load vs. displacement response appears to be due to the shear deformation component, as expected. The flexural deformation component of the response remains practically linear elastic.

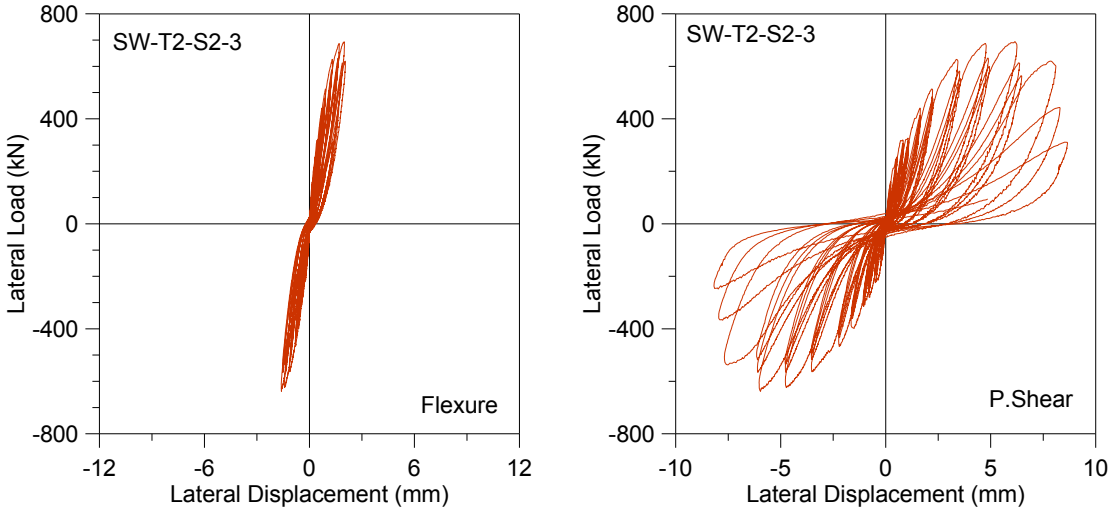

Figure 4.16. Flexural and Shear Deformation Components, Specimen T2-S2.

As well, the flexural deformation component has a much smaller contribution to the total lateral displacement of the wall, compared with the shear deformation component. Flexural deformation values change between 10% and 20% of the shear deformation.

Lateral load vs. shear deformation measurements from the on-wall sensors, and the lateral load vs. sliding deformation measurements are provided in Figure 4.17. The shear deformations shown, which were measured by the on-wall displacement sensors, produce an asymmetric (and therefore biased) load-deformation response. The sliding deformation measurements are small in magnitude, indicating their relatively small contribution to the overall lateral displacement of the wall.

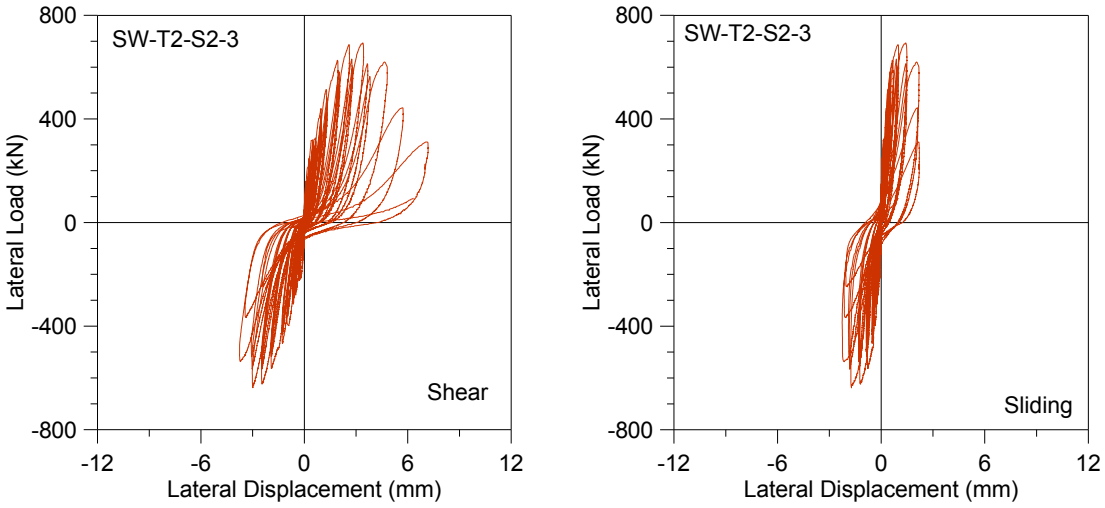

Figure 4.17. Shear and Sliding Deformation Components, Specimen T2-S2.

4.3.3. Lateral Deformation Components of Specimen T1-N10-S1

This specimen was tested under an axial load level corresponding to 10% its axial capacity. The lateral load capacity of the specimen was increased by approximately 23%, with respect to zero axial load case. The failure mode was diagonal tension, with very sudden crushing along the diagonal strut. The lateral load vs. top displacement response of the specimen, as well as the lateral load vs. the sum of the flexural and shear deformation components measured by the local sensors, are provided in Figure 4.18. The measured data for all the other were provided up to same data point, for consistent comparison purposes. Results presented in Figure 4.18 show that the total deformation measured by the local sensors slightly exceeds the measured lateral top displacement, in the positive loading direction.

Figure 4.19 presents the flexural and shear deformation components of the lateral load – displacement response, for the specimen. The flexural and shear deformations shown in the figure were measured by the pedestal-to-pedestal sensors; since pedestal-to-pedestal measurements provide more reliable data, and include sliding shear deformations, as discussed in Section 4.1. As observed in the figure, the shape and pinching properties of the shear deformation component of the response resembles the shape of the measured load – displacement response. This also shows that the main contribution to lateral displacement comes from shear deformation.

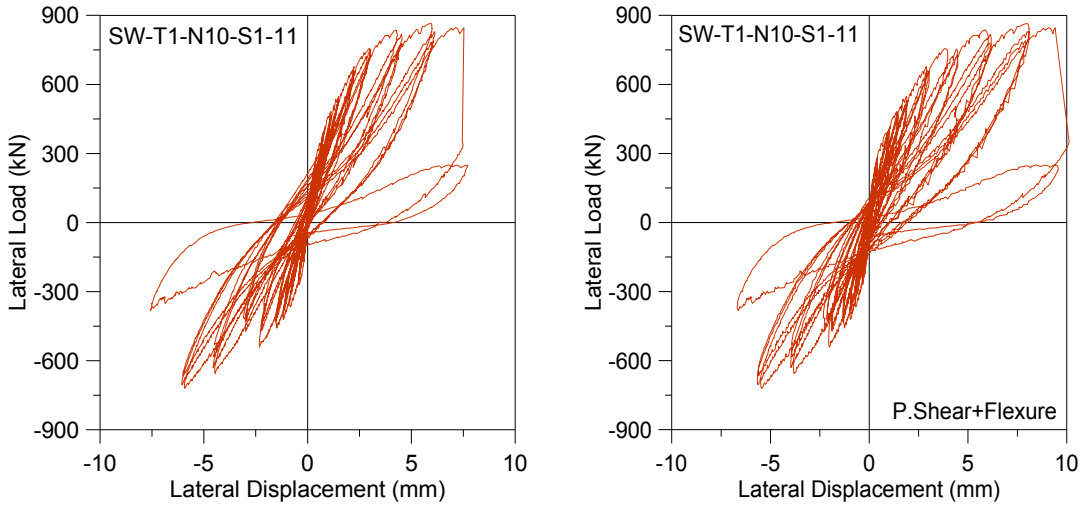

Figure 4.18. Lateral Load vs. Displacement Response from External and Local Sensors, T1-N10-S1.

The shear deformation (measured by on-wall sensors) and sliding deformation components of the lateral load – displacement response are compared in Figure 4.20. Results presented on the figure indicate that the on-wall shear deformation readings do not provide symmetric hysteresis loops. As well, on-wall shear deformation readings do not consistently represent the lateral displacements measured at the top of the wall. This further verifies that on-wall shear deformation measurements are much more reliable, in representing the behavior.

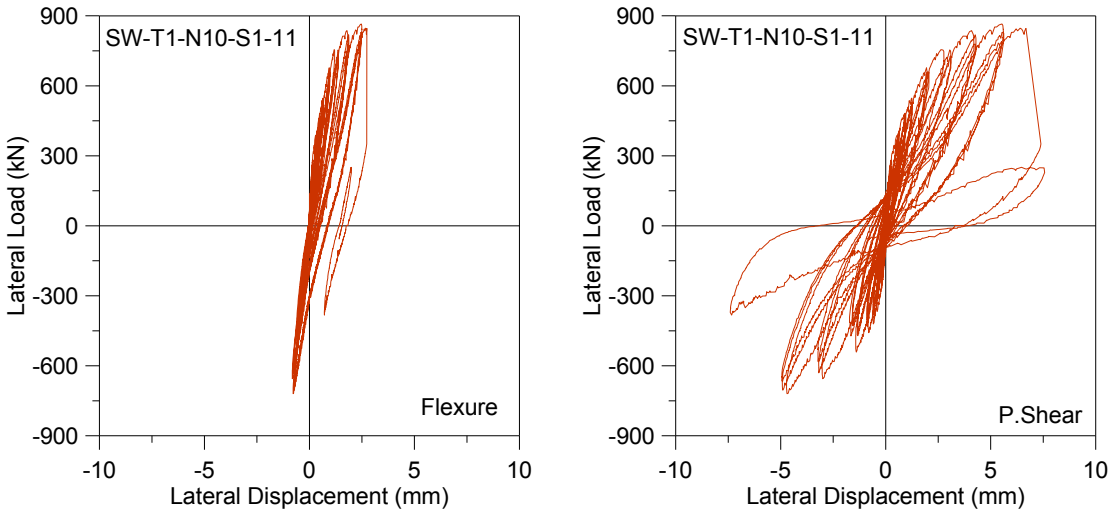

Figure 4.19. Flexural and Shear Deformation Components, Specimen T1-N10-S1.

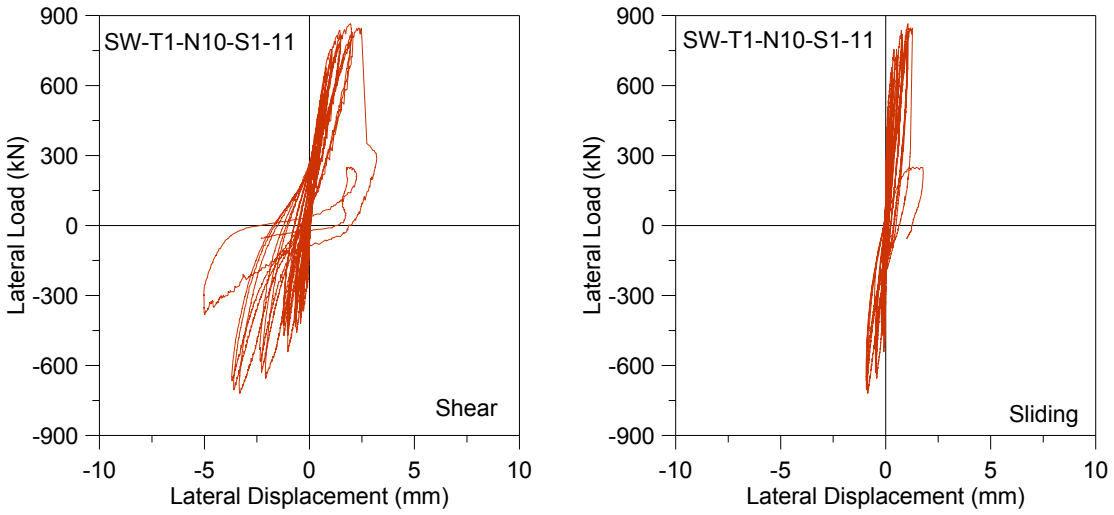

Figure 4.20. Shear and Sliding Deformation Components, Specimen T1-N10-S1.

The sliding deformations were measured using the two displacement sensors attached on the wall on both sides, at the wall-pedestal interface. Results shown in Figure 4.20 also illustrate that the sliding deformations measured at the base of the wall are small in magnitude, compared with shear deformations. It must be noted that the pedestal-to-pedestal shear deformation measurements provide the sum of the shear and sliding deformations, whereas on-wall shear deformation measurements do not include sliding deformations.

4.3.4. Lateral Deformation Components of Specimen T3-S1

This specimen had only 2-ϕ8 boundary reinforcement at both ends, and it failed due to sliding shear at the bottom. Figure 4.21 compares the lateral load vs. top displacement response of the specimen, with the lateral load vs. the sum of the shear and flexural deformation components, measured using the local sensors. The total deformation values measured by the local sensors are not symmetrical in the positive and negative loading directions. Considering the average deformation contributions, via calculating the average of the total deformations in the positive and negative loading directions, seems more reasonable in this case. Figure 4.22 presents the percentage contribution of deformation components, to the lateral displacement of the wall, within different drift bands.

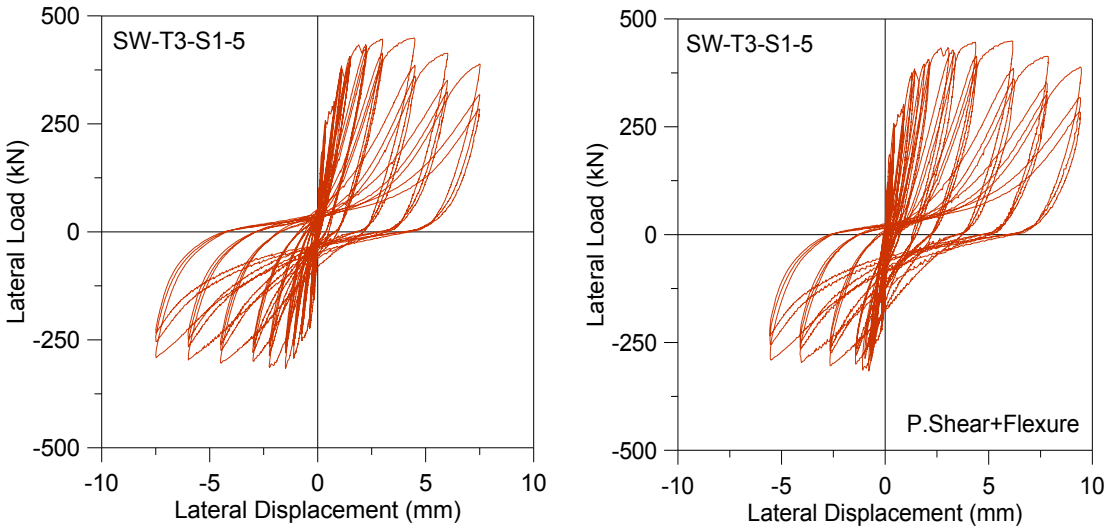

Figure 4.21. Lateral Load vs. Displacement Response from External and Local Sensors, T3-S1.

Figure 4.23 compares the flexural and shear deformation components of the lateral load vs. top displacement response. In this case, the flexural deformation component of the response is significant, with the flexural deformations being approximately 50% of the shear deformations. The failure mode of this specimen was governed by sliding shear; however, the specimen apparently experienced significant amount of flexural deformation.

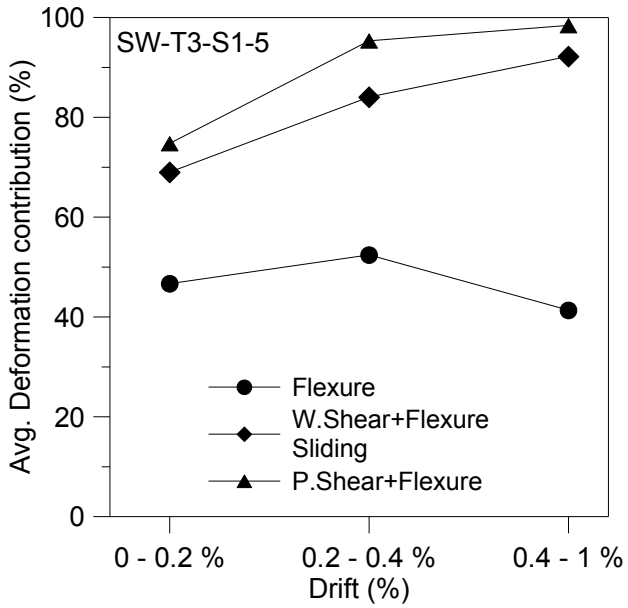

Figure 4.22. Average Deformation Contributions, Specimen T3-S1.

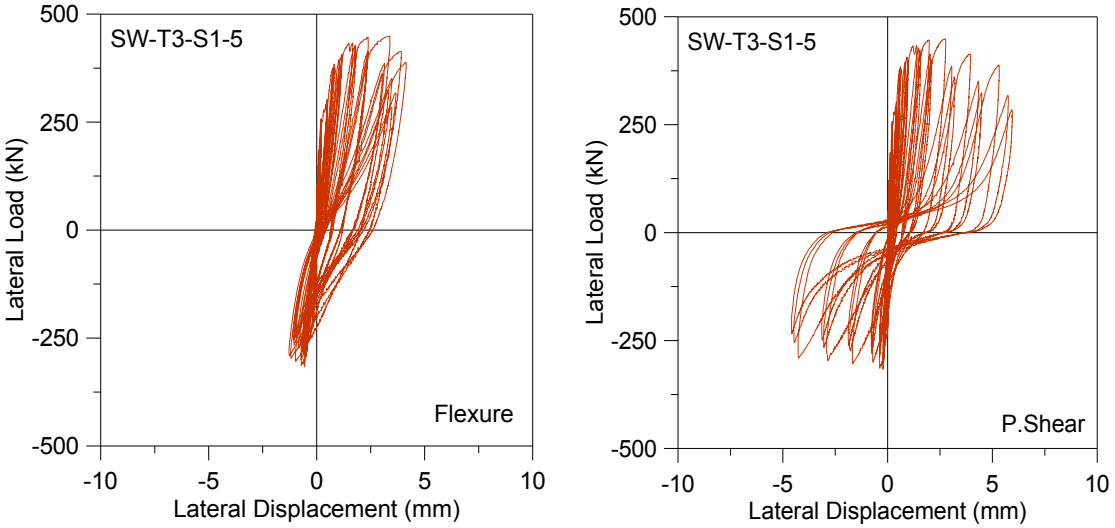

Figure 4.23. Flexural and Shear Deformation Components, Specimen T3-S1.

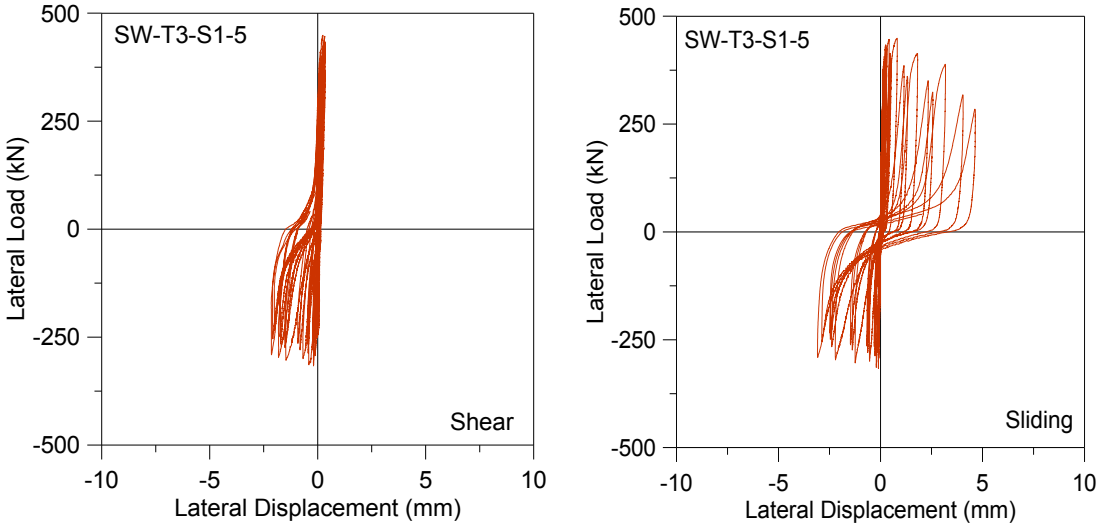

Figure 4.24. Shear and Sliding Deformation Components, Specimen T3-S1.

The shear deformation readings obtained from on-wall diagonal sensors is not representative of the response, because the on-wall shear sensors were placed above wall-pedestal interface, where the sliding crack developed. On the other hand, as depicted in Figure 4.24, the lateral load vs. sliding deformation response show stable hysteresis loops, which resemble the shape of lateral load – top displacement response. For this specimen, the lateral load vs. sliding deformation behavior is nonlinear, and sliding shear deformations contribute to approximately 40% of the top displacement, at high drift levels.

Looking at the all test results it can be concluded that the lateral shear deformation components were around four times greater than the lateral flexural deformations. This finding is also consistent with the theory of elasticity calculations. For the tip deflection calculations of a cantilever beam the following equation was provided by Timoshenko, (1933).

$$v_{(y=0)} = \frac{Px^3}{6EI} - \frac{Pl^2x}{2EI} + \frac{Pl^3}{3EI} + \frac{Pc^2}{2IG}(l - x) \tag{4.5}$$

Where x is the position along the height and y is the position along length. The formula provided for the mid-length deflection and parabolic shear loading at x = 0 (at the free end of the cantilever). l is the height and 2c is the total length of the specimen. At x = 0 the formula become:

$$v_{(y=0)} = \frac{Pl^3}{3EI} + \frac{Pc^2}{2IG}l \tag{4.6}$$

Where the first term represents the flexural deformations and the second term stands for the shear deformations at the tip. For 0.5 aspect ratio specimens *l/2c* = 0.5. And for concrete shear modulus, G can be taken as 0.4E. The flexural and shear deformations become as follows:

$$\delta_f = 0.33\frac{Pc^3}{EI} \quad \& \quad \delta_S = 1.25\frac{Pc^3}{EI} \tag{4.7}$$

Where δ_f is the flexural deformations and δ_s is the shear deformations at the top of the specimen. As it can be seen from the theoretic calculations, shear deformations are around four times greater than flexural deformations.

4.4. Average Horizontal Normal Strain (ε_x) Profiles

The average horizontal normal strain (ε_x) profiles, measured along wall height at different drift levels, are plotted in Appendix A for all specimens tested. In this section,

two representative strain profiles are shown; one for a Type2 specimen, and one for a Type6 Specimen.

Average horizontal normal strains were measured using horizontally placed LVDTs along the height of the specimens. The longitudinal deformations (elongations) were measured between two threaded rods placed at both ends of the wall, where the ends of the sensors were attached. Average horizontal normal strains were calculated via dividing the elongation measurements with the gauge length of the sensors. The measurements indicate that the average horizontal strains generally tend to increase towards the wall mid-height, due to the lateral constraining effect of the top and bottom pedestals. However as cracking is initiated at the bottom of the wall, horizontal strains start to amplify at the bottom part of the wall, and they may exceed the strain values measured at wall mid-height due to progressive crushing close to the bottom. Also each diagonal crack formed contributes to these strain values. Therefore these strains are not the concrete strain at that level. Figure 4.25 shows the average horizontal normal strain distributions measured for Type2 – Specimen3, at different positive and negative drift levels.

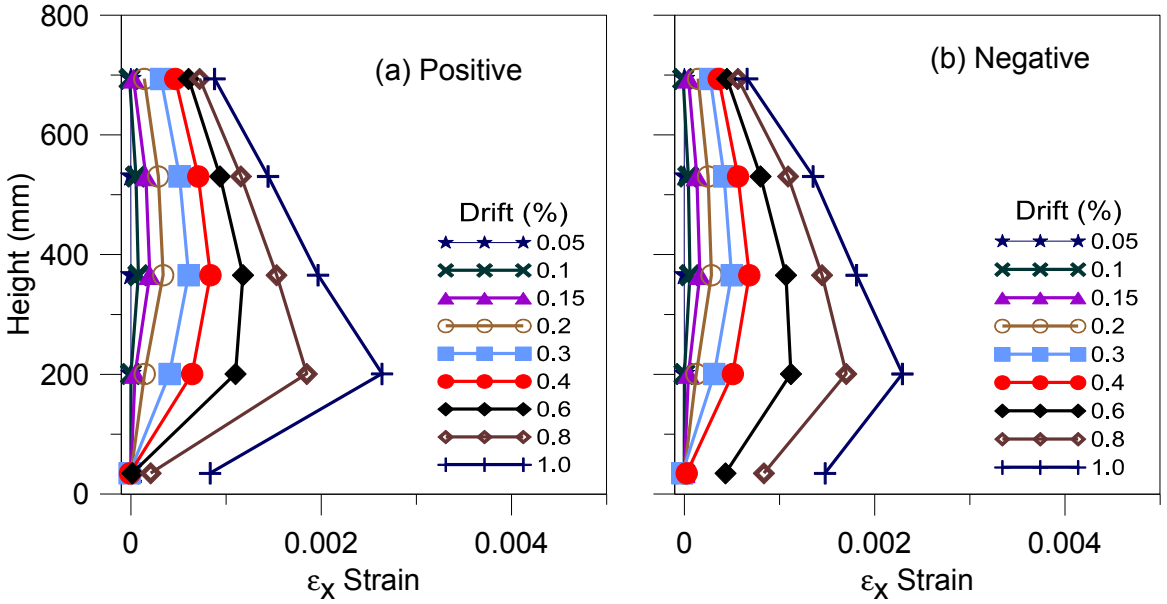

Figure 4.25. Average Horizontal Normal Strain Profiles, Specimen T2-S3.

The measurements indicate that at the initial drift levels, horizontal normal strains were greater in magnitude, at the wall mid-height due to rigid boundary constraints at top and bottom pedestals. At 0.6% drift level, the specimen reaches its lateral load capacity

and crushing starts close to the bottom of the wall. Therefore, the second-level (200 mm height) horizontal normal strains are amplified. Average horizontal normal strain profiles for all Type2 specimens show similar trend, and the strains measured for the positive and negative loading directions are comparable, at all levels along wall height.

Figure 4.26 shows the average horizontal normal strain distribution for Type6 – Specimen1. Again, there is a clear trend in the distribution of the strains along the height of the wall. Low average strain values are measured close to the top and bottom of the wall, due to the constraining effect of the pedestals. The strains increase towards the mid-height of the specimen. For this specimen type, maximum strain values were typically measured at wall mid-height. The Type6 specimen showed similar a strain distribution. For other specimen types, less systematic distributions were also observed, as shown in Appendix A.

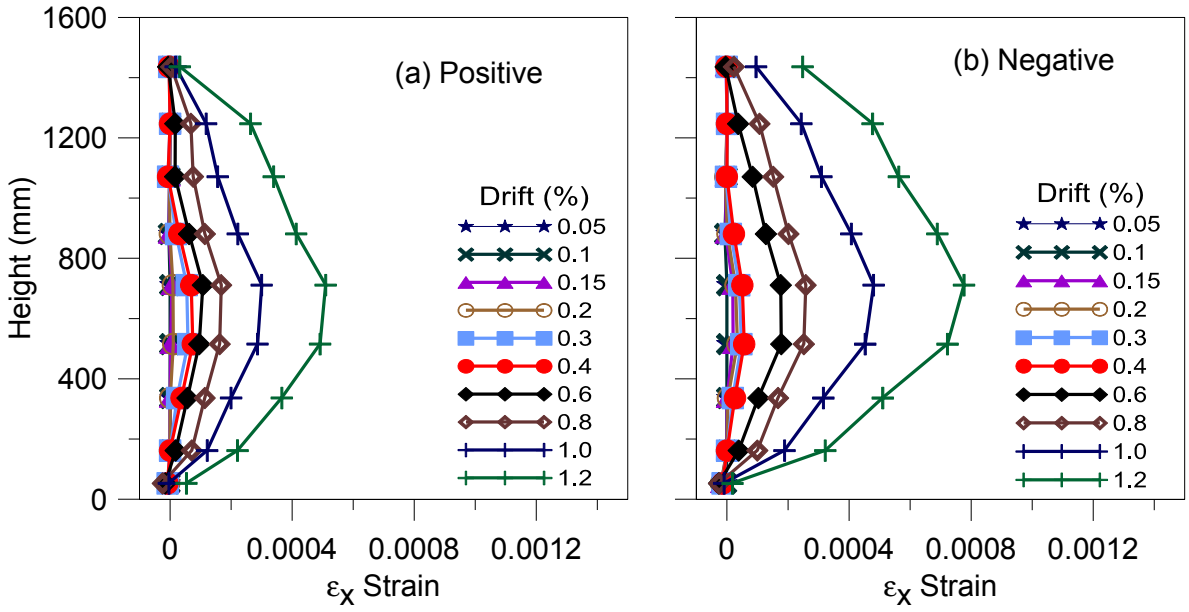

Figure 4.26. Average Horizontal Normal Strain Profiles, Specimen T6-S1

5. ASSESSMENT OF WALL LATERAL LOAD CAPACITY

5.1. Assessment of Wall Shear Strength

FEMA 356 requirements for assessment of the lateral load capacity of reinforced concrete structural walls are provided in Section 6.8, and are summarized in this section. Structural walls are considered as slender, if their aspect (height/length) ratio is larger than 3.0, and are considered as short or squat if they have an aspect ratio smaller than 1.5. Slender wall responses are normally controlled by flexural behavior, and the response of squat walls are normally controlled by shear. Since all of the wall specimens tested in the scope of this experimental project fall in the definition of squat walls, their lateral load capacities are calculated based on the nominal shear strength equations provided in the code provisions.

The nominal shear strength of the walls tested was calculated based on FEMA356 provisions. According to FEMA356, the nominal shear strength of a shear wall shall be determined using the procedure and equation provided in Section 21 of ACI 318. In ACI 318 the aforementioned equation is in the form of:

$$V_n = A_{cv}\left(\alpha_c \lambda \sqrt{f_c'} + \rho_t f_y\right) \tag{5.1}$$

Where A_{cv} is the gross are of the wall section bounded by the thickness of the web portion and the length of the section, in the direction of shear force considered. Considering the wall specimens tested in this project, the gross area of the wall is identical to the total cross sectional are of the wall, since the thickness of the wall is the same along the length of the wall. The ACI equations provided is in terms of SI units. The coefficient α_c is 0.25 for walls having an aspect ratio (h_w/l_w) $\leq$1.5, is 0.17 for (h_w/l_w) $\geq$2.0 and varies linearly for the aspect ratios between 1.5 and 2.0. The λ coefficient is a modification factor for reflecting the mechanical properties of lightweight concrete, relative to normal weight concrete of the same compressive strength. For normal weight concrete, which was used in the

construction of all test specimens, the λ coefficient is defined 1.0. f_c' represents the compressive strength of concrete.

The second part of the equation $\rho_t f_y$ stands for the contribution of the transverse reinforcement to the shear strength. Here, ρ_t is the transverse reinforcement ratio, and f_y is the specified yield stress of the transverse reinforcing steel. According to ACI 318M-08, (Section 21.9.4.3), the vertical reinforcement ratio shall not be less than the horizontal reinforcement ratio, for walls with aspect ratios (h_w/l_w) not exceeding 2.0. For calculating the shear strength of walls, where the longitudinal and transverse reinforcement ratios are different, the lower of the two reinforcement ratios is used together with the corresponding yield stress. This means $\rho_t f_y$ is taken as the minimum of the $\rho_t f_{yt}$ and $\rho_l f_{yl}$. This approach is consistent with the common interpretation of the ACI318 requirement (Sozen and Moehle, 1993, Wood, 1990).

Another ACI318 requirement states that the nominal shear strength of an individual wall shall not be taken larger than $0.83A_{cw}\sqrt{f_c'}$. This requirement provides an upper bound for shear strength calculations. In this equation, A_{cw} is the cross sectional area of the entire wall. This term is the same as A_{cv} for the walls having a constant thickness throughout the length.

The distributed web reinforcement ratios in longitudinal and transverse directions, ρ_l and ρ_t, shall not be less than 0.0025, if the ultimate shear force demand V_u exceeds $0.083A_{cv}\lambda\sqrt{f_c'}$. Reinforcement spacing each way shall not exceed 450 mm, and reinforcement contributing to V_n shall be continuous. For walls where the shear force demand is below $0.083A_{cv}\lambda\sqrt{f_c'}$, ρ_l and ρ_t shall be permitted to be reduced to the values specified in Section 14.3 of ACI 318, which are the minimum reinforcement requirements.

FEMA 356 has an additional requirement on the use of reinforcement ratio values in nominal shear strength calculations. FEMA 356 states that when a wall or wall segment has a transverse reinforcement ratio, ρ_n (replacing ρ_t, in ACI 318M-08), less than the minimum value of 0.0025 but greater than 0.0015, the shear strength of the wall shall be calculated using the ACI 318 equation provided previously. For transverse reinforcement

ratios less than 0.0015, the contribution from the wall reinforcement to the shear strength of the wall shall be held constant at the value obtained using a ratio of 0.0015. This modification to ACI provisions is based on the work of Wood, (1990) who found that wall shear strength is relatively insensitive to changes in the reinforcement ratio ρ_n, particularly for low ratios of ρ_n.

ACI 318 also requires that the reinforcement contributing to V_n shall be distributed across the shear plane. At least two curtains of reinforcement shall be used in a wall if the shear force demand V_u exceeds $0.17A_{cv}\lambda\sqrt{f_c'}$, where the A_{cv} is the gross area of the wall section bounded by the web thickness and the length of the wall in the direction of shear force applied, and f_c' is the compressive strength of concrete. If this section is strictly applied, it implies that the shear strength of a wall having one curtain of reinforcement cannot be taken greater than the shear strength of concrete ($0.17A_{cv}\lambda\sqrt{f_c'}$). The aim of this provision is to ensure that the shear reinforcement is distributed across the shear plane. However when applied to walls with single curtains of web reinforcement, it has an unintended impact of limiting the wall nominal shear strength, due to neglecting of the contribution of the single-curtain reinforcement. This unintended impact was investigated by Orakçal et al (2009), where a modification was proposed for calculation of nominal shear strength of walls having one curtain of reinforcement. Orakçal et al. (2009) also showed that the nominal shear strengths calculated using equation 21.7 of ACI 318 and the FEMA 356 procedure are agreeable with test results for lightly-reinforced wall spandrels, and the same nominal shear strength calculation procedure can be used, even if the two-curtain reinforcement requirement is violated.

The second modification to the ACI318 equation was to use of expected material properties for the nominal shear strength calculation for walls. Use of specified concrete compressive strength and steel yield stress values were found to underestimate the expected shear strength of walls. ASCE/SEI 41 currently relates the calculated shear strength to the nominal (lower bound) values for concrete compressive strength and reinforcement yield stress. Test data by Hidalgo (2002) have demonstrated that the shear strength of walls could be better represented using expected (mean) material properties. The ASCE41 committee has proposed revising the calculation of wall shear strength to be based on expected material properties to get a better estimate of wall behavior and to be

more consistent with the rest of the standard. These proposals are included in Supplement1 of ASCE/SEI 41.The section on calculation of the shear strength of walls in the original ASCE 41 document is identical to FEMA 356.

Table 5.1. Properties and Shear Strength of Tested Specimens.

Specimen ID	α_c	f_c', MPa	ρ_t, %	f_{yt}, MPa	ρ_l, %	f_{yl}, MPa	$V_{n,FEMA}$, kN	V_{TEST}, kN
SW-T2-S1-1	0.25	19.3	0.68	500	0.68	500	656.34	798.6
SW-T2-S2-3	0.25	25.8	0.68	500	0.68	500	758.86	666.1
SW-T2-S3-4	0.25	29	0.68	575	0.68	575	804.54	813.3
SW-T3-S1-5	0.25	32.1	0.68	575	0.68	575	846.45	382.7
SW-T4-S1-6	0.25	34.8	0.68	575	0.68	575	881.33	874.1
SW-T5-S1-7	0.25	35	0.68	575	0.34	575	618.12	709.6
SW-T6-S1-8	0.25	22.6	0.68	575	0.68	575	710.24	735
SW-T1-S2-9	0.25	24	0.34	575	0.34	575	572.35	563
SW-T1-N5-S1-10	0.25	26.3	0.34	575	0.34	575	582.68	789
SW-T1-N10-S1-11	0.25	27	0.34	575	0.34	575	585.73	793
SW-T1-S1-2	0.25	23.7	0.34	500	0.34	500	525.07	635

The nominal shear strength of each wall specimen tested during the experimental program was calculated using the code provisions described above, based on specifications of FEMA 356, ACI 318M-08, and ASCE/SEI 41 Supplement1. Properties and the calculated nominal shear strengths of the test specimens are listed in Table 5.1. The lateral load capacities measured during the tests (V_{TEST}) are the average of the maximum lateral loads applied in the positive and negative loading directions. The comparison of the test results with the nominal shear strength calculations according to FEMA 356 (V_{TEST} / $V_{n,FEMA}$) are also presented in the table.

The walls tested during the experimental program have continuous longitudinal reinforcement, with sufficiently embedment length into top and bottom pedestals, or 90-degree hooks. The longitudinal web reinforcement ratio for Type1 and Type5 specimens is 0.34% and for Types2, 3, and 4, it is 0.68%. If there is any discontinuity in the longitudinal reinforcement or insufficient embedment (development) length, such bars should not be included in the longitudinal web reinforcement ratio. Since all of the tested specimens have continuous longitudinal web bars with sufficient development length, the longitudinal reinforcement ratios listed in Table 5.1 were directly used in the shear strength calculations.

The specimens tested have transverse (horizontal) web reinforcement ratios of 0.34% for Type1, and 0.68% for Type2, 3, 4, and 5 specimens. If there were no hooks provided on the transverse reinforcement, due to deficient anchorage conditions, this should be considered as reduction in the effective transverse reinforcement ratio. This reduction shall be implemented via applying the minimum reinforcement ratio for the shear strength calculation. FEMA 356 recommends a minimum reinforcement ratio of 0.15% for nominal shear strength calculations. As well, according to common interpretations of ACI 318, the shear strength computed using Equation (5.1) should be based on the minimum value of $\rho_t f_{yt}$ and $\rho_l f_{yl}$. Since all the transverse reinforcing bars have 180-degree hooks, the transverse reinforcement ratios listed in Table 5.1 were directly used in the shear strength calculations.

In Table 5.1, the ratio ($V_{TEST}/ V_{n,\ FEMA}$) shows how accurately the FEMA 356 procedure (based on the ACI318 equation) estimates the nominal shear strength of the wall specimens tested. If this ratio is greater that 1.0, this means the FEMA 356 procedure provides a conservative estimate. As shown in the table, 5 of the specimens have ($V_{TEST}/ V_{n,\ FEMA}$) ratios greater than 1.0, meaning that the test specimen shows a higher lateral load capacity than the FEMA 356 estimation. Only Type2-Specimen2 yields a ratio of 0.88, which is reasonably close to 1, but indicates an unconservative FEMA 356 estimation. The measured lateral load capacity of the Type5 specimen was not compared with the FEMA 356 nominal shear strength estimation, since the specimen did not experience a true shear failure. The Type5 specimen had a very low boundary reinforcement ratio, and

experienced a premature sliding shear type of failure at wall bottom, triggered by flexural cracking and yielding of boundary reinforcement.

The nominal shear strength of the specimens was also calculated according to the Turkish Seismic Code (TSC, 2007), for comparison purposes. The results are presented in Table 5-2. The shear strength formula provided in TSC is:

$$V_r = A_{ch}\left(0.65 f_{ct} + \rho_{sh} f_{yw}\right) \quad (5.2)$$

Where A_{ch} is the area of the concrete cross section in the direction of shear force applied, f_{ct} is the direct tensile strength of the concrete ($0.35\sqrt{f_c`}$), ρ_{sh} is the horizontal web reinforcement ratio, and f_{yw} is the yield strength of the horizontal web reinforcement. When compared with the FEMA-356 nominal shear strength formula, the coefficients relating the shear strength to the square root of concrete compressive strength are close to each other. The coefficient in TSC becomes 0.65x0.35 = 0.23, and it is 0.25 in FEMA-356. Although the terms related to contribution of reinforcing steel to shear strength appear to be similar, there are slight differences between TSC and FEMA 356. The FEMA 356 equation considers the minimum of the transverse (horizontal) and longitudinal (vertical) web reinforcement in shear strength the equation, whereas the TSC equation considers only the transverse reinforcement. Due to this discrepancy, the TSC equation provides unconservative estimates for the shear strength of a wall, which incorporates smaller amount (ratio) of vertical reinforcement than the horizontal reinforcement. But other than that special case, the nominal shear strength estimations of FEMA-356 and TSC are close to each other, and in reasonable agreement with the test results.

5.2. Assessment of Wall Flexural Capacity

Although none of the specimens tested experienced flexural failure, the flexural lateral load capacities of the specimens were also calculated, to be able to compare their flexural and shear capacities. Nominal flexural lateral load capacities ($V_{n,\ ACI\text{-}FLEX}$) of the specimens were calculated according to the Equation (5.3), considering the single curvature (cantilever) loading condition imposed during the tests:

$$V_{n,ACI-FLEX} = \frac{M_n}{Wall\ height} \quad (5.3)$$

Table 5-2. Shear Strength according to TSC and FEMA-356.

Specimen ID	f_c', MPa	V_{TEST}, KN	$V_{n,FEMA}$, kN	$V_{n,TSC}$, kN	$V_{TEST}/V_{n,FEMA}$	$V_{TEST}/V_{n,TSC}$
SW-T2-S1-1	19.3	798.60	656.34	791.90	1.22	1.01
SW-T2-S2-3	25.8	666.10	758.86	820.00	0.88	0.81
SW-T2-S3-4	29	813.30	804.54	924.32	1.01	0.88
SW-T3-S1-5	32.1	382.70	846.45	935.81	-	-
SW-T4-S1-6	34.8	874.10	881.33	945.37	0.99	0.92
SW-T5-S1-7	35	709.60	618.12	946.06	1.15	0.75
SW-T6-S1-8	22.6	735.00	710.24	898.47	1.03	0.82
SW-T1-S2-9	24	563.00	572.35	552.51	0.98	1.02
SW-T1-N5-S1-10	26.3	789.00	582.68	561.91	1.35	1.40
SW-T1-N10-S1-11	27	793.00	585.73	564.68	1.35	1.40
SW-T1-S1-2	23.7	635.00	525.07	505.36	1.21	1.26
				Average	1.12	1.03
				Standard Deviation	0.16	0.24

Nominal moment capacities at the wall sections, where the bending moment is maximum (wall base), were calculated according to Sections 10.2, 10.3 and 10.7 of ACI 318M-08, based on the following principles. The flexural moment strength of a member requires static equilibrium and compatibility of strains. Equilibrium between the compressive and tensile forces acting on the cross section at nominal strength should be satisfied. The compatibility between stress and strain for concrete and reinforcement at nominal strength conditions should also be provided. For normal members, strain in reinforcement and concrete shall be assumed directly proportional to the distance from the neutral axis. But deep beams shall be designed taking into account nonlinear distribution of strains. A member can be classified as deep beam if the clear span is smaller or equal to four times the depth of the member. According to Section 10.7 of ACI 318M-08, the wall

specimens tested can be considered as deep beams. The maximum compressive strain at crushing is assumed as 0.003. The relationship between concrete compressive stress distribution and concrete strain shall be considered rectangular, trapezoidal, parabolic or any other shape that results in agreement with results of comprehensive tests. For the assessment of the tested specimens rectangular stress block has been used as concrete compressive stress distribution. Tensile strength of concrete shall is neglected in the nominal moment capacity calculations. Stress in the reinforcement below yield strength shall be taken as the elastic modulus of steel times the steel strain. For strains greater than that corresponding to the yield strength, steel stress is kept constant at the yield strength value. The increase in strength due to strain hardening of the reinforcement is neglected for strength computations. In case of an applied axial load, the effect of an axial load is taken into account, for the nominal moment capacity calculations. If there is any kind of discontinuity of reinforcing bars at the section that the moment capacity is being calculated, this reinforcement should not be considered in the moment capacity calculations.

The nominal moment capacities of the wall specimens were calculated according to the ACI 318 code provisions described above. Actual (measured) material properties were used in the calculations. For the nominal moment capacity calculations, concrete compressive strengths listed in Table 2.2 were used. The reinforcing bars used for the specimens tested for the first set of tests (Type1 and Type2 Specimen1, 2) has 500 MPa and 440 MPa yield strengths for 8 mm and 16 mm reinforcing bars, respectively. Four different types of reinforcing bars were used for the second set of tests. ϕ8 bars have 575 Mpa, ϕ14 bars have 535 MPa, ϕ16 bars 525 MPa and ϕ22 bars have 550 MPa yield strengths. Table 5.3 shows a summary of test results and the nominal flexural lateral capacities of wall specimens tested.

The results show that all specimens have higher flexural lateral load capacities compared with their FEMA 356 nominal shear strengths and their measured lateral load capacities, with the exception of Specimen T3-S1, which suffered a premature sliding shear failure. This confirms the shear failure modes observed during the tests.

Table 5.3. Comparison of Test Results with Nominal Strength Calculations.

Specimen ID	f_c', MPa	$V_{n, FEMA}$, kN	$V_{n, ACI-FLEX}$, KN	$V_{n, ACI - SF}$, kN	V_{TEST}, KN
SW-T2-S1-1	19.3	656.34	1056.00	694.80	798.6
SW-T2-S2-3	25.8	758.86	1075.00	928.80	666.1
SW-T2-S3-4	29	804.54	1255.00	1011.60	813.3
SW-T3-S1-5	32.1	846.45	610.00	709.35	382.7
SW-T4-S1-6	34.8	881.33	1648.00	1095.12	874.1
SW-T5-S1-7	35	618.12	890.00	1098.00	709.6
SW-T6-S1-8	22.6	710.24	987.00	813.60	735
SW-T1-S2-9	24	572.35	875.00	864.00	563
SW-T1-N5-S1-10	26.3	582.68	1300.00	946.80	789
SW-T1-N10-S1-11	27	590.02	1700.00	997.20	793
SW-T1-S1-2	23.7	525.07	874.00	853.20	635

5.3. Assessment of Wall Shear Friction Capacity

Nominal shear friction capacities of the tested specimens were also calculated according to Section 11.6 of ACI 318M-08. With the exception of Section 11.6, all code provisions regarding shear are intended to prevent diagonal tension failure. The purpose of this section is to provide design methods where it is appropriate to consider shear transfer across a given plane, such as an existing crack or potential crack, or an interface between dissimilar materials and components.

According to ACI 318 Section 11.6, a crack is be assumed to occur along the shear plane considered. Where shear friction reinforcement is perpendicular to the shear plane V_n, shear friction capacity, shall be computed by:

$$V_n = A_{vf} f_y \mu\, b \tag{5.4}$$

Where A_{vf} is the area of the reinforcement perpendicular to the considered shear friction plane. f_y is the yield strength of the considered reinforcement. Each reinforcing bar shall be considered together with its specific yield strength value. $\mu$is defined as the coefficient of friction, and is equal to 1.4λ for monolithically cast concrete, 1.0λ for concrete placed against hardened concrete with surface intentionally roughened, and 0.6λ for concrete placed against hardened concrete not intentionally roughened. The λ parameter depends on the concrete type. λ is 1.0 for normal weight concrete, is 0.75 for lightweight concrete. If normal weight and lightweight concrete is used together, the λ coefficient is determined according to the volumetric proportions of lightweight and normal weight aggregates, but cannot exceed a value of 0.85.

ACI 318M-08 also provides an upper bound for the shear friction capacity calculation based on to equation (5.4). For normal weight concrete either placed monolithically or placed against hardened concrete with surface intentionally roughened, V_n shall not exceed the smallest of $0.2f_c'A_c$, $(3.3 + 0.08f_c')A_c$ and $11A_c$. For all other cases, V_n shall not exceed the smallest of $0.2f_c'A_c$ and $5.5A_c$, where A_c is the area of the concrete section resisting shear transfer and f_c` is the compressive strength of concrete. It is stated in Section 6.4.4 of FEMA 356 that "shear-friction capacity shall be calculated according to ACI 318, taking into consideration the expected axial load due to gravity and earthquake effects," and ACI 318-08 Section 11.7.7 permits a permanent net axial compression force across a shear plane to be taken as additive to the force in the shear-friction reinforcement $A_{vf}f_y$.

Nominal shear friction capacities of all the wall specimen tested were calculated according to the code provisions described above, for monolithically-placed normal weight concrete, based on number and type of reinforcing bars across the wall-pedestal interface. The calculated shear-friction capacities of the specimens are listed in Table 5.3. The values

listed in the table show that all of the specimens have higher shear friction capacities compared with their FEMA 356 nominal shear strengths, with the exception of Specimen T3-S1, which suffered a sliding shear failure. This confirms the sliding shear failure observed in Specimen T3-S1. However, this specimen experienced sliding shear failure at a significantly lower lateral load level than its shear-friction capacity, indicating that the shear friction estimation of ACI 318 may be unconservative for walls with low amount of boundary reinforcement. This is consistent with prior experimental observations on squat walls by Orakçal et al. (2009).

6. ASSESMENT OF WALL LATERAL DEFORMATION CAPACITIES

The lateral load behavior and failure modes of all of the tested wall specimens were governed by shear. Therefore, all specimens exhibited brittle behavior overall. However, the behavior of the specimens was noticeably different from each other, in terms of deformation capacities. The displacement ductility capacities (μ) calculated for each specimen is presented in Table 6.1. The ultimate displacement, Δ_u, is considered as the displacement corresponding to the displacement at 80% of the lateral load capacity after load degradation has started. The yield displacement, Δ_y, is determined from the idealistic bilinear load displacement curve, as being the displacement at the yield strength. Idealistic load displacement curve was shown in Figure 1.2. Displacement ductility is the ratio of ultimate displacement to the yield displacement. It can be defined as the displacement capacity of the specimen at the ultimate load level without showing any significant capacity degradation. The cracking load and drift level (at first diagonal crack), as well as yield drift and ultimate drift levels are also provided in Table 6.1.

For all the tested specimens it can be concluded that the ductility properties were poor. Lateral load level degraded rapidly after reaching the lateral load capacity. Some of the specimens can be said to have relatively high ductility. Specimen T3, the one that experienced sliding shear mode of failure, had shown around two times higher ductility compared to other types. Also specimen T5 showed relatively high ductility compared to other 1 aspect ratio specimen. This is due to the low amount of vertical reinforcement leading to yielding of boundary and vertical bars onset of lateral load capacity. This yielding contributed to flexural top deformations increasing the displacement ductility of this specimen.

Table 6.1. Cracking shear and Displacement Ductility.

SPECIMEN	V_U, KN	V_{Cr}, KN	Cracking Drift (%)	Yield Drift (%)	Δ_y, mm	Ultimate Drift (%)	Δ_u, mm	μ
SW-T2-S1-1	798.6	254	0.1	0.8	6	1.2	10	1.67
SW-T2-S2-3	666.1	212	0.1	0.8	6	1.2	9	1.50
SW-T2-S3-4	813.3	380	0.1	0.4	3	1.2	9	3.00
SW-T3-S1-5	382.7	255	0.1	0.3	2.25	1.2	9	4.00
SW-T4-S1-6	874.1	360	0.05	0.4	2	1.4	7	3.50
SW-T5-S1-7	709.6	170	0.05	0.4	6	1.6	24	4.00
SW-T6-S1-8	735	140	0.05	0.6	9	1.4	21	2.33
SW-T1-S2-9	563	160	0.05	0.6	4.5	1.2	9	2.00
SW-T1-N5-S1-10	789	300	0.05	0.6	4.5	1.2	9	2.00
SW-T1-N10-S1-11	793	275	0.05	0.6	4.5	1.2	9	2.00
SW-T1-S1-2	635	180	0.05	0.8	5.9	1.2	10.2	1.73

6.1. FEMA-356 Backbone Curves

Experimental results obtained for the wall specimens were also used for comparison with the modeling parameters recommended in FEMA 356 and ASCE 41 documents, to be used in analysis procedures for performance assessment and rehabilitation of existing buildings. FEMA 356 defines several types of analysis procedures in Section 2.4 for performance evaluation of existing buildings, including the nonlinear static analysis procedure. Nonlinear static analysis is often used to simulate the seismic response of the structure under equivalent static seismic loading. In order to model a structural system to perform nonlinear structural analysis, the nonlinear force-deformation of the structural

elements should be represented with reliable behavioral models. The ideal way to calibrate the element models is to conduct cyclic tests on specimens representing each structural element, and obtains the experimental force-deformation envelope (called the backbone curve) of the elements. In the absence of test results, the generalized backbone curves defined in FEMA 356 are to be used for modeling purposes for nonlinear static analysis. These backbone curves are based on the nominal strength calculations; stiffness values, and modeling parameters (deformation parameters) defined in FEMA 356 recommendations. In Chapter 2.4 of FEMA 356, generalized force vs. deformation relationships are provided. Provided backbone relationships are used to determine modeling and acceptance criteria for deformation-controlled actions. The generalized backbone curves for shear-controlled and flexure-controlled responses in FEMA 356 are illustrated in Figure 6.1

In backbone curves shown in Figure 6.1, linear force-deformation response is assumed between point *A* (zero load) and the effective yield point *B*. The load effect (*Q*) is defined as normalized with respect to the effective yield force (or moment). The stiffness of the element within the linear portion of the response is defined in corresponding sections for different elements. The slope from *B* to *C* is a small percentage (0 – 10 %) of the elastic slope, and is included to represent behavioral phenomena such as strain hardening. *C* has an ordinate that represents the strength of the component and abscissa value equal to the deformation at which significant strength degradation has started. The line *CD* stands for the strength degradation and beyond point *D*, the component responds with substantially reduced strength (residual strength) up to point *E*. At deformations greater than point *E*, the load-carrying capacity of the element is zero.

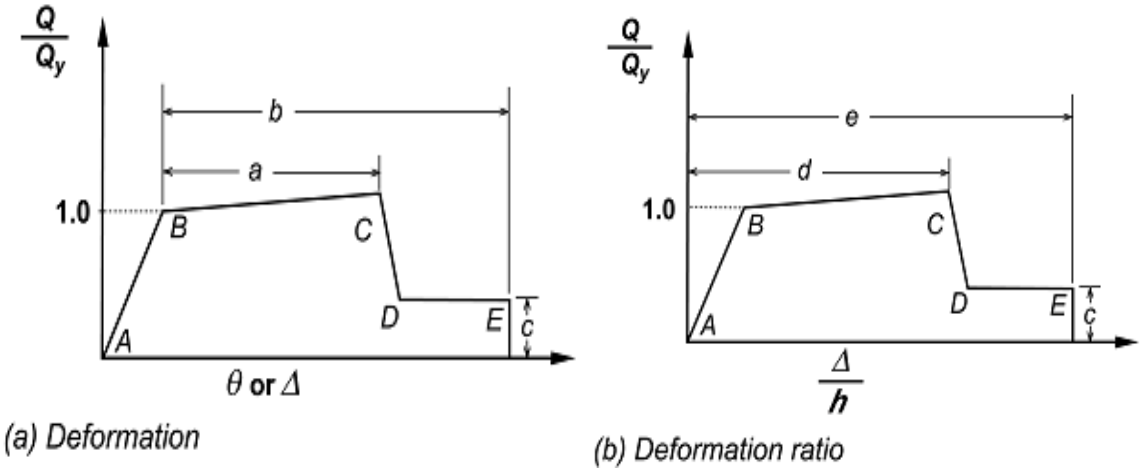

Figure 6.1. Generalized Force-Deformation Relations (FEMA-356).

A sharp transition between points *C* and *D* can result in computational difficulty or inability to converge when used as modeling input for nonlinear analysis software. Therefore, a small slope provided between points *C* and *D* to avoid such difficulty. The acceptance criteria can be prescribed in terms of deformations or deformation ratios (normalized deformation with respect to yield deformation). Elastic stiffness values and values for the parameters *a*, *b*, *c*, *d*, and *e*, which can be used for modeling of various structural components, are presented in Chapter 5 through 8 in FEMA 356.

It is also stated in FEMA 356 that an idealized lateral force – deformation backbone curve can be determined from the experimental data. The procedure is defined in Section 2.8.3 of FEMA 356 for determining modeling parameters and acceptance criteria based on experimental data. The backbone curve based on experimental load – deformation data shall be drawn using points at the intersection of the first loading cycle to the $(i)^{th}$ drift level with the second unloading cycle from the $(i-1)^{th}$ drift level. The backbone curve derived using this approach shall be approximated by linear segments joining the intersection points. As a result, a multi-segmented backbone curve shall be drawn.

6.2. Modeling Parameters for Structural Walls

As mentioned above, the modeling parameters in FEMA 356 are defined differently for different structural components and material types. In Chapter 6 of FEMA 356, modeling parameters for reinforced concrete components are provided. The code provides

backbone curves for various type of structural components, the responses of which are controlled by either shear or flexural deformations. Table 6.18 provides plastic hinge rotation values and residual strength ratios (Figure 6.1(*a*); parameters *a*, *b* and *c*) for structural walls, columns supporting walls, and coupling beams controlled by flexure. Table 6.19 reports the modeling parameters *c*, *d*, and *e* denoted in Figure 6.1(*b*), for structural wall members controlled by shear. This experimental study concentrates on the behavior of squat walls, and in general, the failure mode of the wall specimens was shear failure. Therefore, the modeling parameters defined in Table 6.19 were used for comparison of the test results with the FEMA 356 backbone curves. According to Table 6.19 of FEMA 356, for structural walls d = 0.75%, *e* = 2% and *c* = 0.4. These parameters indicate that the strength degradation starts at 0.75% drift level, followed by a strength drop to a residual strength level, which is 40% of the maximum strength, and is maintained up to 2 % drift level. Since strain hardening effects are typically not observed in squat wall behavior, no strain hardening is considered in the backbone curves, after the yield point. Therefore, segment *BC* on the backbone curve is horizontal, at the nominal shear strength level. Segment *CD* on the backbone curve is drawn as a sudden vertical drop, as stated in FEMA 356.

In Section 6.4, use of the Type II curve (Figure 6.1 (*b*) for reinforced concrete components, is described. It is stated that parameters d and e refer to the total deformations measured from the origin. Parameters *c*, *d* and *e* are defined numerically in corresponding tables, for different type of components. Alternatively it shall be permitted to determine these parameters directly from analytical procedures justified by experimental evidence. Based on that statement, alternative modeling parameters have been developed by Wallace et al. (2006), part of which were reported in ASCE/SEI 41 Supplement 1.

6.2.1. ASCE 41 Modified Backbone Curves for Squat Walls

ASCE/SEI 41 backbone curve definitions and parameters are identical to those in FEMA 356. However, in the ASCE/SEI 41 Supplement 1, a number of modifications were proposed to the modeling parameters and acceptance criteria for squat structural walls.

Although the terms squat and slender are not explicitly defined in Section 6.7 of ASCE/SEI 41, in C6.7.1 of the commentary, it is stated that structural walls shall be considered as slender (normally controlled by flexure) if their aspect ratio (height/length) is greater than 3.0, and short or squat (normally controlled by shear) if their aspect ratio is smaller than 1.5. Modifications proposed in Supplement 1 include revision of the load–deformation backbone relationship for shear-controlled walls.

Research by Wallace et al. (2006) has demonstrated that the current bilinear elastic – perfectly plastic envelope curve prior to strength degradation does not well represent the behavior of shear-controlled walls. The alternative tri-linear backbone curve (prior to strength degradation) shown Figure 6.2 was proposed to model shear-controlled wall behavior, in order to account for the softening of the backbone curve after first diagonal cracking has occurred. The proposed curve incorporated an initial elastic stiffness (*AF*) up to the 60% of the expected nominal shear strength, followed by a reduced (post-cracked) stiffness (*F-B*) reaching the nominal shear strength at a total deformation ratio 0.4%. The parameter d is increased to 1% drift level and residual strength for walls with axial loads below $5\%f_c'A_g$ reduced from the value of 0.4 specified in FEMA-356 for all walls controlled by shear to 0.2.

Changes to acceptance and modeling criteria for walls controlled by shear were proposed to reflect previous experimental results (Hidalgo et al., 2002, Wallace et al., 2006). While FEMA 356 had only one category encompassing all walls regardless of axial load, modifications proposed in ASCE 41 Supplement 1 to Table 6.19, subdivide shear-controlled walls into two categories; one for walls with low axial loads and another for walls with significant axial load demands. This change is based on tests on wall piers carried out by Wallace et al. (2006), which showed reduced wall deformation capacity for axial loads equal to or greater than $5\%f_c'A_g$ (Wallace et al., 2006). The same tests showed negligible residual strength for walls with axial loads greater than $5\%f_c'A_g$, leading to additional proposed modifications. Based on the tests by Wallace et al. (2006), it was proposed that the residual strength coefficient for walls with axial loads equal or greater than $5\%f_c'A_g$ be reduced from the value of 0.4 specified in FEMA 356 for all walls controlled by shear, to zero at 1% drift level. Although experimental evidence substantiates a residual strength coefficient of 0.4 for well-detailed squat walls with zero axial load, the

tests by Wallace et al. (2006) indicate that the residual strength may be significantly lower for axial loads near 5%$f_c'A_g$, and for walls with poor detailing.

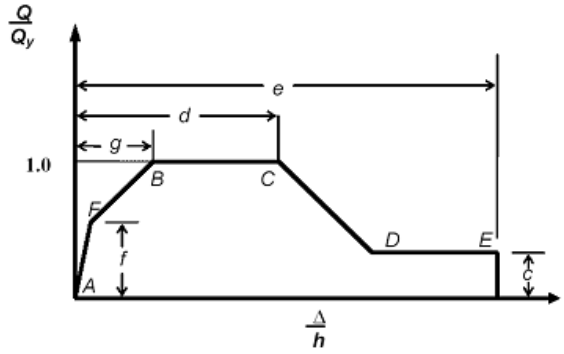

Figure 6.2. Modified Trilinear Backbone Curve for Shear Controlled Walls.

In the supplement it is also proposed that section 2.8, which provides instructions to draw multi segmented backbone relations from experimental data, should be modified. Research done by Massone, (2006) has shown that the FEMA-356 procedure for obtaining experimentally obtained backbone curves exaggerates the rate of strength degradation. Therefore in the supplement it is proposed that the backbone curves can be drawn through the peak displacement points of the first cycles of each drift levels.

6.3. Backbone Curves and Experimental Observations

The specimens tested in the experimental program showed a linear elastic load-displacement response during the initial drift levels. The specimens were carefully monitored through cycles to be able to relate stiffness degradation with formation of the first diagonal crack, in order to evaluate the modifications proposed in ASCE 41 Supplement 1 to the backbone curves. According to the modified backbone curves, a stiffness decrease should be expected at approximately 60% of the wall lateral load capacity, due to diagonal cracking. The test results have also shown that the lateral stiffness of the specimens reduced significantly due to formation of the first diagonal tension crack.

For the first set of tests, the first diagonal tension cracks formed at the 0.1% drift level, corresponding to approximately 30% of their lateral load capacities. The first set

specimens have reached their maximum lateral load capacities at 1.0% – 1.2% drift levels. Drift levels larger than 1.2 % resulted in permanent strength degradation. For the second set of tests, the first diagonal cracks formed at the 0.05% drift level, corresponding to approximately 45% of the lateral load capacities. They reached their ultimate capacity at the 0.6% drift level. Drift levels larger than 0.8% resulted in strength degradation. ,

The second set of specimens reached the first diagonal cracking point and the lateral load capacity at the earlier drift levels. This may be due to the difference in concrete stiffness between two sets, since the second set of specimens had higher concrete strength. This may have caused reaching higher stresses at an earlier drift levels. Only the Type3 specimen in the second set experienced first cracking at 0.05% drift level, as formation of a flexural crack.

For the third set of specimens, initial diagonal cracks formed at 0.05% drift level, at approximately 35% of the lateral load capacities. These specimens reached their lateral load capacity at 1% drift level, and drift levels of 1.2% and higher resulted in rapid strength degradation.

Table 6.2 shows the failure modes and residual strength characteristics for all of the wall specimens tested. For most of the specimens residual strength level comes out to be smaller than 15% of the lateral load capacity of the specimen. Most of the time residual there was no constant strength at the residual, the load level was gradually degrading. This leads us to use the average lateral load values at the residual strength level.

In the following sections, the lateral load-displacement curves of all the wall specimens, as well as the experimentally obtained backbone curves, were compared with the current (FEMA 356) and modified (ASCE 41 Supplement-1) backbone relationships. The experimental backbone curves were drawn per recommendations provided in the ASCE41 Supplement 1, using the maximum displacement point at the first loading cycle of each drift level. In the FEMA 356 and ASCE 41 backbone relationships, the lateral load capacity of the wall is defined per the FEMA 356 nominal shear strength calculation described in the previous chapter.

Table 6.2. Failure Modes and Residual Strength Characteristics.

SPECIMEN	V_U, KN	$V_{Residualr}$, KN	% of V_U	Δ_r, mm	Δ_{ru}, mm	μ_r	Failure Mode
SW-T2-S1-1	798.6	82	10.3	14.6	18	1.23	Diagonal Compression
SW-T2-S2-3	666.1	66	9.9	13.4	53.8	4.01	Diagonal Compression
SW-T2-S3-4	813.3	68	8.4	14.5	17.5	1.21	Diagonal Compression
SW-T3-S1-5	382.7	0	0.0	-	-	-	Sliding Shear
SW-T4-S1-6	874.1	226	25.9	12	19.7	1.64	Diagonal Compression
SW-T5-S1-7	709.6	410	57.8	30	48	1.60	Diagonal Compression
SW-T6-S1-8	735	70	9.5	27	54	2.00	Diagonal Compression
SW-T1-S2-9	563	265	47.1	15	36	2.40	Diagonal Tension
SW-T1-N5-S1-10	789	80	10.1	15	24	1.60	Diagonal Tension
SW-T1-N10-S1-11	793	0	0.0	-	-	-	Diagonal Tension
SW-T1-S1-2	635	107	16.9	17	52	3.06	Diagonal Tension

Most of the specimens showed very low residual capacity and degrading residual lateral strength. Backbone relationships of the specimens were used to determine the starting point of the residual strength portion of the curve. The transition point at the transition from load degradation portion to residual plateau is defined as the starting point of the residual strength level. The displacement at that transition point was denoted as Δ_r. The ultimate displacement observed during the test is denoted as Δ_{ru}. The residual strength was calculated as the average of all lateral loads between Δ_r and Δ_{ru} in both positive and negative directions. Also a quantitative parameter μ_r is introduced to define the ductility characteristics at the residual strength level. All the above mentioned quantities for all specimens were presented in Table 6.2. It should be mentioned that the actual residual

ductility, μ_r, can be greater than the values reported in Table 6.2 for specimens T1-S2 and T5-S1, since these specimens retained their residual capacity at the end of the test.

6.3.1. Backbone Relationships for Type-1 Specimens

The experimental backbone curves of Type1 specimens were compared with the backbone relationships recommended in FEMA 356 and ASCE 41 Supplement1. Figure 6.3 compares the backbone relationships for Type1-Specimen1.

The shear strength estimation of FEMA 356 shows good agreement with the experimental results. The modified backbone relationship (ASCE-41) can better represent the degradation of the wall stiffness after first cracking. The first main diagonal shear crack formed at 0.2% drift level and at 55% of the lateral load capacity.

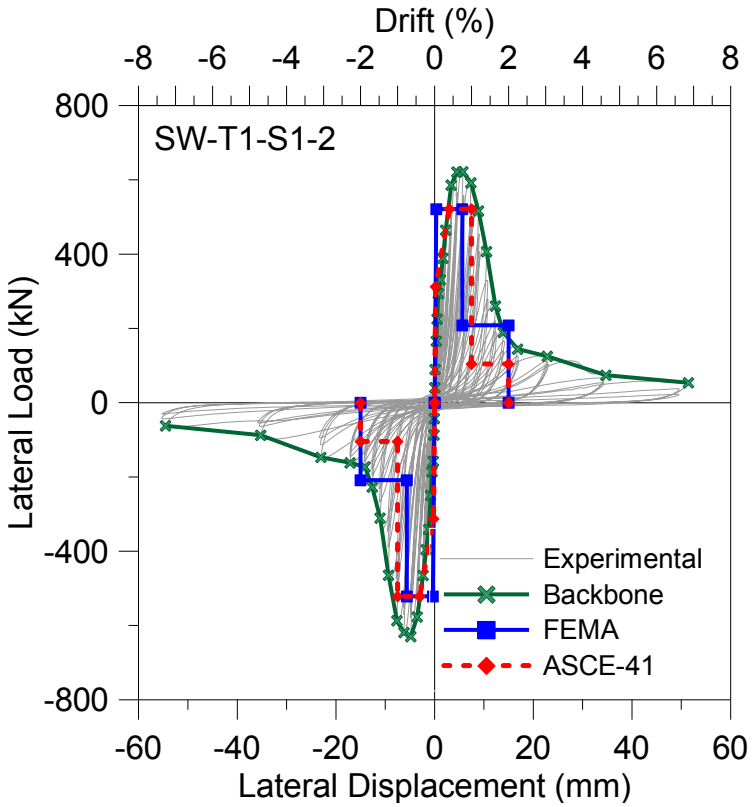

Figure 6.3. Shear-Controlled Response, Backbone Curve and Modeling Criteria, T1-S1.

The ASCE41 Supplement 1 backbone relationship can better represent the ductility of the wall at lateral load capacity, since strength degradation is defined at 1% drift. On the

other hand, both FEMA and ASCE-41 curves cannot accurately represent the deformation attributes of the wall at post-peak load levels. After reaching its lateral load capacity, the strength of the specimen degrades gradually with increasing drift levels. Using a straight-line segment from 1% drift level at capacity load to 2% drift level at zero load can better represent this response.

Figure 6.4 shows the backbone relations and modeling criteria for Type1-Specimen2. This specimen has similar geometric and material properties with Specimen1, but boundary reinforcement was confined. For this specimen, the modified (ASCE-41) backbone curve provides a better estimate of the deformation behavior. The main diagonal crack formed at 1% drift level at a load level 35% of the lateral load capacity. A residual strength of approximately 40% of the lateral load capacity was reached at 2% drift level, and the specimen maintained its residual strength up to 4.8% drift. The improved ductility and residual capacity of the specimen may be attributed to the confined boundary regions.

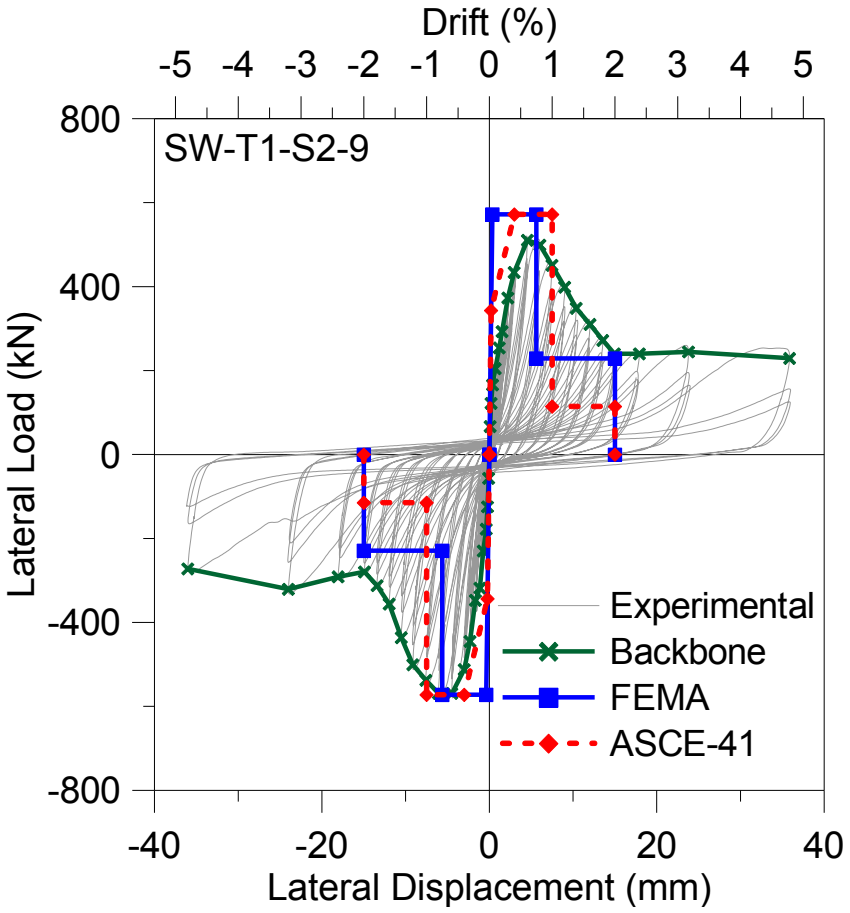

Figure 6.4. Shear-Controlled Response, Backbone Curve and Modeling Criteria, T1-S2.

Figure 6.5 shows the backbone relations for the Type-1 specimen (T1-N5-S1) tested under an axial load level of 5% of its axial load capacity. The lateral load capacity of the specimen was higher by 25%, with respect to Type1-Specimen1. The lateral load capacity estimation of FEMA 356 is conservative, since it does not consider the effect of axial load on lateral load capacity. The stiffness estimation of the modified (ASCE 41) backbone relationship appears to be in good agreement with the test results. After the capacity is reached, the lateral strength of the specimen degrades rapidly and reduces to almost zero at the 3.2% drift level, without showing any residual capacity.

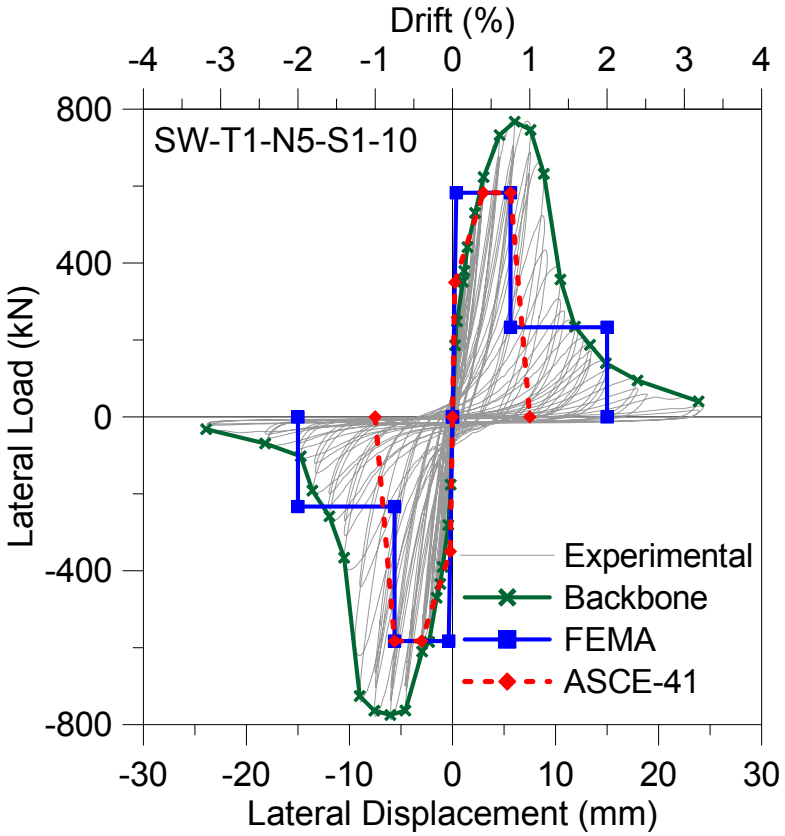

Figure 6.5. Shear-Controlled Response, Backbone Curve and Modeling Criteria, T1-N5-S1.

Figure 6.6 shows the backbone relations for Type1-N10-Specimen1, which was tested under an axial load level of 10% of its axial load capacity. The lateral load capacity of this specimen was reached at 1% drift level, at approximately the same lateral load with the 5% axial load level specimen. However this time the lateral strength decreased much more suddenly, to 10% of its capacity, immediately after the 1% drift level. As well, the specimen did not show any significant residual strength capacity.

Experimentally observed lateral load – deformation relationships were better represented by ASCE41 backbone estimations. Test results confirmed that there is no significant residual strength for the specimens tested under axial load levels of 5% or greater. However it is better to drop the lateral load level to zero at 1.5% drift level.

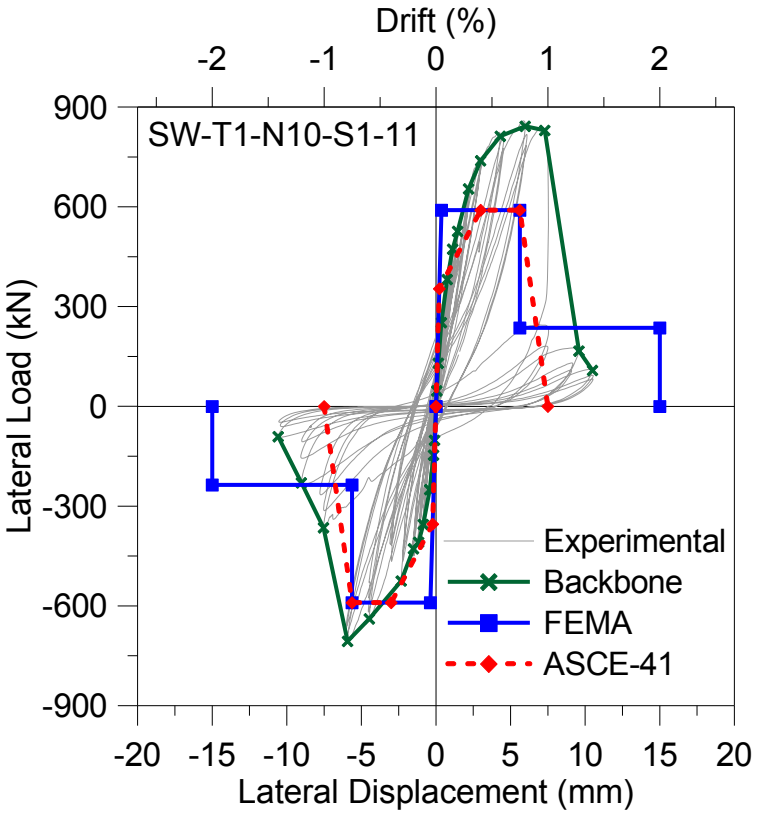

Figure 6.6. Shear-Controlled Response, Backbone Curve and Modeling Criteria, T1-N10-S1.

6.3.2. Backbone Relationships for Type-2 Specimen

Type2 specimens have 0.68% reinforcement ratio for both vertical and horizontal directions. Three identical specimens have been tested. However, there were problems related to placement of concrete, for Type2 Specimens 1 and 2. Therefore, the first two specimens were not used for backbone comparisons. Figure 6.7 shows the backbone relationships for Type2 Specimen3. The lateral load capacity was reached at 0.6% drift level. The FEMA 356 shear strength estimation is in agreement with the experimental result. The first main diagonal crack has formed at 0.15% drift level at 56% of the ultimate load capacity. The modified (ASCE 41) backbone relationship can realistically capture the

degradation of the stiffness, as seen from the figure. The residual strength of the specimen is below 10% of the lateral load capacity. Although the modified backbone relationship represents the strength degradation characteristics of the specimen, the residual strength of the specimen was significantly lower than the code backbone relationships. A better representation of the experimental backbone curve can be achieved by using a linear variation from the strength degradation point (1% drift) to zero capacity, once 2% drift level has reached. It must be mentioned that although not compared here, the other two Type2 specimens showed somewhat similar strength degradation characteristics. They lateral load drops to a level of approximately 10% of the capacity, which can be deemed as negligible residual strength, at around 2% drift level.

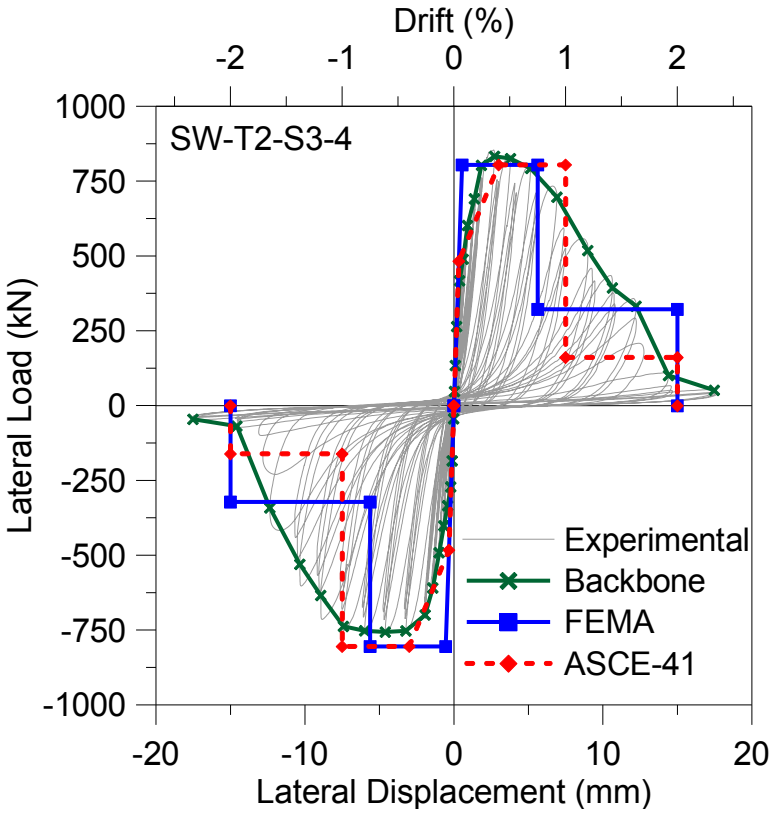

Figure 6.7. Shear-Controlled Response, Backbone Curve and Modeling Criteria for T2-S3.

ASCE 41 better represents the ductility characteristics of the specimen. However it is better to linearly drop the lateral load level from capacity at 1% drift level to zero at 2% drift level.

6.3.3. Backbone Relationships for Type-3 Specimen

The Type3 specimen has the same amount of web horizontal and vertical web reinforcement ratios (0.68%) as the Type2 specimens. However, the low amount of boundary reinforcement used in this specimen caused initial cracking to occur under flexure at the wall bottom, and ultimately a premature sliding shear failure at the wall-pedestal interface. Figure 6.8 shows the backbone relationships of the Type3 specimen.

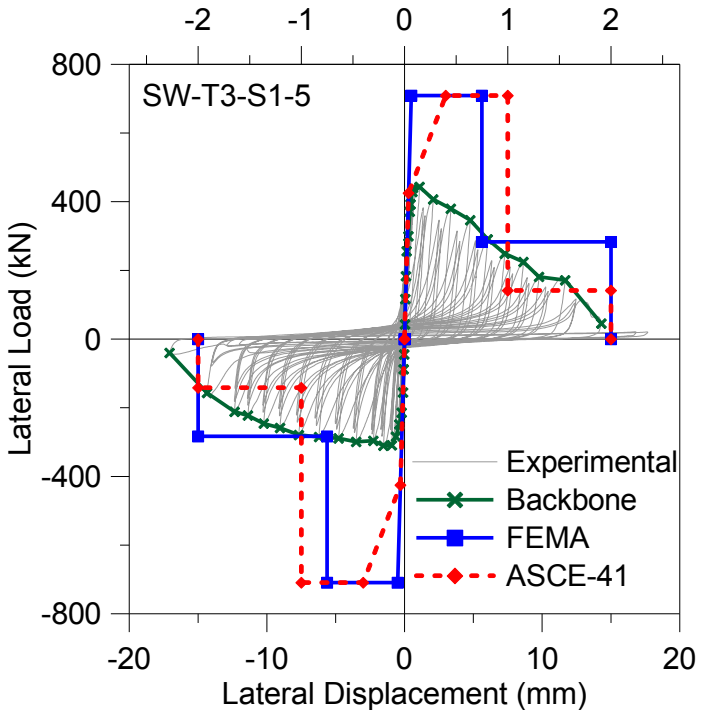

Figure 6.8. Shear-Controlled Response, Backbone Curve and Modeling Criteria, T3-S1.

The first interface crack on the specimen formed at 1% drift level, at 65% of the lateral load capacity. The wall specimen did not experience any diagonal cracking or significant shear deformation. The specimen reached its lateral load capacity at 0.6% drift. The shear strength of the wall in the FEMA 356 and ASCE 41 backbone relationships was estimated using the shear-friction capacity calculation procedure provided in ACI318. As discussed previously, the shear friction capacity of the specimen was hugely overestimated by the ACI318 procedure. In terms of load-deformation behavior, the FEMA356 and ASCE41 backbone relationships failed to represent the test results, which is expected since the response of the wall is not shear-controlled, by definition.

6.3.4. Backbone Relationships for Type-4 Specimen

The type-4 specimen is the shortest specimen tested in the scope of this experiment. The wall has 500 mm height and 1500 mm length. The web reinforcement ratio in the longitudinal and horizontal direction is 0.68%, being same as the type-2 and type-3 specimens. The specimen has four-ϕ14 boundary reinforcement, which makes its flexural capacity and sliding shear capacity much higher than the diagonal shear capacity. This specimen has failed under diagonal shear.

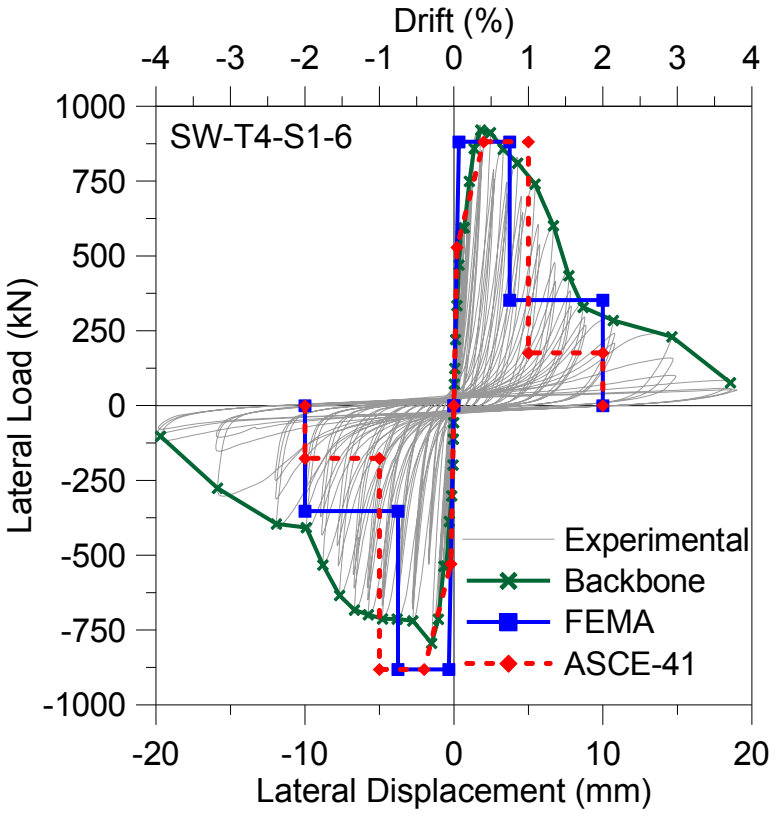

Figure 6.9. Shear-Controlled Response, Backbone Curve and Modeling Criteria for Type-4 Specimen.

The shear strength calculation using FEMA356 code provisions shows good agreement with the test results. The experimental lateral load capacity is almost same as the shear strength calculation according to FEMA. After reaching the ultimate load level the specimen immediately started to lose its lateral strength. But the strength degradation has occurred gradually. There is no instantaneous decrease in the lateral strength that resembles the code backbone models. The first diagonal tension crack has occurred at 0.15

% drift level at 60% of the lateral load capacity. The softening portion of the modified backbone model resembles the real softening of the stiffness after first crack. The specimen does not have a significant residual strength capacity. After gradual strength degradation the specimen loses 60% of its lateral load capacity at around 2% drift level and then it loses 90% of its capacity at around 4% drift level. Therefore using a linear variation from the degrading point to 2% drift level can better represent the energy dissipation capacity.

6.3.5. Backbone Relationships for Type-5 Specimen

The type-5 specimen has 1 height/ length ratio. It has 0.68% transverse web reinforcement ratio and 0.34 % vertical web reinforcement ratio. However, it still has flexural capacity being greater that the shear capacity of the wall.

Figure 6.10 shows the backbone relation of the type-5 specimen. The failure of the wall has been dominated by diagonal tension mode. Therefore the shear strength formula given in FEMA356 provided a good estimate of the lateral capacity. The first diagonal tension crack has occurred at 0.15% drift level at 48% of lateral load capacity. After the formation of the first crack, successive diagonal cracks had occurred and the existing cracks started to widen. Although the failure mechanism has been dominated by shear, the flexural component of the lateral deformation is about 50% of the total lateral deformation. This means that the wall has failed under the combined action of shear and flexure. After the initiation of the first crack the stiffness has been decreased but not as much as the previous ones. The modified backbone curve has overestimated the stiffness degradation. The FEMA 356 backbone model shows a better agreement with the experimental stiffness up to capacity. Both FEMA and ASCE41 gives over-conservative ductility estimations for this specimen.

6.3.6. Backbone Relationships for Type6 Specimen

Type6 specimen has 0.68% reinforcement ratio in both vertical and horizontal directions. Wall aspect ratio (height/length) is 1.0. The specimen has shown diagonal compression failure mode. The diagonal cracks formed but at the ultimate load level at 1% drift level the bottom corners crushed due to diagonal compression.

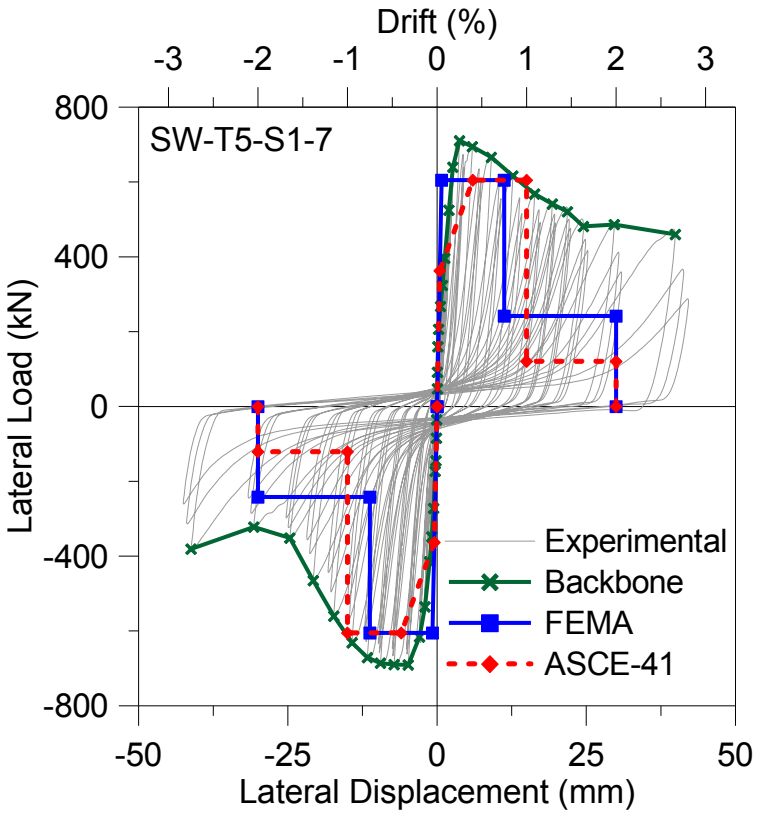

Figure 6.10. Shear-Controlled Response, Backbone Curve and Modeling Criteria for Type-5 Specimen.

Figure 6.11 shows the backbone relations and modeling criteria for Specimen T6-S1. It can be seen that the capacity of the specimen is well estimated. On the other hand, stiffness degradation at 60% of the capacity seems a little late. The stiffness degraded at 0.05% drift level at 20% of the lateral load capacity. The estimated backbone curve for both FEMA 356 and ASCE-41 suplement1 remains outside the experimental backbone curve. However these estimations shall provide more conservative capacities and stiffness. In terms of residual strength same comments can be made as the type2 specimens. The residual capacity attained at 1.8% drift level at a load level below 10% of the lateral load capacity. Therefore modeling criteria estimations was too high.

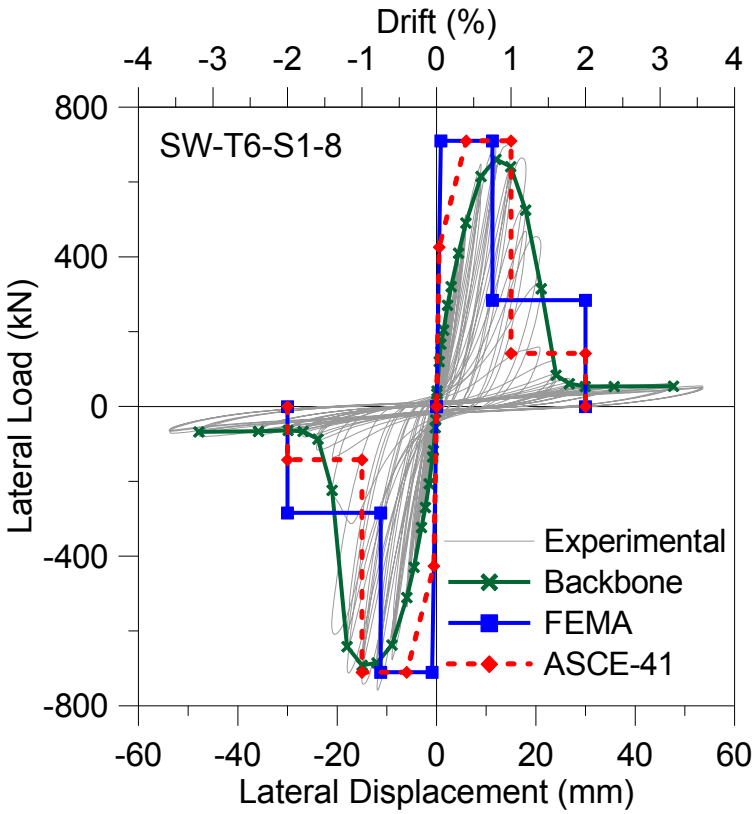

Figure 6.11. Shear-Controlled Response, Backbone Curve and Modeling Criteria, T6-S1.

7. CONCLUSIONS

The objective of this experimental study was to investigate the lateral load behavior of squat structural walls, for better understanding and representation of their lateral load capacity, ductility, and residual capacity, as well as their behavioral characteristics and different failure modes. The wall specimens investigated were differentiated by their aspect ratios, amounts of horizontal and vertical web reinforcement, amounts of boundary reinforcement, and axial load levels. The results and conclusions of this study can be summarized as below:

- The behavior and failure modes of all the test specimens investigated were shear-controlled. The three types of failure were observed for the test specimens included diagonal tension failure (associated with crushing along diagonal struts), diagonal compression failure (crushing at bottom corners propagating along the wall base), and sliding shear failure at wall base, triggered by flexural cracking and yielding of boundary reinforcement.

- It was observed that the horizontal and vertical web reinforcement ratios of the walls are critical in determining whether a diagonal tension failure or a diagonal compression failure will develop. In these tests, regardless of the wall aspect ratio and axial load level, specimens with 0.34% web reinforcement ratio (both horizontal and vertical) experienced diagonal tension failure, whereas specimens with 0.68% web reinforcement ratio experienced diagonal compression failure.

- Comparing the test results for the specimens with aspect ratio of 1.0, the vertical web reinforcement amount was found to influence both the lateral load capacity and the distribution of the diagonal cracks. Increased vertical web reinforcement ratio resulted in an increase in the lateral load capacity, and also provided a more uniformly distributed diagonal crack pattern.

- It was observed that using a low amount of longitudinal boundary reinforcement can cause a premature sliding shear type of failure at the interface of the wall, triggered by flexural cracking and yielding of boundary longitudinal reinforcement.

- The lateral load – displacement behavior of all specimens were dominated by shear deformations. Lateral load degradation was rapid after the lateral load capacity was reached. In general, the specimens showed poor ductility characteristics, as expected for squat walls. The specimen with confined boundary zones showed better ductility characteristics at the residual strength level. However confinement at the boundaries did not increase the lateral load capacity. For squat walls experiencing diagonal tension or diagonal compression failure, confinement of wall boundaries seems to increase the residual load capacity of the wall, as well as ductility characteristics at the residual load level.

- It was observed that axial loading on a squat wall increases its lateral load capacity, but has negative effect on ductility characteristics and the residual capacity. Axially-loaded walls showed significantly lower residual load capacities and poor ductility characteristics, compared with the zero-axial-load specimens that failed in diagonal tension. As well, it was observed that higher levels of axial load on a wall (e.g., 10% of axial load capacity) can results in a very rapid degradation of the lateral load capacity.

- The nominal shear strength calculations recommended in FEMA356 (or ASCE41) provided reasonable accurate and slightly conservative lateral load capacity predictions, for the specimens experiencing diagonal tension and diagonal compression modes of failure, and no axial load. For walls with very low amounts of boundary reinforcement, which are prone to a sliding shear type of failure triggered by flexural cracking, both the FEMA356 shear strength calculation procedure and the ACI318 shear friction capacity equation may give unconservative predictions of the lateral load capacity. On the other hand, for walls subjected to axial load, FEMA356 shear strength predictions become over-conservative, since the influence of axial load is neglected in the calculations.

- The force-deformation backbone relationships provided in FEMA356 and the modified backbone relationships presented in ASCE41-Supplement1 were in reasonable agreement with the test results. However, the initial stiffness and ductility capacity modifications in the ASCE41-Supplement1 backbone relations are more representative for test results. However, for walls experiencing diagonal compression failure, the ASCE41-Supplement1 backbone relationships provide an unconservative estimate of the residual capacity. Overall, for shear-controlled walls subjected to no axial load, it is recommended that the backbone relationships are ASCE41-Supplement1 are used, with the only modification that the lateral load degrades gradually (along a straight line) from the lateral load capacity at 1% drift level to zero at 2% drift level.

- On the other hand, for walls subjected to axial load, the backbone relationships presented in ASCE41-Supplement1 may be over-conservative in predicting the ductility characteristics, since they consider a very sudden degradation in lateral load, which is not the experimentally-observed case for walls subjected to moderate axial load levels ($5\%A_g f'_c$). Overall, for shear-controlled walls subjected to axial load, it is recommended that the backbone relationships of ASCE41-Supplement1 are used, with the only modification that the lateral load degrades gradually (along a straight line) from the lateral load capacity at 1% drift level to zero at 1.5% drift level.

As recommendations for future studies, further experimental research can be conducted on investigating the lateral load – deformation response of squat structural walls with high web reinforcement ratios (e.g. 0.68%), which would likely experience a diagonal compression mode of failure, under various axial load levels. This would allow evaluation of the FEMA356 and ASCE41 lateral load capacity calculations and load–deformation backbone relationships, also for axially-loaded walls failing under diagonal compression. As well, additional squat walls with intermediate amounts of boundary (as well as web) reinforcement can be tested to assess the limiting reinforcement ratios, which would trigger a premature sliding shear failure mode. Finally, the extensive experimental data and local deformation measurements provided in this study can be used for development and experimental verification of new analytical modeling approaches to

predict the reversed cyclic lateral load behavior of shear-controlled wall elements, as well as for evaluation of the accuracy of existing analytical modeling methodologies.

APPENDIX A: GRAPHS

A.1. Lateral Load – Top Displacement Relations

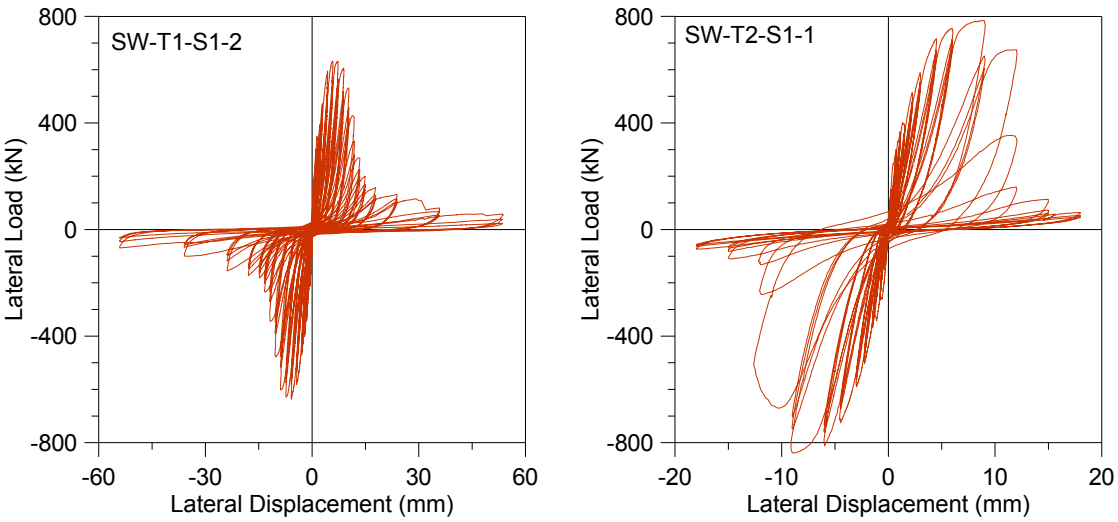

Figure A. 1. Load – Top Displacement, Specimen T1-S1 and T2-S1.

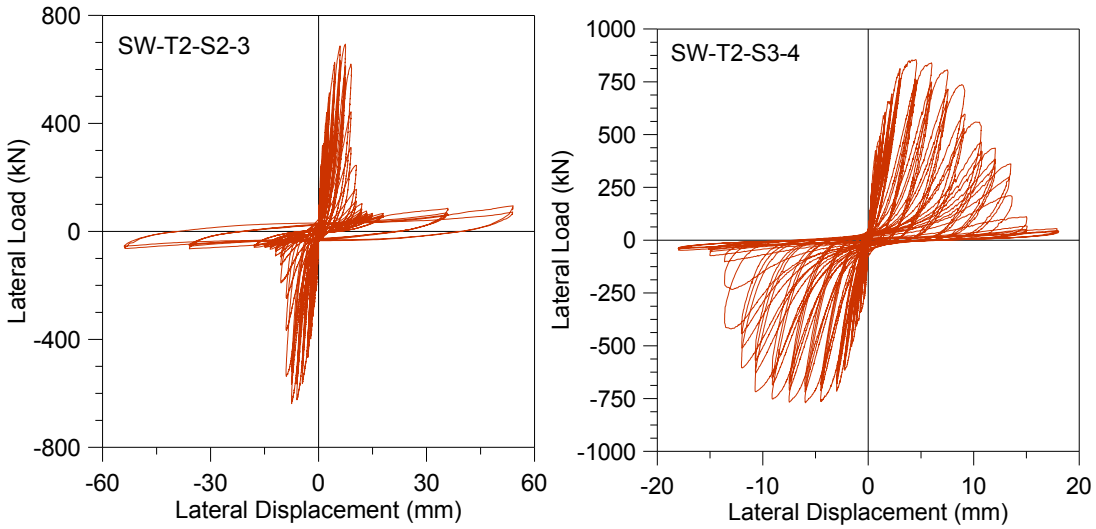

Figure A. 2. Load – Top Displacement, Specimen T2-S2 and T2-S3.

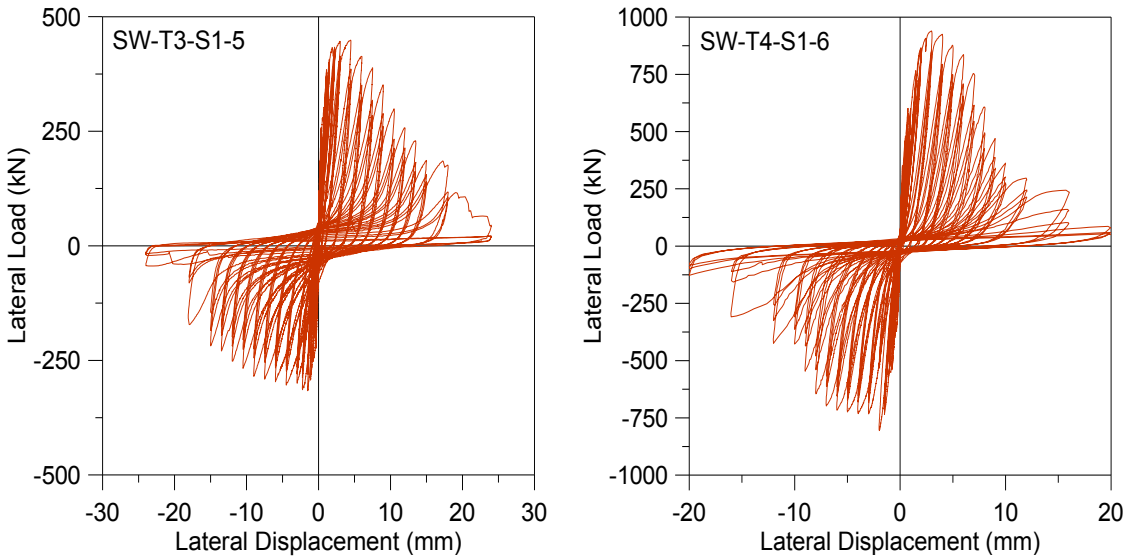

Figure A. 3. Load – Top Displacement, Specimen T3-S1 and T4-S1.

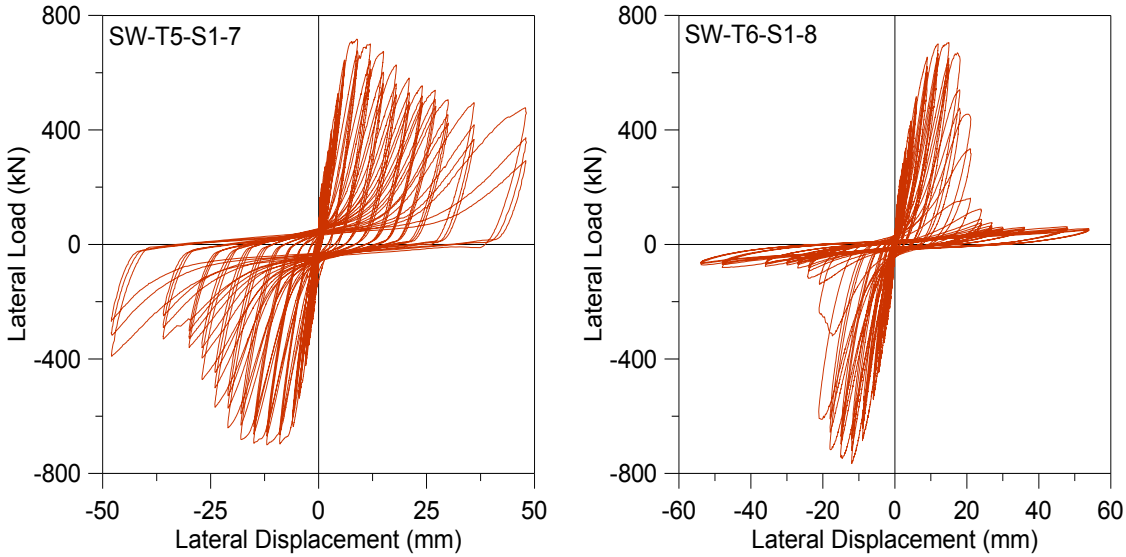

Figure A. 4. Load – Top Displacement, Specimen T5-S1 and T6-S1.

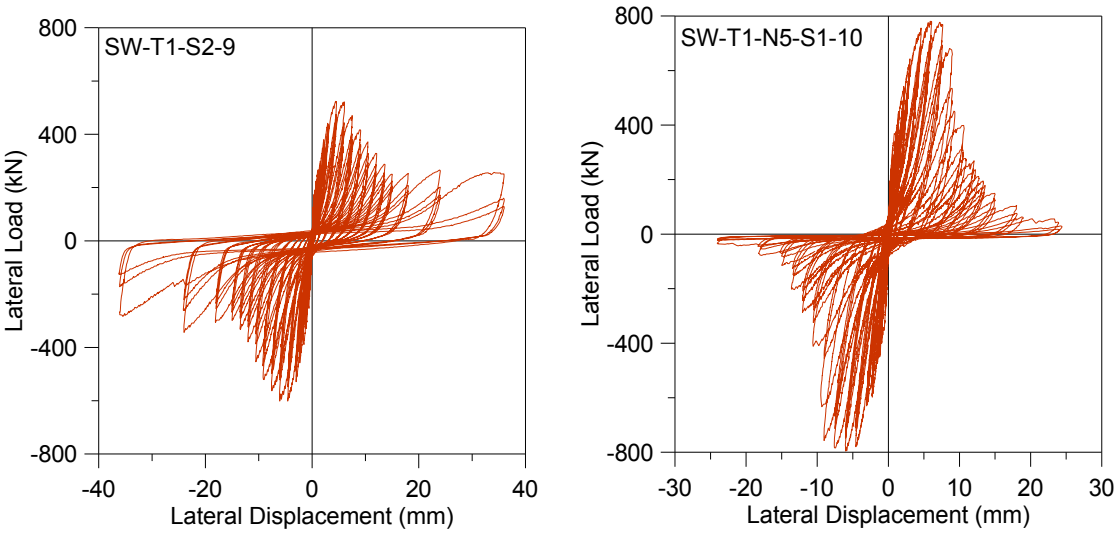

Figure A. 5. Load – Top Displacement, Specimen T1-S2 and T1-N5-S1.

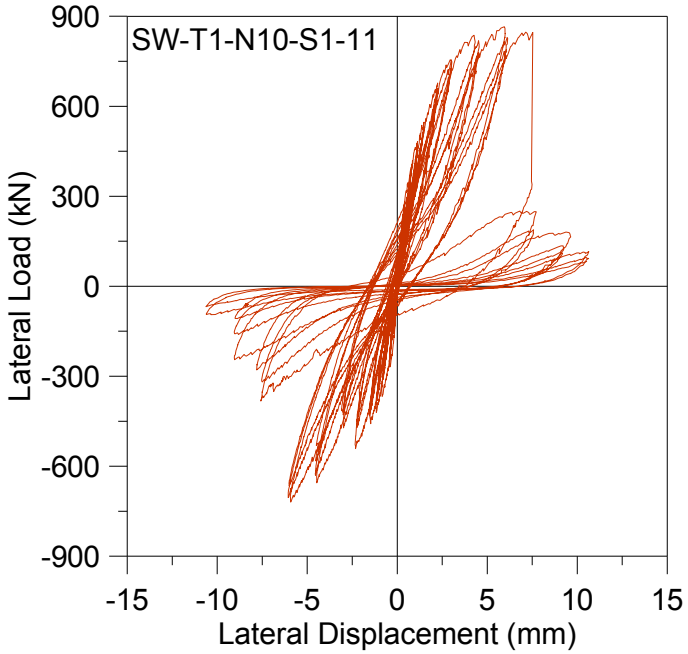

Figure A. 6. Load – Top Displacement, Specimen T1-N10-S1.

A.2. Top Lateral Deformation Components, Specimen T2-S2

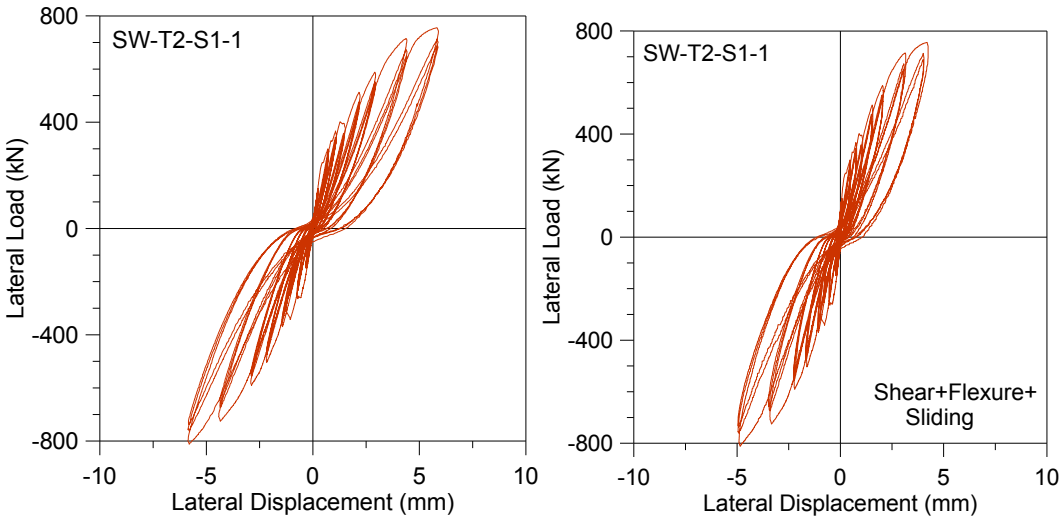

Figure A. 7. Top Lateral Deformation from External and Local Sensors, Specimen T2-S1.

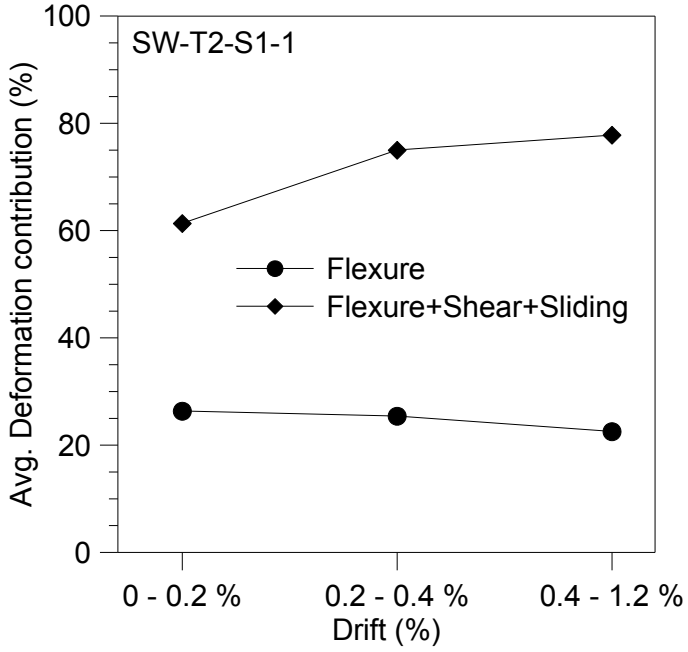

Figure A. 8. Average Deformation Contribution, Specimen T2-S1.

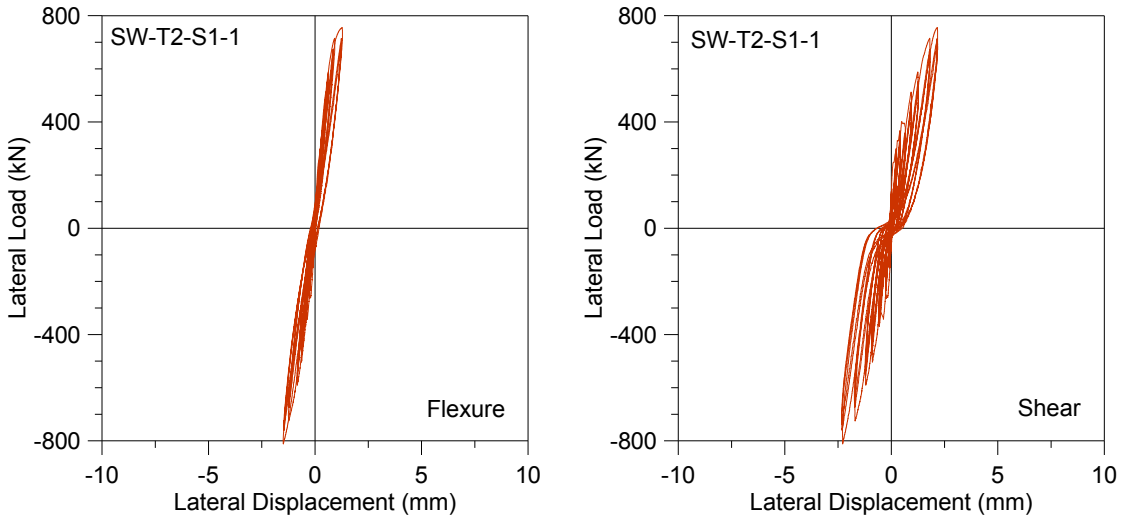

Figure A. 9. Top Lateral Flexure and Shear Deformation, Specimen T2-S1.

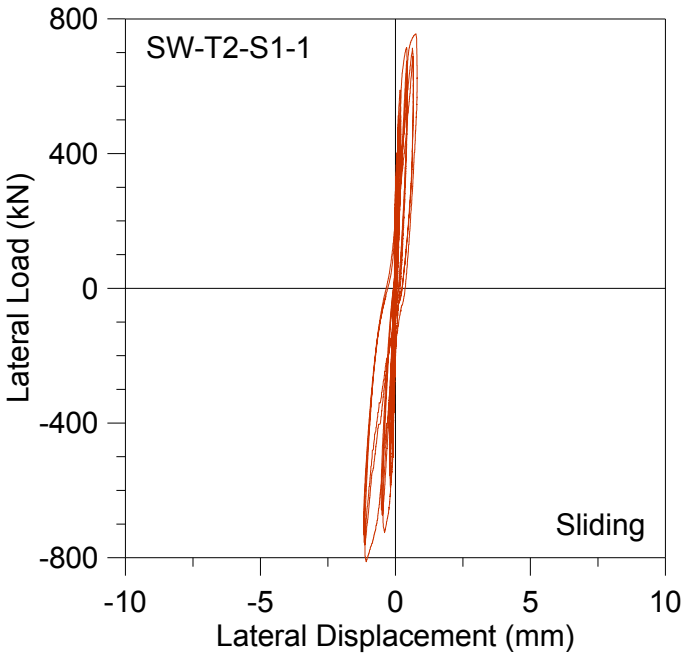

Figure A. 10. Sliding Deformation, Specimen T2-S1.

A.3. Top Lateral Deformation Components, Specimen T2-S3

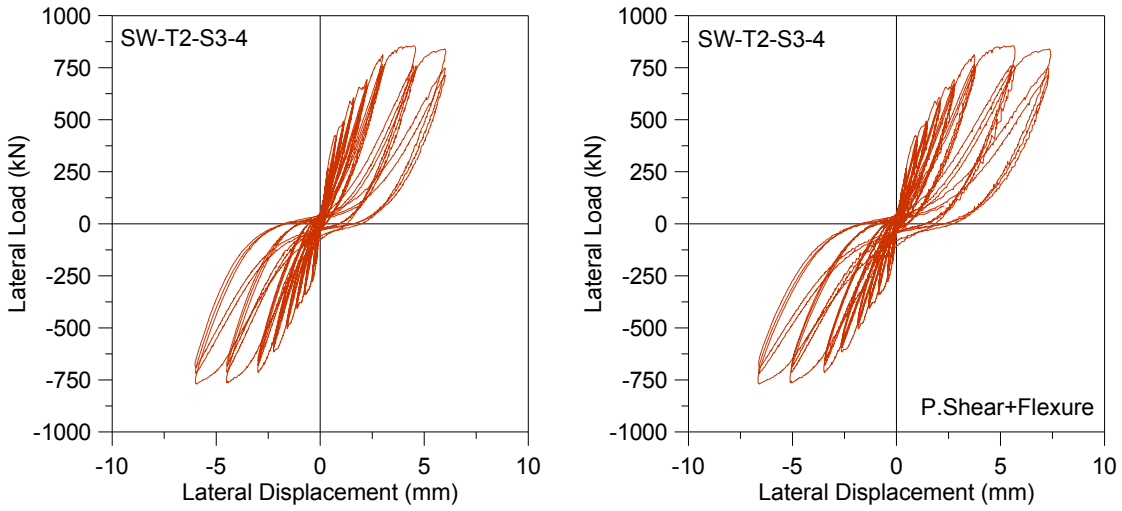

Figure A. 11. Top Lateral Deformation from External and Local Sensors, Specimen T2-S3.

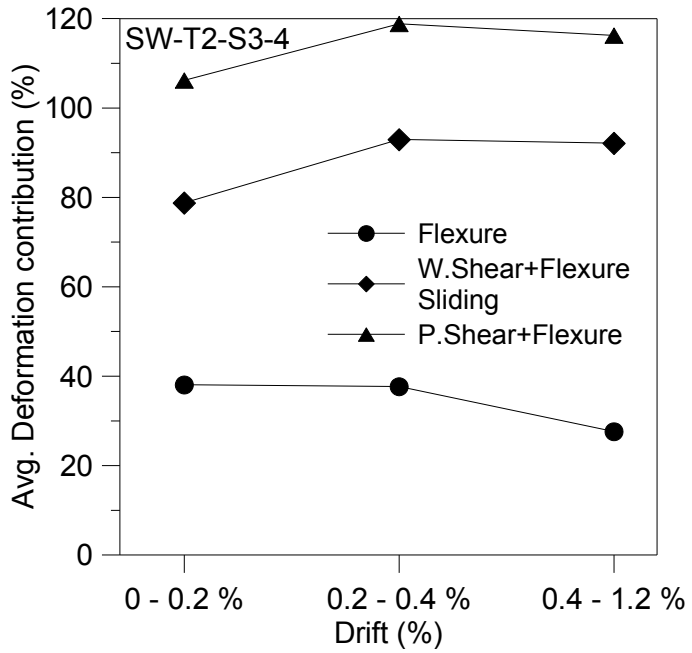

Figure A. 12. Average Deformation Contribution, Specimen T2-S3.

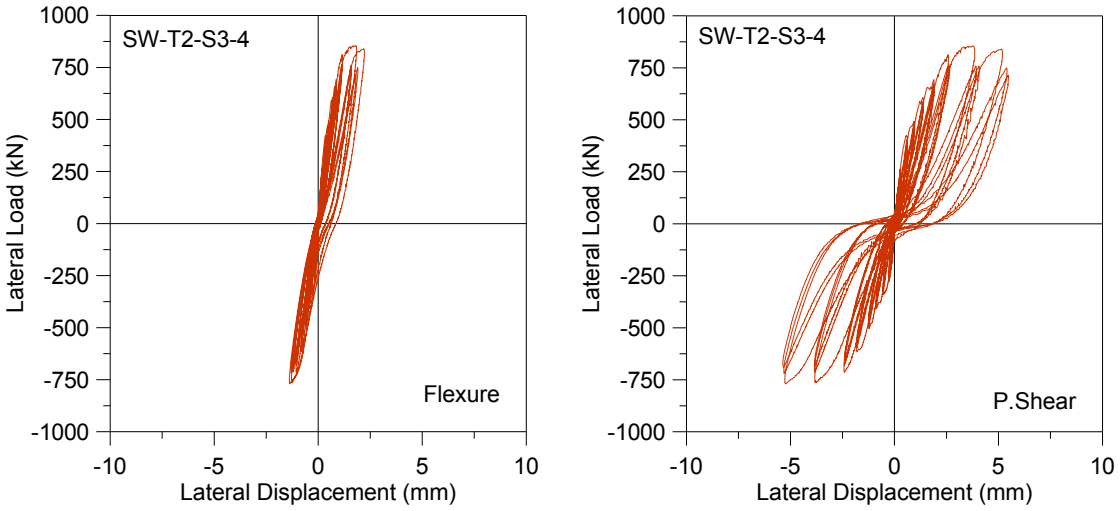

Figure A. 13. Top Lateral Flexure and Shear Deformation, Specimen T2-S3.

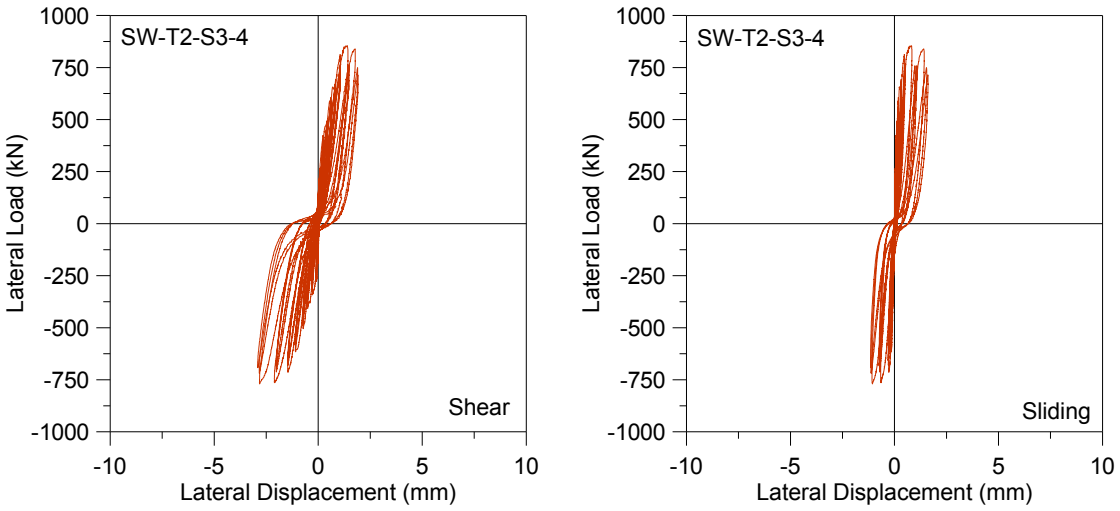

Figure A. 14. Top Lateral Shear and Sliding Deformations, Specimen T2-S3.

A.4. Top Lateral Deformation Components, T4-S1

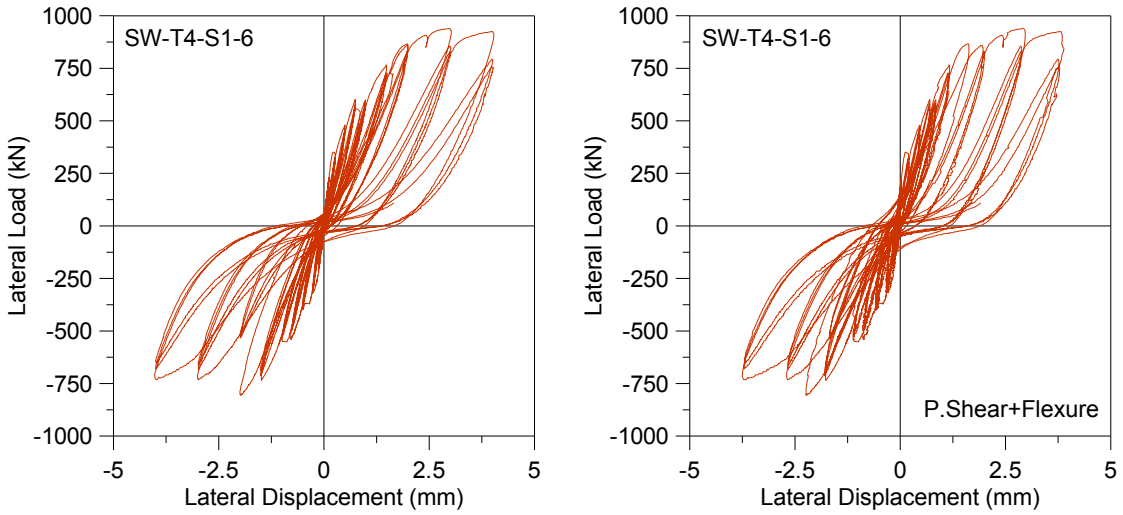

Figure A. 15. Top Lateral Deformation from External and Local Sensors, Specimen T4-S1.

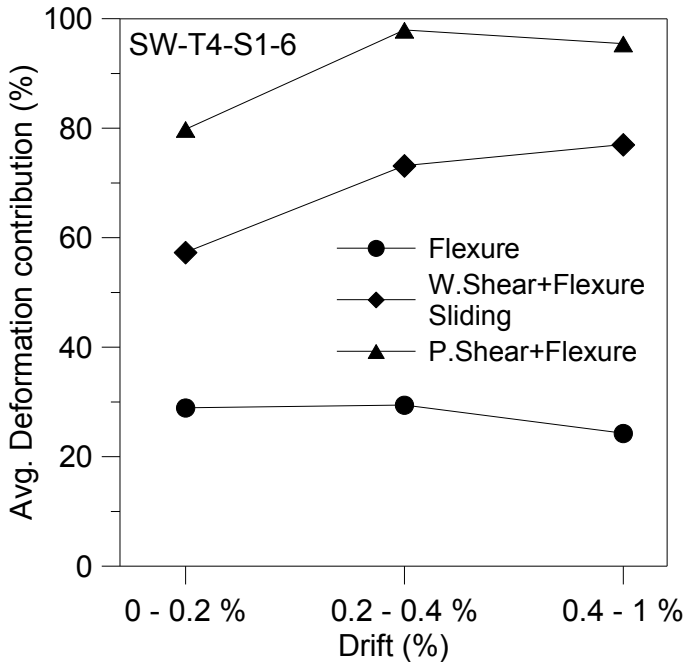

Figure A. 16. Average Deformation Contribution, Specimen T4-S1.

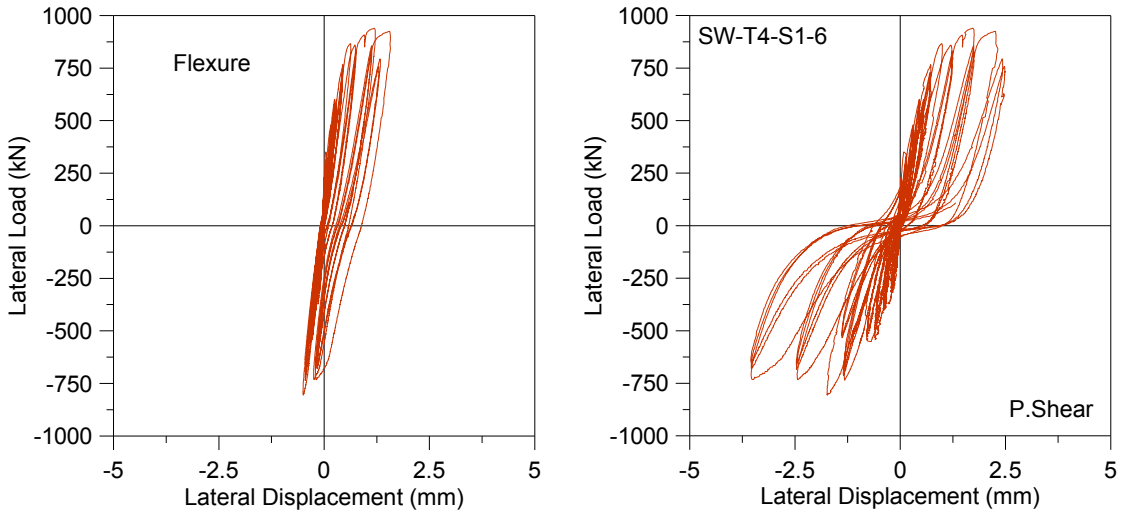

Figure A. 17. Top Lateral Flexure and Shear Deformations, Specimen T4-S1.

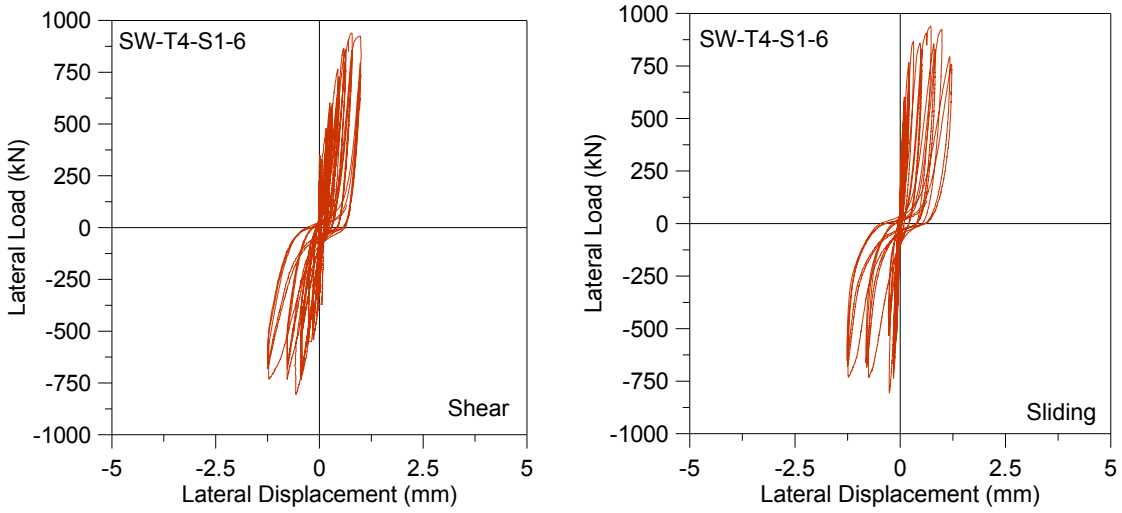

Figure A. 18. Top Lateral Shear and Sliding Deformations, Specimen T4-S1.

A.5. Top Lateral Deformation Components, Specimen T5-S1

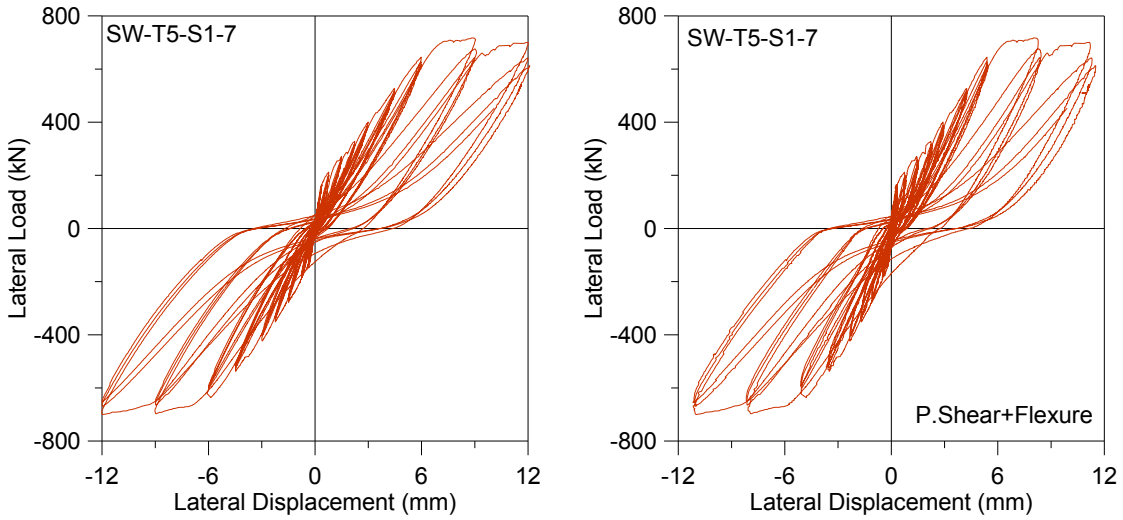

Figure A. 19. Top Lateral Deformation from External and Local Sensors, Specimen T5-S1.

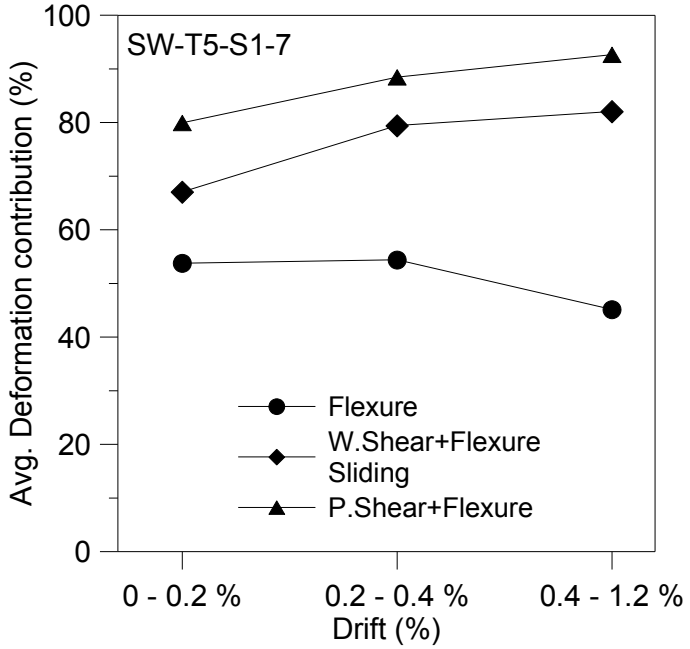

Figure A. 20. Average Deformation Contributions, Specimen T5-S1.

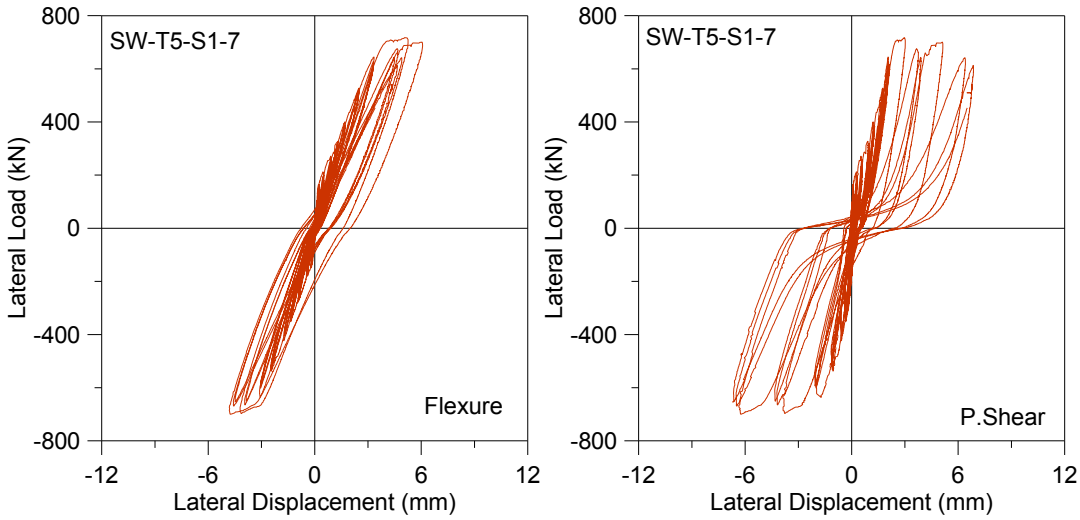

Figure A. 21. Top Lateral Flexure and Shear Deformations, Specimen T5-S1.

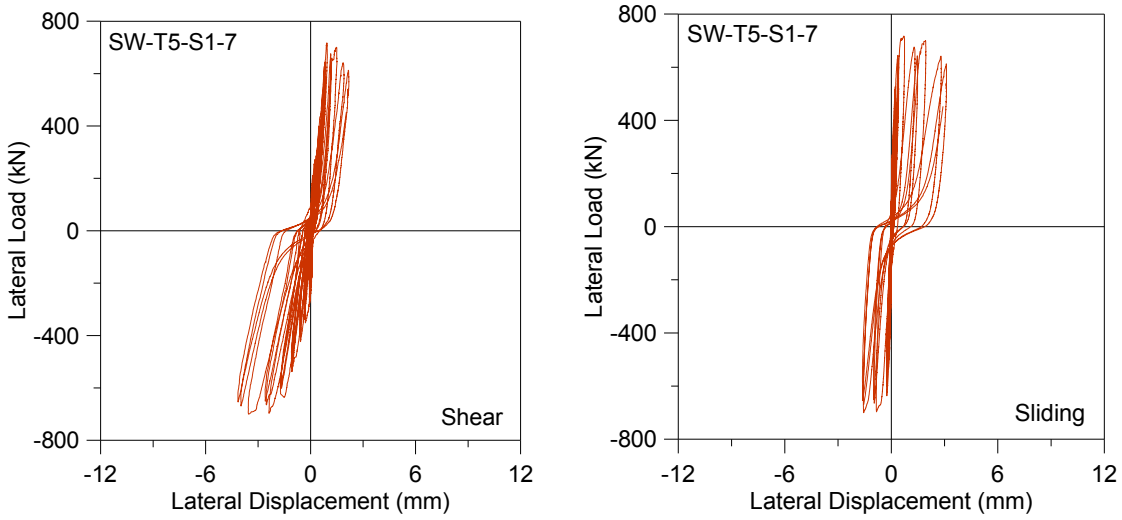

Figure A. 22. Top Lateral Shear and Sliding Deformations, Specimen T5-S1.

A.6. Top Lateral Deformation Components, Specimen T6-S1

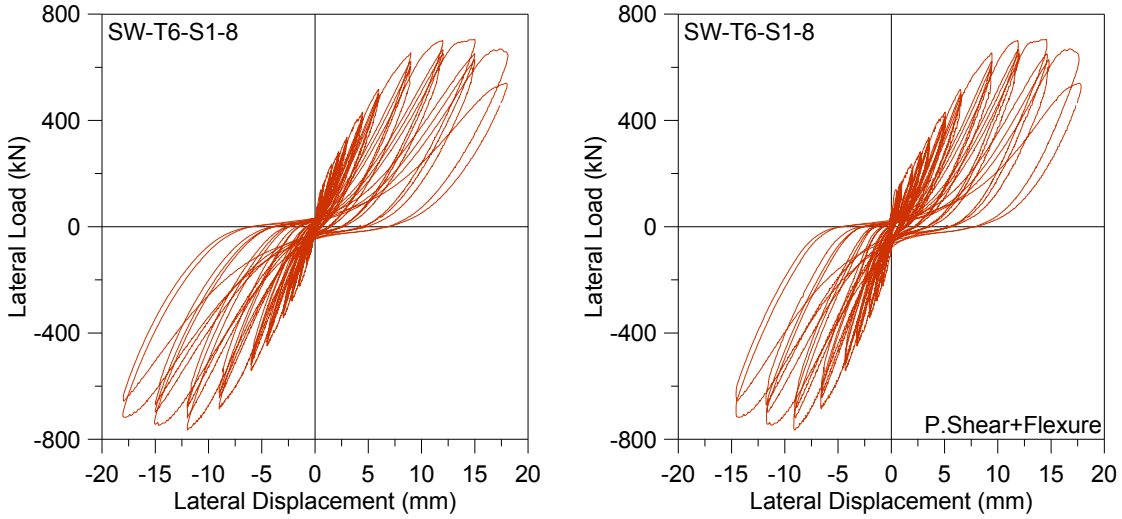

Figure A. 23. Top Lateral Deformation from External and Local Sensors, Specimen T6-S1.

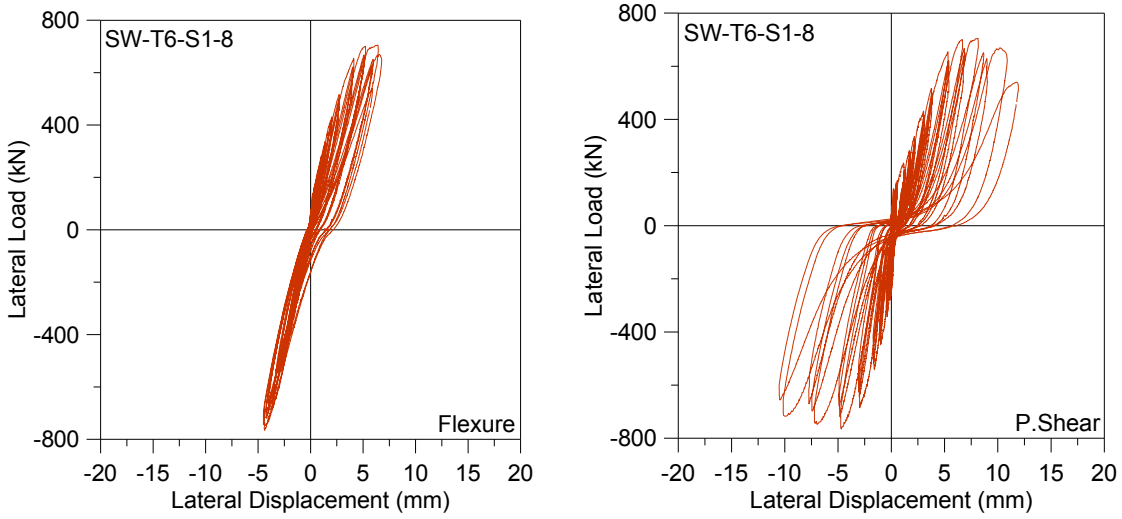

Figure A. 24. Top Lateral Flexure and Shear Deformations, Specimen T6-S1.

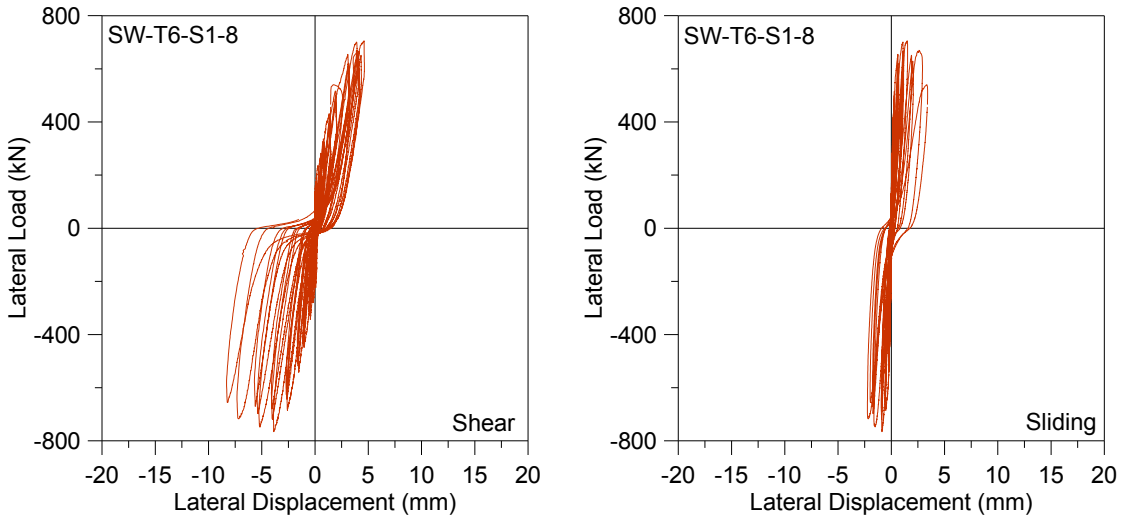

Figure A. 25. Top Lateral Shear and Sliding Deformations, Specimen T6-S1.

A.7. Top Lateral Deformation Components, Specimen T1-S2

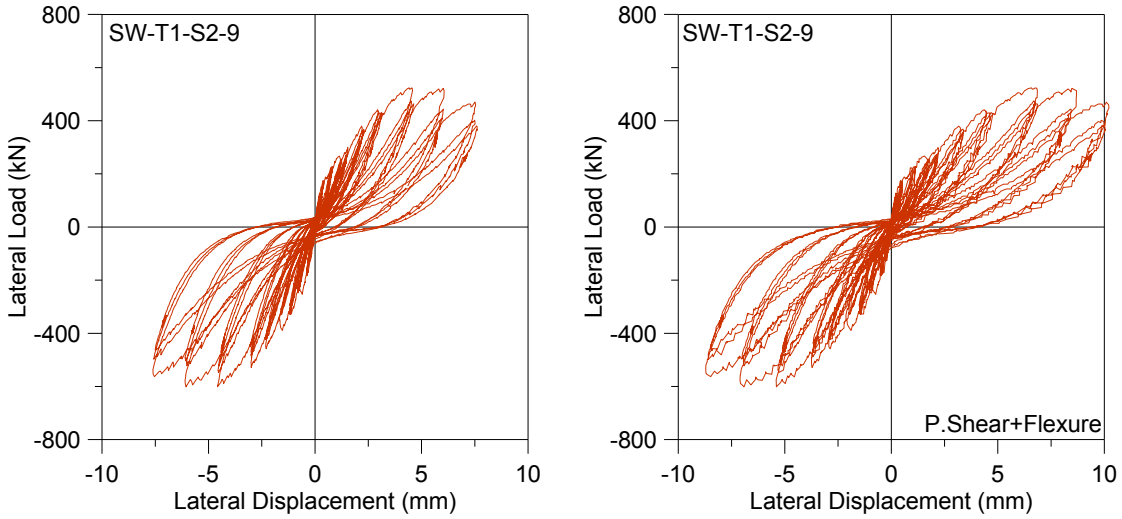

Figure A. 26. Top Lateral Deformation from External and Local Sensors, Specimen T1-S2.

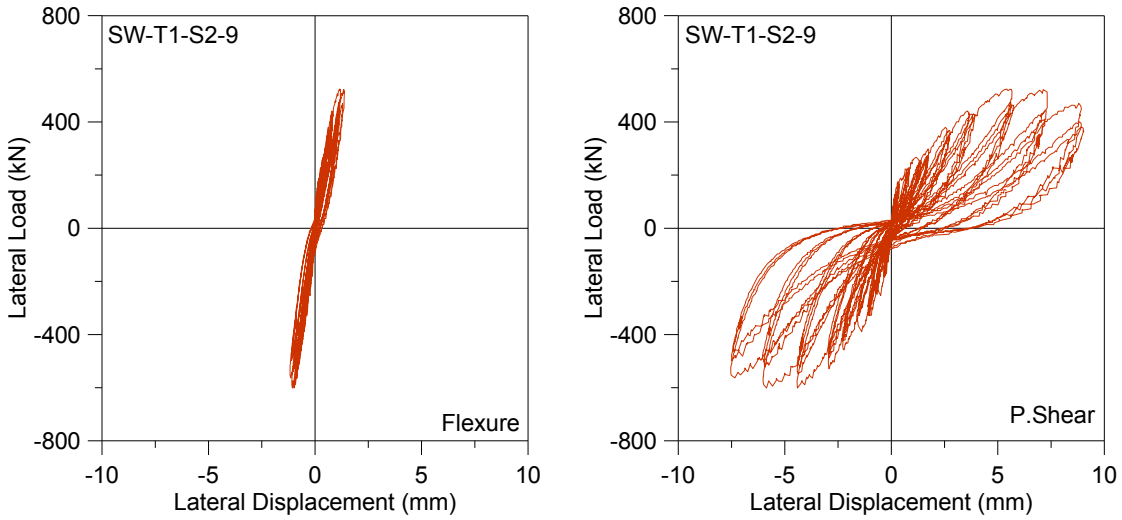

Figure A. 27. Top Lateral Flexure and Shear Deformations, Specimen T1-S2.

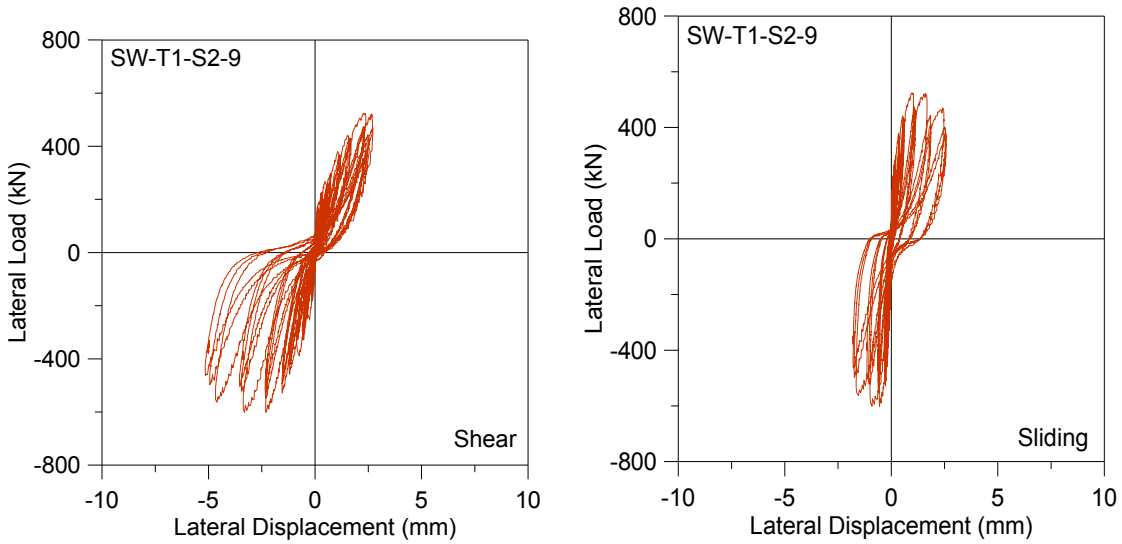

Figure A. 28. Top Lateral Shear and Sliding Deformations, Specimen T1-S2.

A.8. Top Lateral Deformation Components, Specimen T1-N5-S1

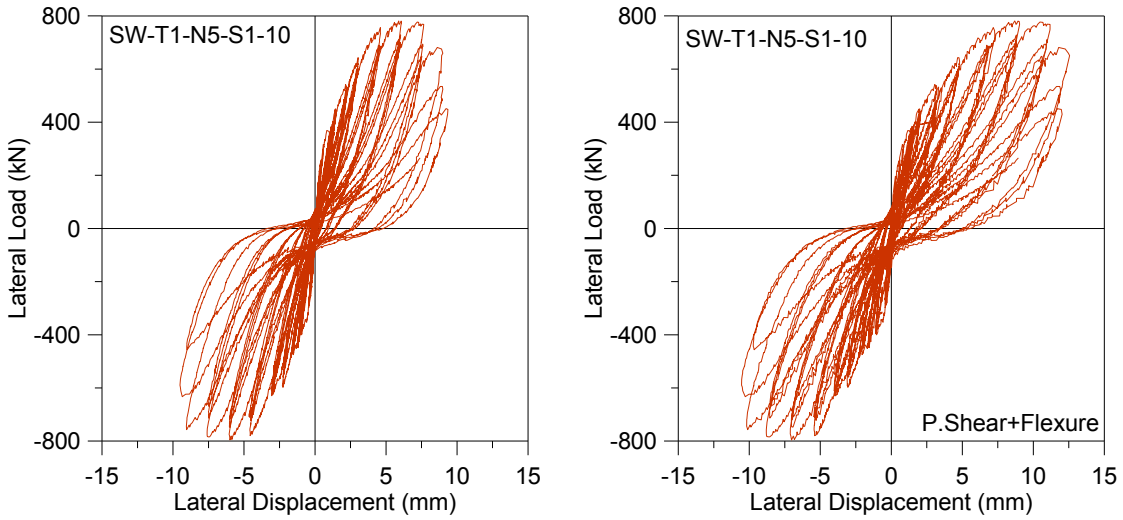

Figure A. 29. Top Lateral Deformation from External and Local Sensors, Specimen T1-N5-S1.

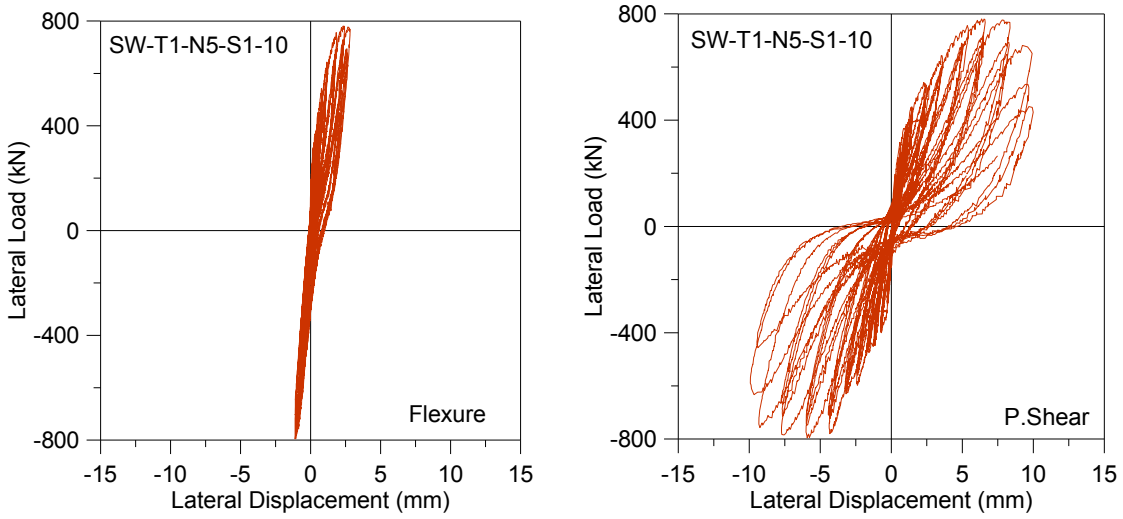

Figure A. 30. Top Lateral Flexure and Shear Deformations, Specimen T1-N5-S1.

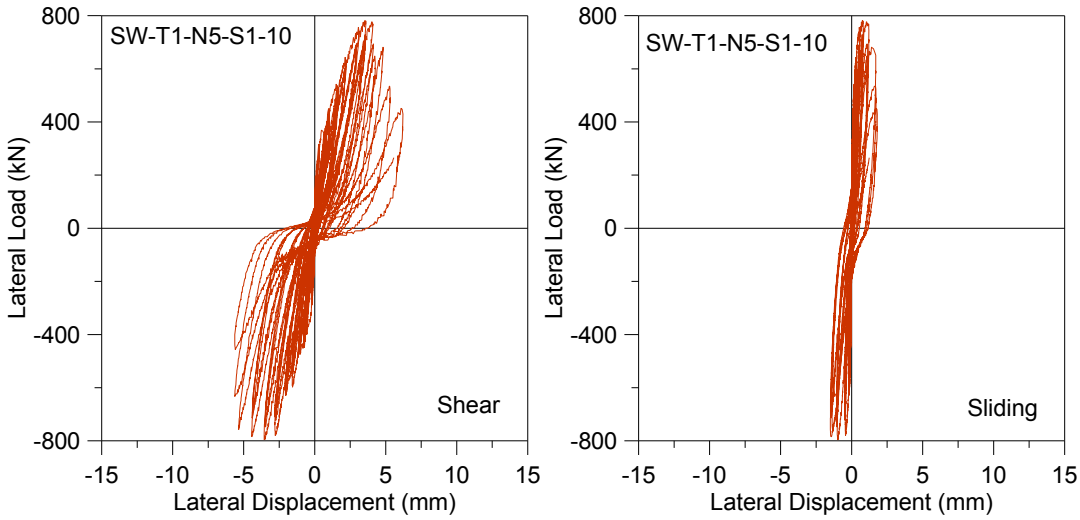

Figure A. 31. Top Lateral Shear and Sliding Deformations, Specimen T1-N5-S1.

A.9. Top Lateral Deformation Components, Specimen T1-N10-S1

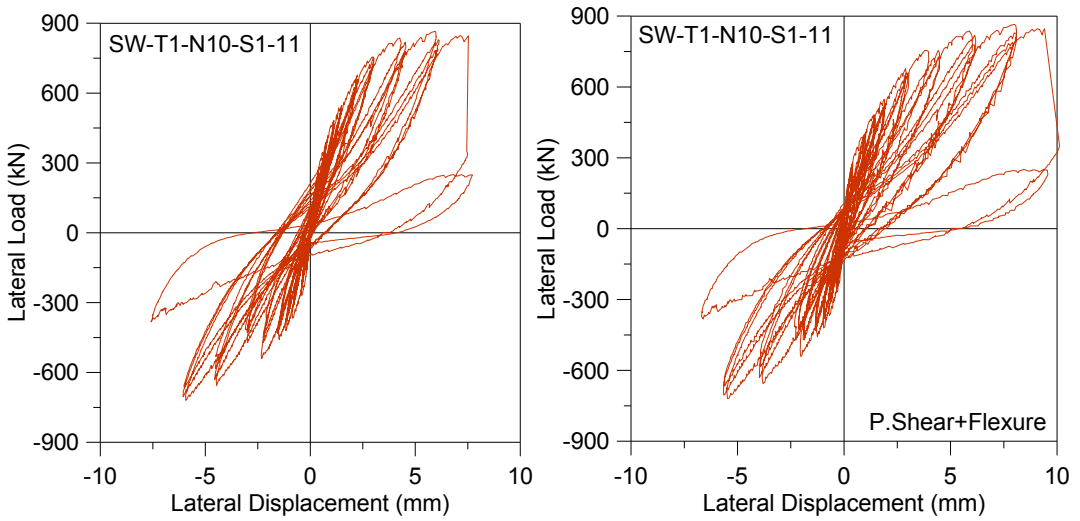

Figure A. 32. Top Lateral Deformation from External and Local Sensors, Specimen T1-N10-S1.

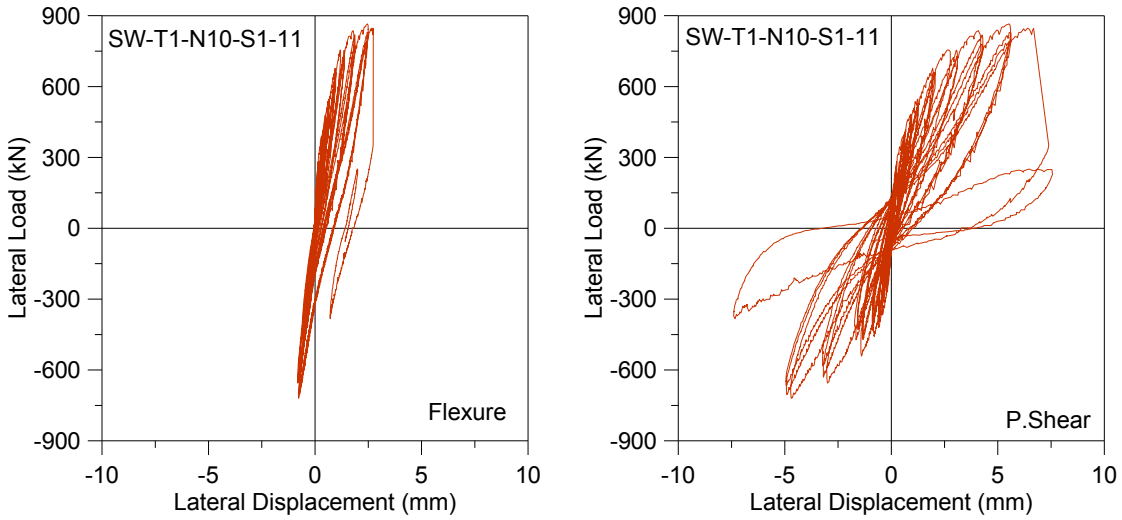

Figure A. 33. Top Lateral Flexure and Shear Deformations, Specimen T1-N10-S1.

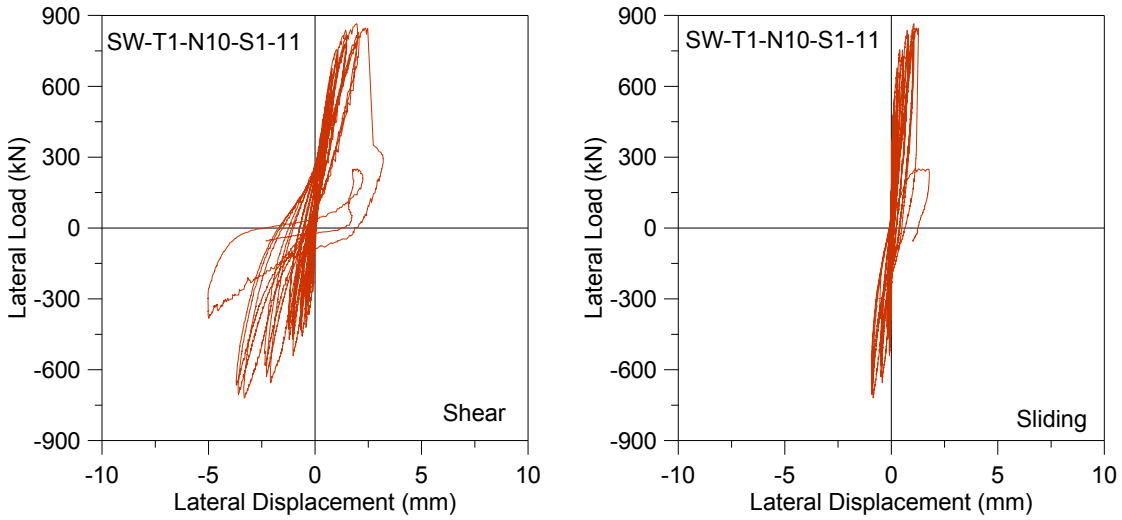

Figure A. 34. Top Lateral Shear and Sliding Deformations, Specimen T1-N10-S1.

A.10. Average Horizontal Strain Profiles

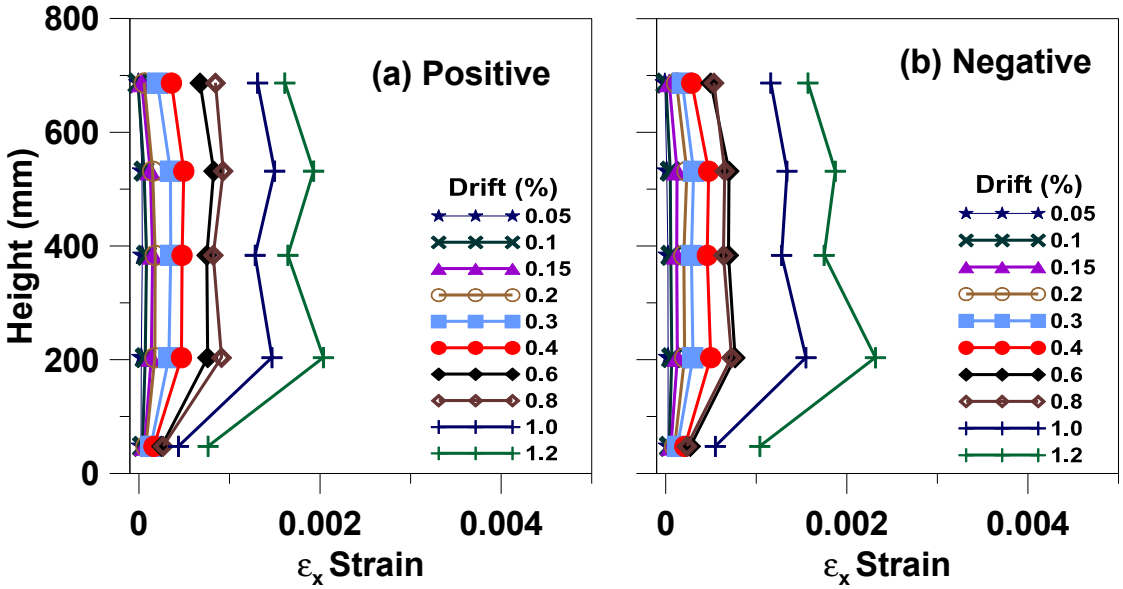

Figure A. 35. Average Horizontal Strain Profile, Specimen T1-S1.

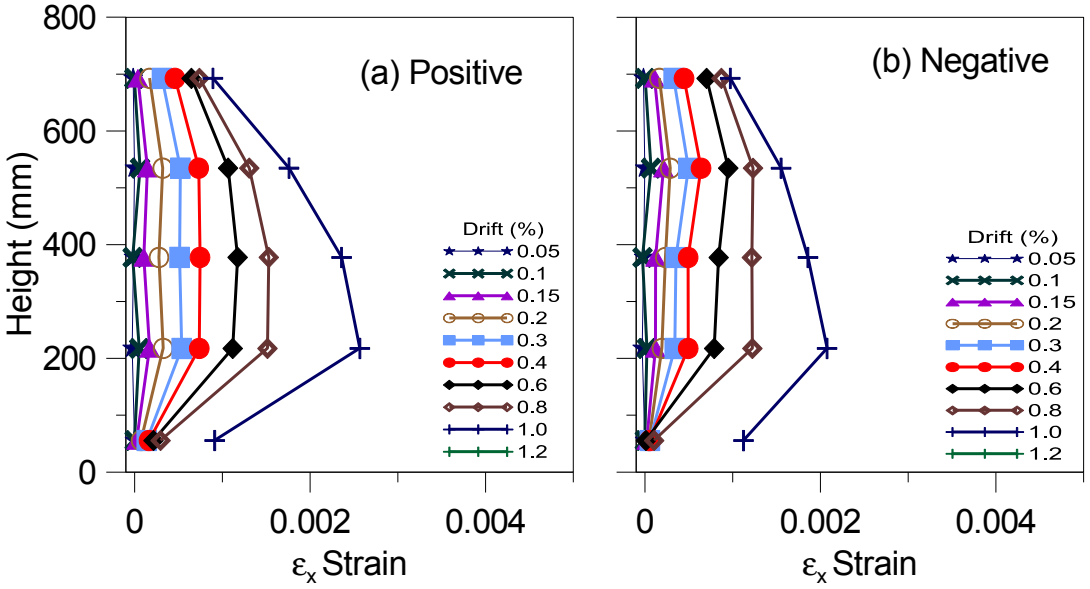

Figure A. 36. Average Horizontal Strain Profile, Specimen T2-S1.

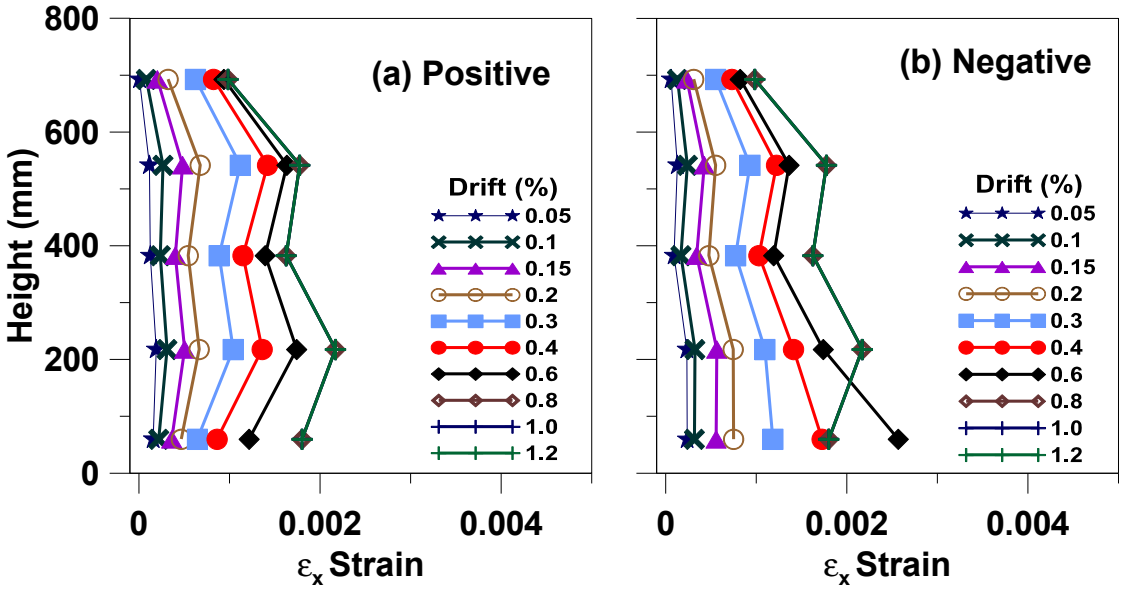

Figure A. 37. Average Horizontal Strain Profile, Specimen T2-S2.

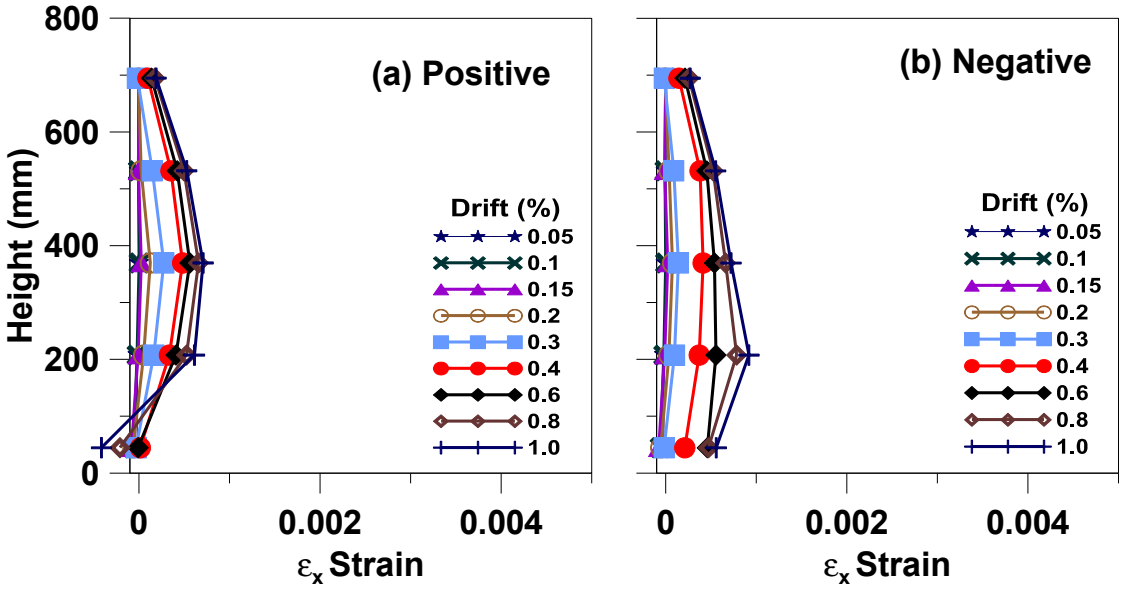

Figure A. 38. Average Horizontal Strain Profile, Specimen T3-S1.

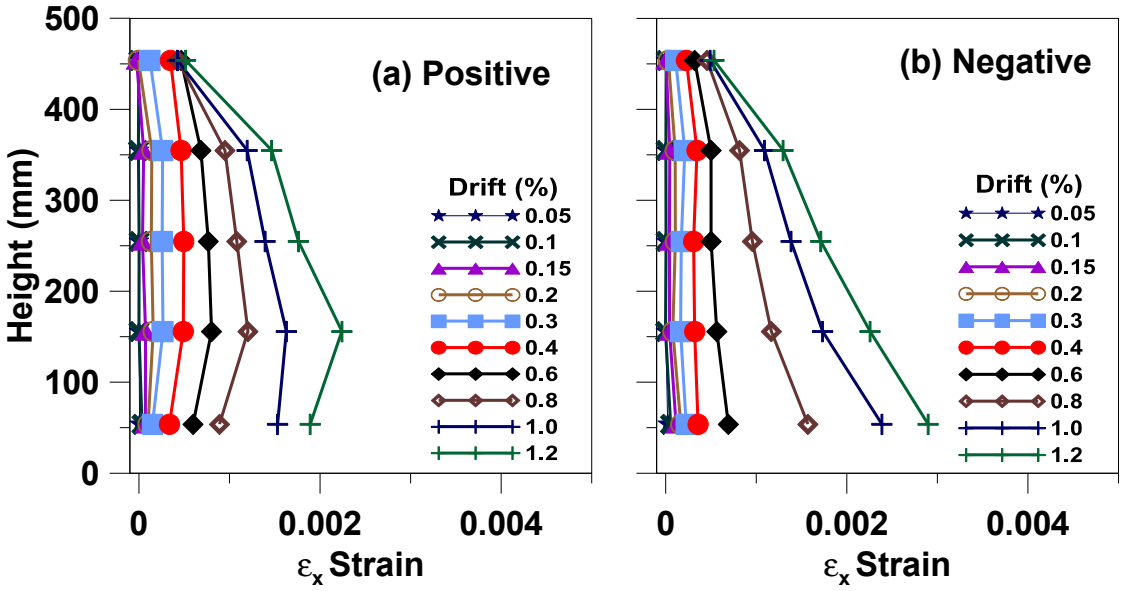

Figure A. 39. Average Horizontal Strain Profile, Specimen T4-S1.

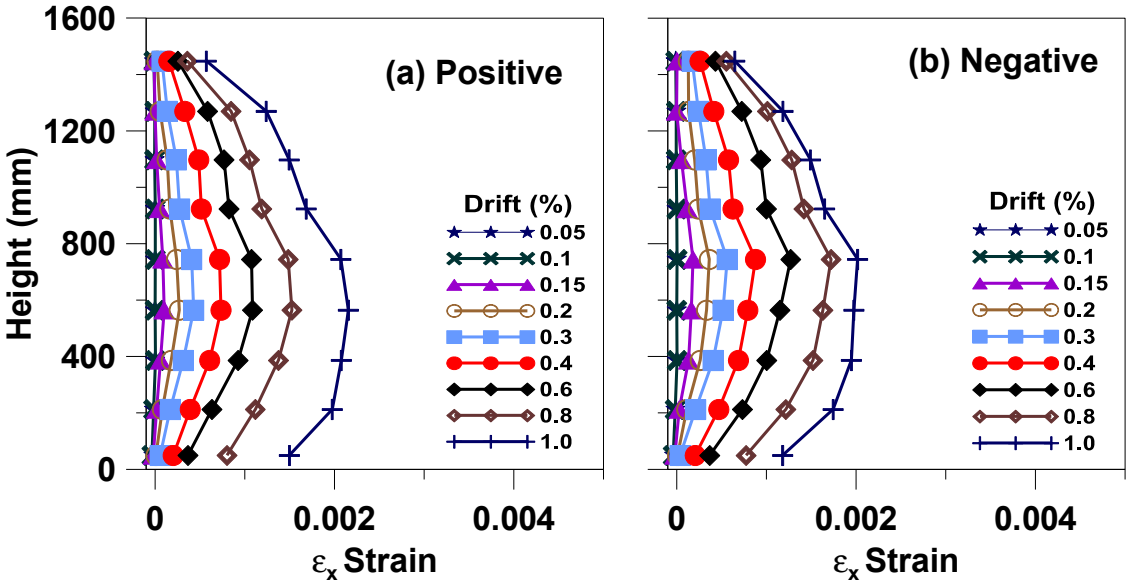

Figure A. 40. Average Horizontal Strain Profile, Specimen T5-S1.

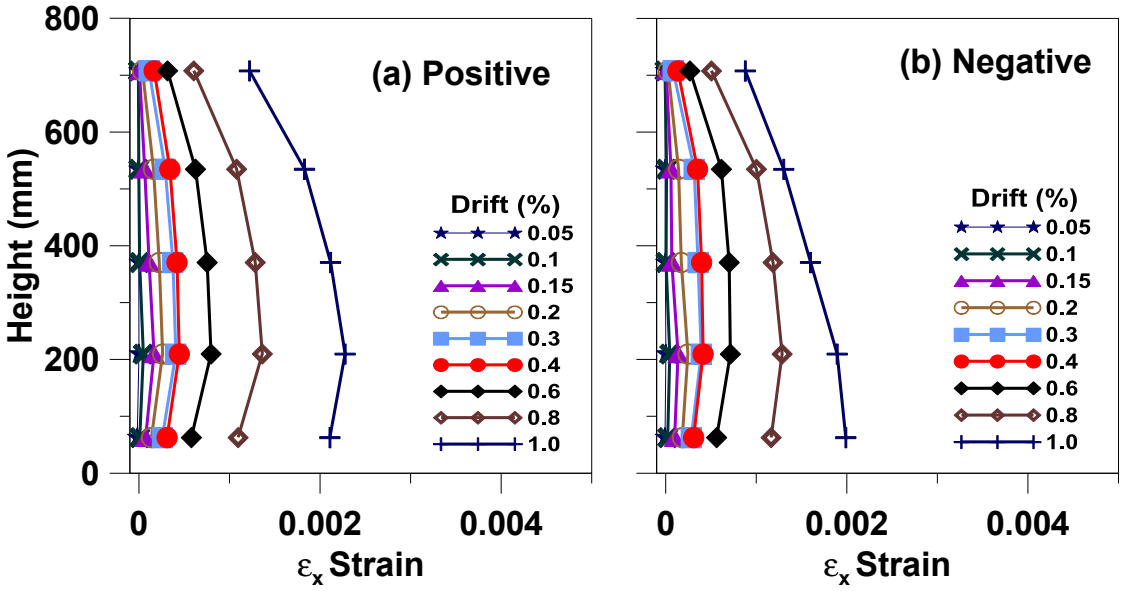

Figure A. 41. Average Horizontal Strain Profile, Specimen T1-S2.

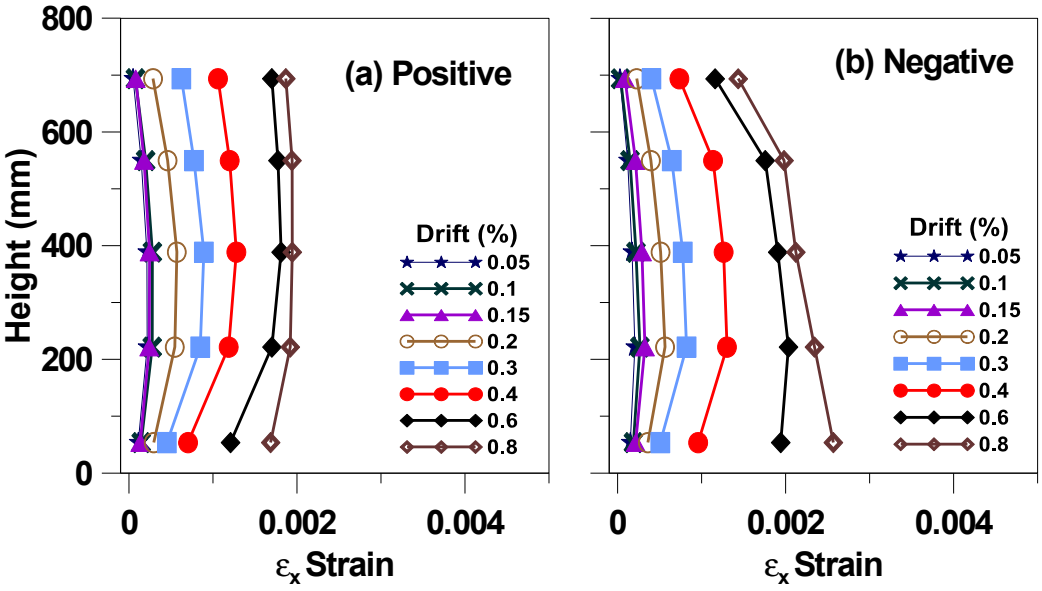

Figure A. 42. Average Horizontal Strain Profile, Specimen T1-N5-S1.

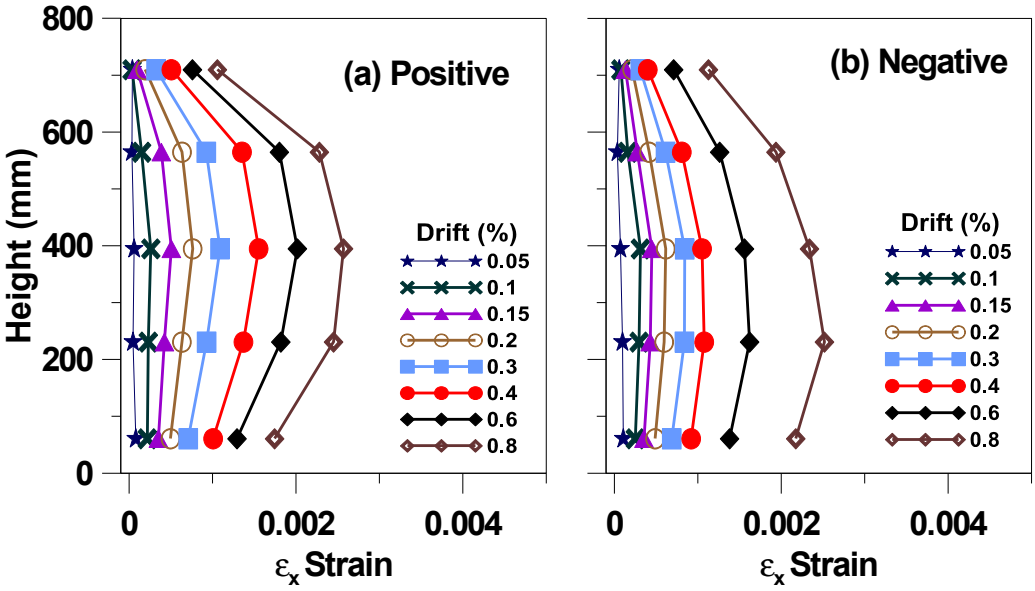

Figure A. 43. Average Horizontal Strain Profile, Specimen T1-N10-S1.

8. REFERENCES

ACI Committee 318, "Building Code Requirements for Structural Concrete (ACI - 318)and Commentary", American Concrete Institute, Farmington Hills, MI, 2008.

ASCE/SEI 41 - Supplement1, "Seismic Rehabilitation of Existing Buildings", Code, American Society of Civil Engineers, Reston, Virginia, 2007.

Barda, F., J. M. Hanson, and W. G. Corley, "Shear Strength of Low-Rise Walls with Boundary Elements", *Portland Cement Association Publication*, no. RD043D, 1976.

Benjamin, J. R., and H. A. Williams, "The Behavior of One-Story Reinforced Concrete Shear Wall", *Journal of the Structural Division, ASCE*, pp. 1-49, May 1957.

Cardenas, A. E., J. M. Hanson, W. G. Corley, and E. Hognestad, "Design Provisions for Shear Walls", *Journal of the American Concrete Institute*, Feb 1972.

Federal Emergency Management Agency, "Prestandard and Commentary for the seismic Rehabilitation of Buildings", FEMA-356, Washimgton, DC, Nov 2000.

Hidalgo, P. A., C. A. Ledezma, and R. M. Jordan, "Seismic Behavior of Squat Reinforced Concrete Shear Walls", *Earthquake Spectra* 18, pp. 287-308, 2002.

Hirosawa, M, "Past Experimental Results on Reinforced Concrete Shear Walls and Their Analysis", *Kenchiku Kenyu Shiryo* (Building Research Institute, Ministry of Construction), pp. 277-290, 1975

Maier, J., and B. Thurlimann, "Bruchversuche an Stahlbetonschieben", *IBK Bericht* I, no. 8003, 1985.

Massone, L. M, "RC Wall Shear – Flexure Interaction: Analytical and Experimental Responses", Dissertation, Civil Engineering, University of California Los Angeles, Los Angeles, 2006.

Orakçal, K, "Nonlinear Modeling and Analysis of Slender Reinforced Concrete Walls", Dissertation, University of California , Los Angeles, 2004.

Orakçal, K., L. M. Massone, and J. W. Wallace, "Shear Strength of Lightly Reinforced Wall Piers and Spandrels", *ACI Structural Journal*, pp. 455-465, July-August 2009.

Park, R., and T. Paulay, *Reinforced Concrete Structure,* New York, NY: Wiley , 1975.

Paulay, T. and M. J. N. Priestly, *Seismic Design of Reinforced Concrete and Masonary Buildings,* New York: John Wiley & Sons, Inc., 1992.

Paulay, T., M. J. N. Priestl, and A. J. Synge, "Ductility in Earthquake Resistant Squat Shear Walls", *ACI Journal*, pp. 257-269, 1982.

Sozen, M. A. and Moehle, J. P., "Stiffness of Reinforced Concrete Walls Resisting In-Plane Shear", 1993.

TSC-2007, "Requirements for Design and Construction of Reinforced Concrete Structures", Turkish Standard Institute, Ankara, 2007.

Wallace, J. W., L. M. Massone, and K. Orakçal, *St. Joseph`s Healthcre Orange California SPC-2 Upgrade: E/W Wing Component Test Program,* Final Report, University of California, Los Angeles, 2006.

Wood, S. L., "Shear Strength of Low-Rise Reinforced Concrete Walls", *ACI Structural Journal* 87, no. 1, pp. 99-107, 1990.